Atomic Layer Deposition of Late First-Row Transition Metals: Precursors and Processes

Katja Väyrynen

Department of Chemistry
Faculty of Science
University of Helsinki
Helsinki, Finland

ACADEMIC DISSERTATION

To be presented, with the permission of the Faculty of Science of the University of Helsinki, for public criticism in Auditorium A129 of the Department of Chemistry, A. I. Virtasen aukio 1, on the 11th of October, 2019 at 12 o'clock.

HELSINKI 2019

Supervisors

Professor Mikko Ritala
Professor Markku Leskelä
Department of Chemistry
University of Helsinki
Helsinki, Finland

Reviewers

Professor Séan Barry
Department of Chemistry
Carleton University
Ottawa, Canada

Professor Hyungjun Kim
School of Electrical and Electronic Engineering
Yonsei University
Seoul, Republic of Korea

Opponent

Professor Martyn Pemble
School of Chemistry and Tyndall National Institute
University College Cork
Cork, Republic of Ireland

ISBN 978-951-51-5494-1 (paperback)
ISBN 978-951-51-5495-8 (PDF)
http://ethesis.helsinki.fi
Unigrafia
Helsinki 2019

When you thought everything would be easy peasy lemon squeezy but it's actually difficult difficult lemon difficult

Abstract

Late first-row transition metals, namely copper, nickel, and cobalt, are pivotal materials in many modern and future applications. Because of its low resistivity, Cu has for long been the metal of choice for interconnects in microelectronic devices. Co is needed in the smallest features of the 10 nm technology node interconnects, as it is more robust than Cu toward electromigration, a phenomenon causing damage to the interconnects. Being ferromagnetic, Co and Ni are in the focal point of developing faster and more durable magnetic memories capable of handling the exponentially increasing amounts of data being generated annually.

The development of faster yet smaller electronic devices requires a constant increase in computational power. To improve the performance without increasing device size, the components on integrated circuits should be shrunk and packed more closely. The shrinking is achieved by using thin films with nanoscale thicknesses preferably arranged in three-dimensional forms. For downscaling to continue, accurate thin film deposition methods are needed. Atomic layer deposition (ALD) provides atomic level accuracy and is thus the number one thin film deposition technique for modern and future devices. ALD is based on a cyclically repeated alternate supply of gaseous precursors that react on a substrate and form a uniform layer of material, atom by atom, even on complex three-dimensional structures.

ALD is based solely on chemistry; to benefit from the many advantages the method has to offer, suitable precursors must first be found for each of the desired materials. ALD has been employed to deposit a myriad of materials ranging from pure elements to, for example, oxides, nitrides, and chalcogenides, but the deposition of metals has been hindered by a lack of reactive precursors and reducing agents. Thermal ALD processes exist mostly for noble metals, but mere thermal activation has often proven insufficient for the reduction of the late first-row transition metals. The aim of this thesis was to find and develop new precursors and processes for the ALD of high-quality Cu, Ni, and Co thin films, thus promoting the development of better microelectronics.

Within the scope of this thesis, several new metal precursors for the ALD of the late first-row transition metals were developed and tested. Out of all of them, the diamine adducts of Co(II) and Ni(II) chlorides showed the best performance in the ALD experiments. In addition to the new metal precursors, the focus of this thesis was also on finding more efficient alternatives for the conventional reducing agents, H_2 and NH_3. Tert-butylhydrazine showed high reactivity to produce Cu and Ni_3N by ALD, providing significant improvement on film purity and resistivity over the existing processes. Tributyltin hydride, another powerful reducing agent, was studied for the ALD of Co and Ni. Instead of producing metallic Co or Ni, intermetallic Co_3Sn_2 and Ni_3Sn_2 were deposited unveiling a new field of ALD: the ALD of intermetallics. The same approach was also applied to the ALD of Ni_2Ge thin films. Postdeposition reduction of the corresponding metal oxides and nitrides was also explored as an alternative route for the preparation of metal thin films.

Preface

The work for this thesis was done in the group of Thin Films and Other Nanostructured Materials at the University of Helsinki between the years 2016 and 2019. Funding from ASM Microchemistry Oy is gratefully acknowledged. I appreciate Dr. Suvi Haukka, Dr. Marko Tuominen, and Mr. Hannu Huotari for all the fruitful discussions along this journey. I would also like to thank the Walter Ahlström Foundation and the Finnish Foundation for Technology Promotion for awarding me with personal grants.

My heartfelt thanks go to my supervisors, Prof. Mikko Ritala and Prof. Markku Leskelä, for seeing my potential and giving me the opportunity to prove my capability in the field of ALD. I thank you both for all the inspirational lectures you have given and the interesting projects that I have been able to be a part of. I am thankful to you for challenging me and for making me feel motivated and thrive.

I am sincerely thankful for the constructive feedback received from the official reviewers of this thesis, Prof. Séan Barry and Prof. Hyungjun Kim. Your insightful comments helped me improve the thesis significantly. I am also deeply grateful to Prof. Martyn Pemble for accepting the task of opposing this work.

I owe my greatest thanks to Dr. Timo Hatanpää who has been the mastermind behind most of the metal precursors introduced in this thesis. Thank you for all the innovative ideas and for fulfilling my precursor needs. This thesis is a product of our teamwork. Without your contribution, I would still be stuck on my first paper.

I am deeply grateful to everyone who contributed to the articles in this thesis. Mr. Miika Mattinen is thanked for all the AFM measurements and his valuable input to the content of the articles. I wish to thank Mr. Mikko Heikkilä for helping me with some of the more complicated XRD measurements. Thank you Dr. Kenichiro Mizohata, Dr. Kristoffer Meinander, and Prof. Jyrki Räisänen for all the work you put into analyzing my films by ToF-ERDA and XPS. Mr. Joosep Link and Prof. Raivo Stern from the Technological Institution of Tallinn are gratefully acknowledged for magnetic measurements. I am deeply thankful to Mr. Anton Vihervaara without whom I could not have finished all my experiments before leaving the university. Dr. Daniel Peeters and Prof. Anjana Devi from the Ruhr-University Bochum are also thanked for collaborating with us on Cu ALD.

I am thankful for all the great people with whom I have had the privilege to work with in the ALD group. Dr. Jaakko Niinistö and Dr. Ville Miikkulainen are thanked for teaching me the gist of ALD during my research training and Master's studies. I am grateful to Dr. Marianna Kemell for her guidance with both SEM and EDS. I wish to thank Dr. Miia Mäntymäki for passing the torch as the official "labranatsi" to me; the added responsibility helped me boost my confidence in the lab and gave me an opportunity to work on my people and time management skills. I also appreciate the help I got from both Miia and Mr. Leo Salmi with the F-120 reactor in the beginning of my PhD. I would like to thank all my office

mates (Miika, Tomi, Georgi, and Elisa) for all the fun conversations, the times playing GeoGuesser, and the traditional B316 Easter Egg Hunt. I am especially thankful to Miika for his never-ending helpfulness and Tomi for cheering me on and for keeping up the team spirit. Thank you, Jani and Sanni, for bringing color and life into my workdays. I loved going to the coffee room knowing there is always good company and crosswords waiting for me.

I would like to thank my family, especially my mom and my sisters, for their endless support throughout this journey. I am also grateful to all my friends for distracting me from my work and for giving me something to talk about besides ALD. Thank you, Kimmo, for all your optimism, love, and the lazy weekend mornings with perfectly fried eggs. I am grateful to you for agreeing to get our dog, Nätti, and for helping me take care of her.

I owe special thanks to my sister Maiju without whom I would not have chosen to study chemistry, let alone join the ALD group for my research training in 2013. Thank you for helping me make smart choices.

I dedicate this thesis to my late father whose last words to me before my high school physics test have kept me going even when things have got tough: Kyllä sinä osaat.

Helsinki, August 2019

Katja Väyrynen

List of publications

This thesis is based on the following original publications referred to in the text by their Roman numerals.

I **Low-Temperature Atomic Layer Deposition of Low-Resistivity Copper Thin Films Using $Cu(dmap)_2$ and Tertiary Butyl Hydrazine**
Katja Väyrynen, Kenichiro Mizohata, Jyrki Räisänen, Daniel Peeters, Anjana Devi, Mikko Ritala, and Markku Leskelä
Chem. Mater. **2017**, *29*, 6502–6510.

II **Diamine Adduct of Cobalt(II) Chloride as a Precursor for Atomic Layer Deposition of Stoichiometric Cobalt(II) Oxide and Reduction Thereof to Cobalt Metal Thin Films**
Katja Väyrynen, Timo Hatanpää, Miika Mattinen, Mikko Heikkilä, Kenichiro Mizohata, Kristoffer Meinander, Jyrki Räisänen, Mikko Ritala, and Markku Leskelä
Chem. Mater. **2018**, *30*, 3499–3507.

III **Atomic Layer Deposition of Intermetallic Co_3Sn_2 and Ni_3Sn_2 Thin Films**
Katja Väyrynen, Timo Hatanpää, Miika Mattinen, Kenichiro Mizohata, Kristoffer Meinander, Jyrki Räisänen, Joosep Link, Raivo Stern, Mikko Ritala, and Markku Leskelä
Adv. Mater. Interfaces **2019**, *6*, 1801291.

IV **Atomic Layer Deposition of Nickel Nitride Thin Films using $NiCl_2$(TMPDA) and Tert-Butylhydrazine as Precursors**
Katja Väyrynen, Timo Hatanpää, Miika Mattinen, Mikko J. Heikkilä, Kenichiro Mizohata, Jyrki Räisänen, Joosep Link, Raivo Stern, Mikko Ritala, and Markku Leskelä
Phys. Status Solidi A **2019**, *216*, 1900058.

V **Nickel Germanide Thin Films by Atomic Layer Deposition**
Katja Väyrynen, Anton Vihervaara, Timo Hatanpää, Miika Mattinen, Mikko J. Heikkilä, Kenichiro Mizohata, Jyrki Räisänen, Mikko Ritala, and Markku Leskelä
Chem. Mater. **2019**, *31*, 5314–5319.

The author has actively participated in planning the research and written all the articles together with the co-authors. The author has executed most of the film depositions and a large part of the characterization including EDS, SEM, XRD, and resistivity measurements.

Abbreviations

3D	three-dimensional
acac	acetylacetonate
AFM	atomic force microscopy
ALD	atomic layer deposition
at.%	atomic percent
a.u.	arbitrary unit
bdepe	1,2-bis(diethylphosphino)ethane
BEOL	back-end-of-line
btsa	bis(trimethylsilyl)amido
CCTBA	hexacarbonyl(3,3-dimethyl-1-butyne)dicobalt
CDO	carbon-doped oxide
CMOS	complementary metal-oxide-semiconductor
cod	1,5-cyclooctadiene
Cp	cyclopentadienyl
CVD	chemical vapor deposition
dad	diazadienyl
DEZ	diethylzinc
dki	1,3-diketiminate
dmamb	dimethylamino-2-methyl-2-butoxide
dmap	dimethylamino-2-propoxide
dmb	3,3-dimethyl-1-butene
dmetda	N,N-dimethylamine ethylen N'-tertbutylamido-aluminumdihydride
DRAM	dynamic random-access memory
EDS	energy dispersive X-ray spectroscopy
Et	ethyl
fcc	face-centered cubic
hcp	hexagonal close-packed
hfac	hexafluoroacetylacetonate
hfip	hydroxyhexafluoroisopropyl
hmds	hexamethyldisilazane
HQ	hydroquinone
HTXRD	high temperature X-ray diffraction
IC	integrated circuit
IoE	Internet of Everything
^{i}Pr	isopropyl
^{iPr}amd	N,N'-diisopropylacetamidinate
ITO	indium tin oxide
Me	methyl
MTJ	magnetic tunnel junction

$^{n}Bu_3P$	tri-n-butylphosphane
nhc	N-heterocyclic carbene
OAc	acetate
OTS	octadecyltrichlorosilane
PEALD	plasma-enhanced atomic layer deposition
Pin	pinacolate
PVD	physical vapor deposition
py	pyridine
pyrim	pyrrolylaldiminate
RC	product of resistance and capacitance
R_q	root-mean-square
SALICIDE	self-aligned silicide
SAM	self-assembling monolayer
^{s}Bu	sec-butyl
sccm	standard cubic centimeters per minute
SEM	scanning electron microscopy
SRAM	static random-access memory
STT-RAM	spin-transfer torque random-access memory
TBGH	tributylgermanium hydride
TBH	tert-butylhydrazine
tbidmb	1-(tert-butylimino)-2,3-dimethylbutan-2-olate
TBTH	tributyltin hydride
^{t}Bu	tert-butyl
^{tBu}amd	N-tert-butyl-N'-ethylpropionamidinate
TGA	thermogravimetric analysis
thd	2,2,6,6-tetramethylheptane-3,5-dionate
TMA	trimethylaluminum
tmeda	N,N,N',N'-tetramethylethylenediamine
tmpda	N,N,N',N'-tetramethyl-1,3-propanediamine
ToF-ERDA	time-of-flight elastic recoil detection analysis
VSM	vibrating sample magnetometer
vtmos	vinyltrimethoxysilane
vtms	vinyltrimethylsilane
XPS	X-ray photoelectron spectroscopy
XRD	X-ray diffraction
XRR	X-ray reflectivity
ZB	zettabyte

Table of contents

1 Introduction

The Internet connects almost four billion people worldwide. Nowadays, nearly everything is linked together, and we are not only talking about machine-to-machine based communications but about a wider, more complex system called the Internet of Everything (IoE) that brings together things, people, and processes. The digitalization of society creates an enormous amount of data that needs to be transferred, analyzed, and stored — fast and efficiently. As Figure 1 demonstrates, the amount of data generated annually has increased exponentially and is expected to hit 163 zettabytes (ZB) in 2025.[1] At the same time, the development of robotics, artificial intelligence, virtual reality, and self-driving cars puts even more pressure on furthering the microelectronics industry. Electronic devices must be smaller, faster, and more efficient. Increasing computational power without increasing device sizes requires downscaling the electronic components on the integrated circuit (IC). So far, this development has followed Moore's law, according to which the number of transistors on an IC increases by a factor of 1.5–2 every two years. Further miniaturization can be achieved by designing three-dimensional (3D) features and by employing thin films with sub-10 nanometer thicknesses. Computational power has grown in huge leaps; a chip less than the size of a pinhead can nowadays store 500 MB of information while in the 1950s, 5 MB could barely fit in a small jet.[2] To ensure similar progress also in the future, the microelectronics industry looks for new nanomaterials and methods that would allow their preparation in a more accurate and controllable manner.

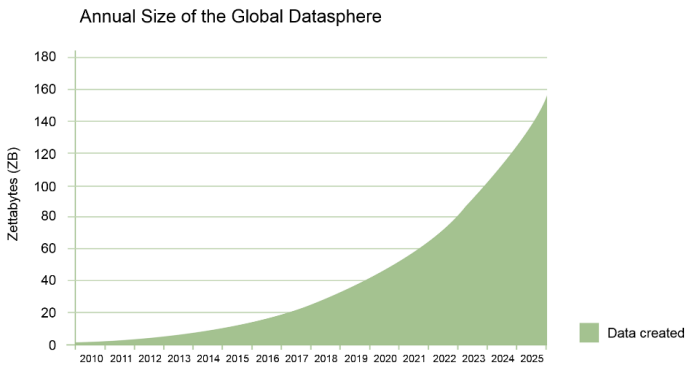

Figure 1. Past and future perspectives regarding the increase of data. Image created based on IDC's Data Age 2025 Study.[1]

Co, Ni, and Cu are late first-row transition metals that find use in many current and future microelectronics applications. Cu replaced Al in interconnects at the 180 nm node in 1997 and has been the primary conductor all the way to the 10 nm node technology.[3,4] The resistance of Cu wires increases as the miniaturization of features is taken further, which causes increased RC (product of resistance and capacitance) delay and electromigration, leading to malfunctioning of the IC.[5–7] The performance of Cu at the very smallest

dimensions has been improved by using Co caps and liners.[8–11] Co may also be used as an alternative conductor and it has, in fact, already been implemented at the bottom layers of Intel's 10 nm technology interconnect.[12] Other possible Cu-replacing metals for narrow interconnects include, for example, Ni, Mo, Rh, and Ru.[13,14] In addition to interconnects, thin films of Co and Ni serve as precursors to the preparation of $CoSi_2$ and NiSi contact materials.[15,16] Owing to their ferromagnetic properties, Co and Ni are also considered as promising materials for magnetic tunnel junctions (MTJ) in memory devices, such as spin-transfer torque random-access memories (STT-RAM).[17,18] Besides being much faster than conventional memories, the STT-RAM also operates with a much lower power consumption and exhibits high endurance.[19,20] By finding the right materials and fabrication methods, magnetic memories could eventually replace all other types of memories, revolutionizing the entire microelectronics industry.

The only thin film deposition method capable of confronting the technological challenges facing the microelectronics industry is atomic layer deposition (ALD). The ALD method was developed and patented in Finland in the 1970s and was first used for the manufacturing of thin film electroluminescent displays.[21,22] Today, ALD is employed all over the world in a wide range of industrial applications; the method has, for example, been a part of the transistor production chain since 2007.[23] ALD is based on saturative, irreversible surface reactions that enable the deposition of thin films in a self-limiting manner, atom by atom — even on complex 3D structures.[24–26] The success of ALD is ascribed entirely to chemistry; the method can be employed only after finding a suitable precursor combination for a desired material. In other words, development of new and improved microelectronics is impossible without fundamental research on ALD chemistry.

This thesis comprises five journal articles introducing both new metal precursors and reducing agents for ALD of the late first-row transition metals. Each publication describes a new ALD process employing the precursors to deposit metals either directly or indirectly by postdeposition reduction of the corresponding metal oxide or nitride film. The motivation for this research is justified in Chapter 2 where both the applications and challenges regarding Co, Ni, and Cu are discussed. Chapter 3 provides a comprehensive literature review to the basic principles of metal ALD and to the previously published ALD chemistries for the late first-row transition metals. Chapter 4 shortly describes the experimental procedures behind publications I–V, and Chapter 5 is a summary of the key results obtained in the course of this research. Finally, Chapter 6 summarizes the most important findings of this thesis and provides some future perspectives on the development of metal ALD and microelectronics.

2 Late first-row transition metals

This chapter highlights the motivation and practical importance behind the research that has been conducted during this PhD project. The late first-row transition metals find use in many modern and future applications, especially in the field of microelectronics. Co has received considerable scientific and industrial interest for its importance in interconnects beyond the 10 nm node technology. Section 2.1 gives a short introduction to the late first-row transition metals and their properties. Section 2.2 presents some relevant applications for Co, Ni, and Cu thin films. The challenges related to developing said applications are outlined in Section 2.3.

2.1 Overview

In this thesis, the concept of late first-row transition metals includes Co, Ni, and Cu, highlighted in the periodic table in Figure 2. Selected properties of these metals are listed in Table 1.[27] Because of the negative standard reduction potentials of Co(II) and Ni(II), their precursors are difficult to reduce to metal, which limits the preparation of Co and Ni thin films by chemical routes. Cu(II) has a standard reduction potential of +0.34 V and is thus easier to reduce; Cu is also one of the few metals that occurs in nature in a pure, metallic form. Typically, the three metals have the face-centered cubic (fcc) structure, but Co and Ni may also occur in the hexagonal close-packed (hcp) structure when prepared at low temperatures.[28] The three metals have similar densities, but the melting point of Cu is lower compared to the other two. Co, Ni, and Cu all exhibit low resistivity, making them highly desirable for many applications. On top of good electrical conductivity, Co and Ni are ferromagnetic and thus suitable for magnetic applications.[17,18]

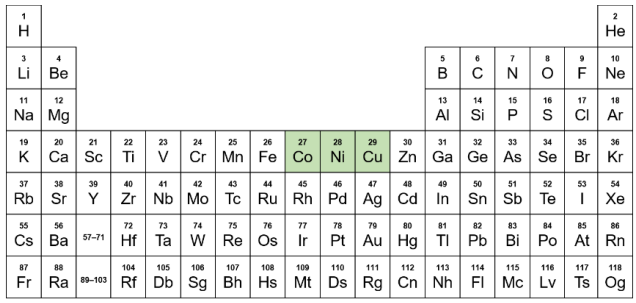

Figure 2. A simplified version of the periodic table. The late first-row transition metals covered in this thesis are shaded.

Table 1. Selected properties of Co, Ni, and Cu.[27]

Metal	Crystal structure	Density (g/cm^3)	Melting point (°C)	Resistivity (μΩcm)	E° (M^{2+}/M^0) (V)
Co	hcp, fcc	8.86	1495	6.2	-0.28
Ni	hcp, fcc	8.90	1455	6.9	-0.26
Cu	fcc	8.96	1085	1.7	+0.34

2.2 Applications

2.2.1 Interconnects

Interconnects form the logistical network of microelectronics devices for transferring messages between individual components on the IC.[4,7,8,29–31] Interconnects are made in the second step of IC fabrication also known as the back-end-of-line (BEOL). For a long time, the BEOL was just an afterthought, while most resources went to developing transistors at the front end. Today, it is the Cu interconnects that are considered as the biggest bottleneck to scaling, and the spotlight has shifted from the front end to the BEOL processing.

Figure 3 shows a scanning electron micrograph (SEM) of a cross-section of Intel's 10 nm node technology interconnect structure.[29] A typical interconnect consists of a conducting metal confined by dielectric layers.[7,29–31] A diffusion barrier, typically a Ta-containing layer, between the two materials prevents the metal from migrating into the dielectric and vice versa. The barrier also improves the adhesion of the metal to the surrounding material. Interconnects are multilayered structures with a specific hierarchy. A modern interconnect may consist of over 17 metal layers. The length of the metal wirings in a typical IBM server chip may sum up to a total of 50–80 km.[31] The narrowest lines at the lowest metal levels are local interconnects forming short, device level connections. The wider lines at the intermediate level connect devices within blocks. Global interconnects form links between the blocks, providing power and clock. Early interconnects were wide Al lines, the performance of which was later improved by filling the grain boundaries with small amounts of Cu. Eventually, the AlCu alloy was replaced by Cu that has served as the workhorse of interconnects ever since. Owing to its low resistivity, Cu performs well as a bulk material but suffers from severe RC delay and electromigration at small linewidths (Section 2.3). Co metal is already in use at the lowest levels of Intel's 10 nm node interconnects but other candidates, such as Ru and Rh, are also under active investigation.

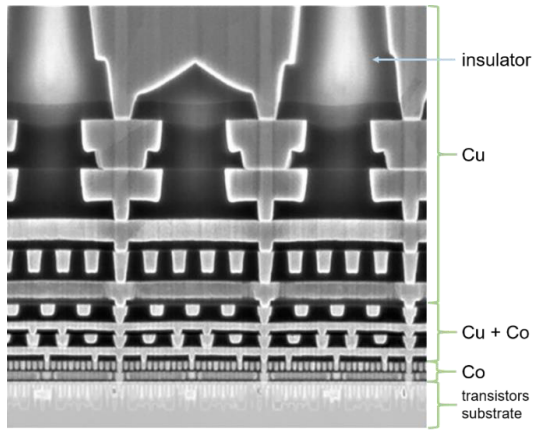

Figure 3. Cross-section of Intel's 10 nm node technology interconnect.[29] Reproduced and modified with permission from ref. 29. Copyright © 2017 IEEE.

Interconnects are fabricated by the dual-damascene process, the schematics of which are presented in Figure 4.[31] The process begins with the deposition of the dielectric material that is then patterned to create vias and trenches. In the next step, the structure is coated with the diffusion barrier. After this, a thin Cu seed layer is deposited to promote the uniform fill of the vias and trenches by Cu electroplating. The process is finished by removing the excess Cu using chemical mechanical polishing and by capping the system with a SiN etch stop layer. The process is then repeated for each of the metallization levels, eventually resulting in the complete interconnect structure.

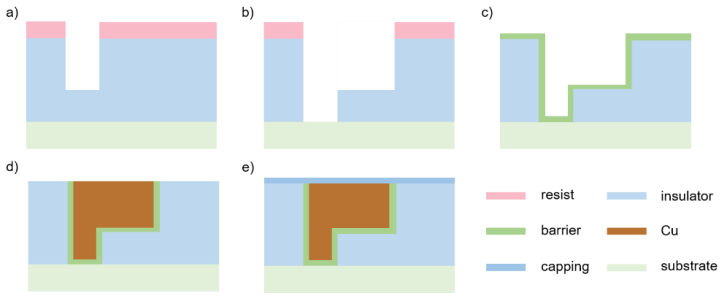

Figure 4. Schematics of the dual damascene process flow: a) and b) deposition and patterning of the insulator, c) deposition of the barrier, d) Cu fill and polishing, and e) deposition of the capping layer.

2.2.2 Contact silicides

All the semiconductor devices on the IC are linked together through a complex network of interconnects. The junction between the semiconductor and the lowest level of the interconnect is called an ohmic contact. To reduce the resistance between the metal line and the semiconductor, silicides with low contact resistance are used.[15,16,32,33] $TiSi_2$ was replaced by $CoSi_2$ as the dominant contact material in complementary metal-oxide-semiconductor (CMOS) technologies at the 130 nm node in the early 2000s. Challenges with $CoSi_2$ scaling have generated interest in NiSi and other Ni-based silicides. Besides its low resistivity, NiSi has advantages that include low resistance at narrow line widths, low Si consumption, and low processing temperatures. On the downside, NiSi suffers from low thermal stability that can, however, be improved by Pt alloying. Table 2 lists some general criteria for the metals used for the contact silicide formation.[15,16]

Table 2. Requirements for contact silicide forming metals.[15,16]

High conductivity	Satisfactory thermal stability
Low contact resistance to n-Si and p-Si	Compatibility with Si device fabrication processes
Low Si consumption	No excessive heat treatments
Good chemical stability in contact with Si	No damaging contamination

The contact silicides between the semiconductor device and the interconnect are prepared through the SALICIDE (self-aligned silicide) process flow illustrated in Figure 5.[15,32] The process is classified as self-aligned, since no additional lithographic patterning is needed. Each silicide has its own tailored process named after the participating metal, that is, the Ti, Co, or Ni SALICIDE process. The procedure begins with the deposition of a metal film. The system is subjected to an initial rapid thermal processing step, allowing the metal layers to react with the exposed Si structures and form metal silicide. The silicide is formed only on the active regions of the device, that is, the source, drain, and gate, leaving the SiO_2 features covered with the original metal film. After the annealing, the remaining metal films are removed by chemical etching. Sometimes, a second annealing step is required to obtain the desired silicide phase. Cobalt, for example, may form CoSi, Co_2Si, and $CoSi_2$ upon reaction with Si, but only the $CoSi_2$ phase is conductive enough to serve as an efficient electrical contact. The SALICIDE processes require careful tailoring to avoid issues such as junction leakage, gate oxide breakdown, and bridging between the silicides caused by Si diffusion.

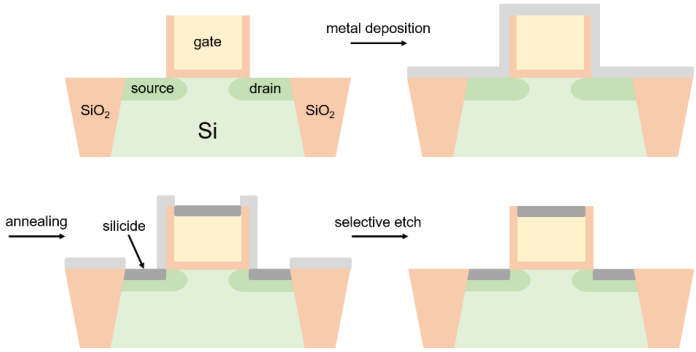

Figure 5. Schematic illustration of the SALICIDE process.

2.2.3 Memory devices

Application spaces like IoE, cloud computing, and social media generate massive amounts of data (Big Data), highlighting the constantly growing importance of efficient memory devices. The majority of conventional memory technologies, such as SRAM (static RAM), DRAM (dynamic RAM), and Flash, store data as charge across a capacitor.[19,34,35] The scaling down of these memories has been successfully continued for decades but is soon facing physical limitations and high manufacturing costs. Device reliability is compromised at small geometries, manifesting as increased problems with leakage current, for example. Instead of fine-tuning existing technologies, the key to furthering miniaturization is finding new types of memories relying on different storage principles. Besides being readily scalable, these memories should exhibit non-volatility, low power consumption and operating voltage, high writing speed and endurance, as well as a simple design.

STT-RAM is one of the most promising candidates for the future universal memory.[19,20,34,35] Figure 6 depicts the schematic structure of a typical STT-RAM cell. As ferromagnetic materials, Co and Ni are considered suitable for magnetic tunnel junctions (MTJ) in STT-RAMs and other magnetic memory devices. The MTJ comprises two ferromagnetic layers, the reference or fixed layer and the storage or free layer, separated by a thin insulator or barrier. Magnetic memories employ the resistance of the MTJ that changes with the direction of magnetization of the free layer. In the STT-RAM, a spin-polarized electron current is passed through the MTJ to switch the magnetic orientation of the free layer with respect to the reference layer. Depending on the polarization of the two layers, the MTJ is changed between the parallel and antiparallel or 0 and 1 states.

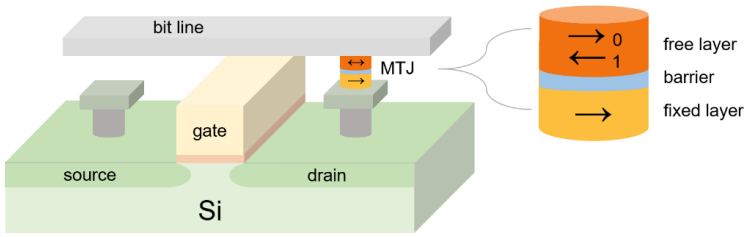

Figure 6. Schematics of an STT-RAM cell.

Table 3 compares the properties of the STT-RAM with the most common memory types, including SRAM, DRAM, NAND flash, and MRAM (magnetic RAM).[19] The STT-RAM essentially combines the advantages of the other memories; it is non-volatile, fast, operates with a low power consumption and suffers no degradation over time. The most critical shortcoming of the STT-RAM is related to the reliability issues of the magnetic switching.[35] Compared to the conventional MRAM, the STT-RAM is considerably smaller in size and thus more scalable and cost competitive.[19,20] Although further tailoring of the cell design is still required, the STT-RAM has potential to become the future leading storage technology and revolutionize the entire microelectronics industry.

Table 3. Comparison of selected existing memory products and the STT-RAM.[19]

	SRAM	**DRAM**	**Flash (NAND)**	**MRAM**	**STT-RAM**
Non-volatile	No	No	Yes	Yes	Yes
Cell size (F^2)	50–120	6–10	5	16–40	6–20
Read time (ns)	1–100	30	50	3–20	2–20
Write / Erase time (ns)	1–100	15	1 ms / 0.1 ms	3–20	2–20
Endurance	10^{16}	10^{16}	10^{5}	$> 10^{15}$	$> 10^{15}$
Write power	Low	Low	Very high	High	Low
Other power consumption	Current leakage	Refresh current	None	None	None
High voltage required	No	3 V	16–20 V	3 V	< 1.5 V

2.3 Challenges and solutions

The performance of microelectronics devices is improved by increasing the number of components on the IC. In practice, this is accomplished by decreasing the feature sizes and increasing the effective surface area using 3D structures. Feature sizes are decreased by using thin films with thicknesses in the nanometer range prepared by a bottom-up (film deposition) or top-down (lithography) approach or a combination of the two. In the case of interconnects, it is important to decrease the line widths of the wirings. The shrinking of dimensions is, however, approaching physical limits beyond which device reliability will be compromised. Interconnects and ohmic contacts cause delayed signals and suffer from electromigration. Improved memories cannot be developed without the adaptation of new storage technology. To overcome these challenges, new materials and designs as well as accurate deposition techniques to make the materials are needed.

2.3.1 RC delay

The RC delay is the delay in signal speed transmitted through the interconnect and is increased by increasing the resistance of conductors and capacitance of the dielectric layers.[6–8] The RC delay is the most significant bottleneck to scaling, hindering the development of high-performance devices. According to researchers at Georgia Institute of Technology, the delay increased by 21.8% from the 22 nm node to 11 nm, and 48% from 11 nm to 7 nm.[8] For decreasing the delay, lowering both the resistance and the capacitance would be ideal, but lowering only the resistance is preferred for its lower cost. The resistance of a wire is defined by its length, cross-sectional area, and resistivity (Figure 7a). The easiest way to lower the resistance would be to make the wires wider, but this would be against scaling down. The other option is to lower the resistivity. Although Cu has a low resistivity in the bulk form, the resistivity of the metal is increased at small linewidths because of electron scattering from interfaces. The effect of electron scattering is more pronounced for materials with long electron mean free paths like Cu, for instance. Therefore, both the resistivity and the electron mean free path should be taken into account when searching for alternative conductors to Cu.

In addition to the interconnects, RC delay is also an issue in the case of ohmic contacts.[6] To ensure the rapid back and forth transmission of a signal from the semiconductor through the contact to the upper levels of the interconnect, the interface resistance should be minimized. The minimal resistance is reached by using low-resistivity $CoSi_2$ and NiSi contacts. For low resistance, the silicide films must be uniform and void-free, which is difficult to achieve with the ever-thinner material layers.

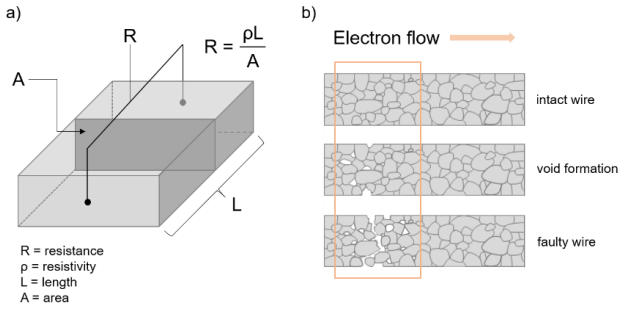

Figure 7. Schematic representation of a) resistance and b) evolution of electromigration in a conducting wire.

2.3.2 Electromigration

Electromigration is a process in which the momentum of a passing electron is transferred to the metal atoms of the metal wire.[5,7] If the current density and temperature in the wire are high enough, the influenced metal atoms may migrate, leading to void formation and ultimately failure of the affected interconnect (Figure 7b). The resistance toward electromigration can be evaluated from the activation energy for grain boundary diffusion or the melting point of the metal. The lower the melting point, the more prone to electromigration the metal is. The poor electromigration resistance of Al was improved by mixing it with 2–4% of Cu. Eventually, Cu replaced Al altogether but is now facing its own limits in terms of reliability at the shrinking geometries.

2.3.3 Alternatives to Cu

Table 4 lists the resistivity, electron mean free path, and activation energy for grain boundary diffusion for selected metals.[7] The activation energy correlates with the melting point of the material. Based on these three properties, IMEC has collected a summary (Figure 8a) of candidates that could potentially outperform Cu as the conductor in the future interconnects.[7,14] Although there are many seemingly good possibilities, the materials must

Table 4. Selected properties of some interconnect materials.[7] The activation energy is for grain boundary diffusion.

Metal	Resistivity (20 °C) (μΩcm)	Electron mean free path (nm)	Activation energy (eV)
Cu	1.7	39	1.4
Al	2.7	15	0.6
Co	6.2	12/7.8	2.1
Mn	144	-	1.8
Ru	7.6	10	3.0
Ta	12	3.8	2.2
Ti	56	0.8	1.4
TiN	22	-	-
W	5.5	14	2.5

also be integrable to the interconnect structure. In other words, the material should be compatible with dry etch patterning or dual-damascene processing. Ideally, no barrier between the metal and the dielectric is needed, meaning that the metal should have good adhesion properties and be resistant toward migration. With interconnect linewidths shrinking, the relative amount of the high-resistivity barrier material gets higher at small cross-sectional areas, increasing the overall resistance of the structure. Finally, the Cu alternative must not exhibit high stress.

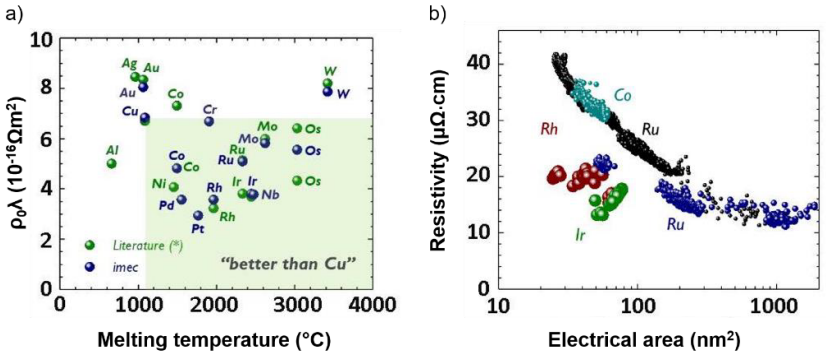

Figure 8. Assessment of Cu alternatives by IMEC: a) first screening based on the product of resistivity and mean free path versus melting temperature and b) comparison of metals tested in actual devices in terms of resistivity and electrical area (the results with Rh, Ir, and Ru marked with blue were treated with postdeposition annealing).[14] Reproduced with permission from ref. 14. Copyright © 2018 IEEE.

From the first screening of Cu alternatives shown in Figure 8a, IMEC selected Ru, Co, Rh, and Ir for testing in actual interconnect structures (Figure 8b).[7,14] Although Rh and Ir showed slightly better performance, Ru and Co are further in the development process and were thus chosen for additional experiments. Neither of the materials needs a barrier layer, since no migration into the dielectric occurs. An adhesion layer is beneficial with both metals but can be limited to a thickness of only a couple of nanometers. Both metals can also be prepared and patterned by conventional techniques, but a more accurate process for the electroplating of Co would be useful for the coating of nanoscale features. Co is already used in trench contacts, wirings (M0 and M1), and caps (M2–M5) in Intel's 10 nm node interconnect stack (Figure 3). By changing from W to Co, the line resistance at the lowest levels was improved by 60%. Furthermore, a fifty-fold improvement was observed in electromigration resistance at the middle levels when adding a Co cap to the Cu lines. Co seems to be a promising material for replacing Cu in interconnects, but time will show which materials take the win beyond the 7 nm node. The outcome is affected not only by the materials themselves but also by the development of the tools and process schemes used at the BEOL.

2.3.4 Deposition techniques

As already mentioned, scaling down requires nanoscale thin films. Films less than 10 nm in thickness are preferred but difficult to prepare in practice. The complex 3D architectures of modern devices bring additional challenges to the fabrication process. The deposition of uniform and conformal films is particularly important in the case of metal seed layers for interconnects. Thin film deposition methods are classified as either physical or chemical. The most common physical vapor deposition (PVD) techniques, especially evaporation but to some extent also sputtering, are line-of-sight methods and thus suitable for coating planar surfaces but not for demanding high aspect ratio structures. In chemical vapor deposition (CVD), film formation is based on volatile precursors reacting or decomposing on a heated substrate. CVD outperforms PVD at nanoscale dimensions but is difficult to control in terms of rate and extent of film growth, making it inadequate a method to meet the needs of future microelectronics.

The only thin film deposition method capable of fulfilling the requirements for thin, conformal films is ALD. ALD is a modification of CVD in which the precursors are delivered into the reaction space separately.[24–26] The ALD method proceeds through saturative, irreversible, and self-limiting surface reactions, providing unparalleled conformality in high aspect ratio trenches. The monolayer per cycle growth allows precise control over film thickness and makes it easier to deposit ultrathin films with good uniformity. Although ALD is the method of choice for furthering miniaturization, finding well-working and integrable processes for the late first-row transition metals has turned out to be rather challenging, as will be elaborated in Chapter 3. Because ALD is based solely on chemistry, finding suitable precursors and reducing agents for the desired material is a requisite for benefiting from the many advantages of the method.

3 Atomic layer deposition of Co, Ni, and Cu

This chapter is an introduction to the fundamentals of ALD. The basic principle of ALD and precursor requirements for metal ALD will be discussed. Sections 3.2 through 3.6 provide an extensive literature review on the ALD of the late first-row transition metals, namely Co, Ni, and Cu. The review covers both thermal and plasma-enhanced processes, the focus being on thermal ALD. In addition to direct metal processes, this chapter also provides information on the indirect approaches to metal ALD. Finally, the effect of the substrate material on metal film growth and properties will be debated.

3.1 Atomic layer deposition

3.1.1 Basic principle

ALD is a gas-phase method for preparing thin films on a solid substrate in a controlled, reproducible manner.[24–26] ALD is based on alternating precursors delivered to a reaction chamber one by one, separated by inert gas purges. Unlike in CVD where the precursors are brought in simultaneously to meet and react already in the gas phase, in ALD all chemical reactions are confined strictly to the deposition surface. ALD proceeds in a cyclic manner, and each cycle comprises four steps. Figure 9 presents a schematic for depositing a monolayer of metal by ALD. In the first step, gaseous metal precursor molecules react with or chemisorb on the reactive sites of a substrate. The reactive site may, for example, be a hydroxyl group. In step two, the excess precursor molecules and byproducts formed upon the reaction are purged away with inert gas, leaving the substrate surface with a saturated layer of chemisorbed precursors. In the third step, a reducing agent is brought in to remove the ligands and reduce the adsorbed metal precursors to elemental metal. As a result, a monolayer of metal atoms is formed. In reality, the film is less than a monolayer because of steric hindrances or a limited number of reactive sites. Finally, in step four, the reaction chamber is purged from excessive reducing agent molecules and byproducts. The cycle is repeated as many times as needed to obtain the desired film thickness.

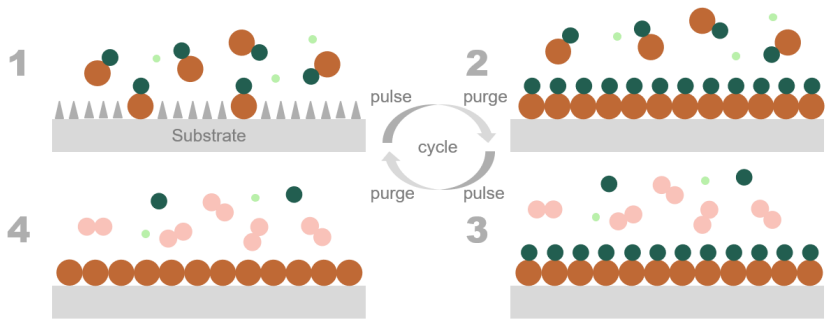

Figure 9. Schematic representation of an ALD cycle for depositing a monolayer of Cu metal.

Not all cyclic processes are ALD even if the precursors are pulsed into the reactor separately. For a process to be truly ALD, each reaction step should be irreversible and saturative. When the film growth is saturative, all the reactive sites on the surface are occupied with precursor molecules, and the precursors do not adsorb on top of each other. Surface saturation ensures self-limiting growth where the amount of deposited material is independent of the precursor dose, assuming that the minimum needed for the saturated layer is exceeded. When the growth is self-limiting, the growth rate becomes constant with increasing precursor pulse time (Figure 10). Deviations from the self-limiting growth regime may occur if the precursors decompose or etch the growing film. The etching reactions may also arise from corrosive byproducts, such as acids.

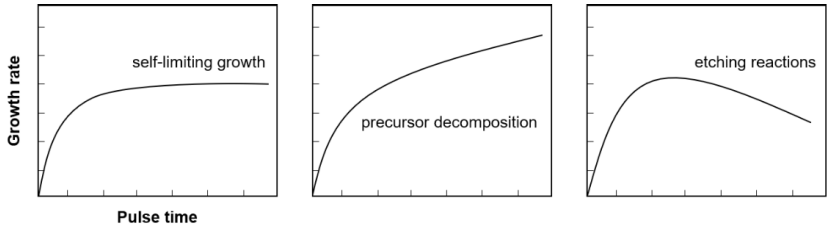

Figure 10. The growth modes of ALD: self-limiting growth and deviations deriving from precursor decomposition and etching reactions.

The self-limiting growth mechanism of ALD is what differentiates this method from the other thin film deposition techniques. Because of saturative surface reactions and self-limiting growth, it is possible to deposit conformal thin films over 3D-structured objects (Figure 11). ALD also enables the deposition of coatings that are uniform in terms of both thickness and composition. By varying the number of deposition cycles, the film thickness can be controlled with sub-nm accuracy. Compared to the other methods, ALD also provides superior reproducibility; both the film thickness and properties can be easily controlled, provided that the deposition is done under saturative conditions. This reproducibility is beneficial when transferring an ALD process from a research tool to a large-scale industrial reactor.

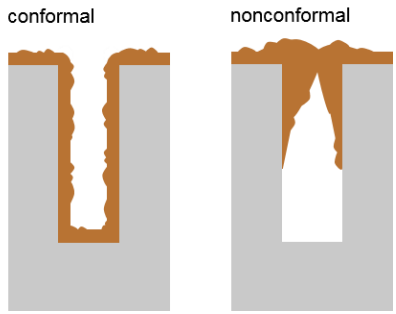

Figure 11. Schematics of a conformal (left) and nonconformal (right) Cu film deposited on a trench substrate.

3.1.2 Precursors for metal ALD

ALD is applicable to the deposition of many materials ranging from metals to metal oxides, nitrides, halides, and chalcogenides. A comprehensive review by Miikkulainen et al. encompasses all the ALD processes reported up to the year 2010.[36] Despite their importance in many applications, the number of processes for the late first-row transition metals has remained low. The main reason for the lack of these processes is the limited selection of suitable precursors and reducing agents. ALD precursors should be volatile, reactive, and thermally stable.[25,37,38] In addition, neither the precursor nor the reaction byproducts are allowed to etch or dissolve into the film or substrate. It is also desirable that the precursors are either gases or liquids, inexpensive, easy to synthesize, and nontoxic. The biggest problems with the ALD of Co, Ni, and Cu are the low reactivity and poor thermal stability of the precursors and the use of the fairly inert reducing agents, H_2 and NH_3. The reactivity issues have typically been circumvented by using high deposition temperatures or plasma-enhancement. Low-temperature reactivity is targeted to minimize film agglomeration and the formation of separate islands (Section 3.1.3). Improving the reactivity of the metal precursor has usually been given top priority, but in the past five years the focus has started to shift toward the reducing agent. Several low-temperature ALD processes have recently been published by combining known metal precursors with unconventional reducing agents.

Metal precursors

As mentioned previously, ALD precursors must be volatile, reactive, and thermally stable.[25,37,38] Figure 12 shows some of the general classes of metal precursors used to deposit Co, Ni, and Cu thin films by ALD. The biggest limitation with most of the metal precursors is the low reactivity; the energy provided by mere thermal activation is often insufficient for complete reduction. Fast and complete reactions between the two precursors is necessary for obtaining pure metal films. The reactivity is a careful balance between nonreactivity in the gas phase and selective reactivity at the surface. To ensure self-limiting growth, it is important that the excess precursor molecules do not adsorb on top of the chemisorbed species. The reactivity is strongly dependent on the co-reactant; some precursors, like metallocenes, react aggressively with water but are often difficult to reduce. Reactions with oxygen sources are relatively easy to predict, whereas surface reduction chemistry is much more complex, making it even more challenging to design highly reactive metal precursors for the ALD of Co, Ni, and Cu.

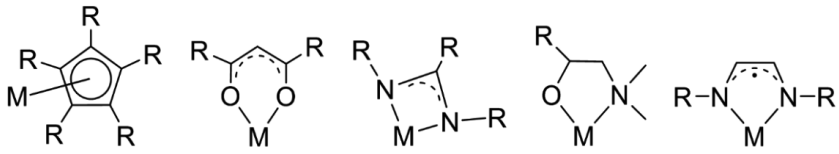

Figure 12. A set of general classes of metal precursors commonly employed in the ALD of Co, Ni, and Cu. From the left: cyclopentadienyl, β-diketonate, amidinate, dimethylamino alkoxide, and diazadienyl.

It is challenging to increase the reactivity of a precursor without compromising, for instance, volatility and thermal stability. For high reactivity, the metal center of the precursor should be open and susceptible for reaction. Steric hindrance lowers the reactivity. Oligomerization should be avoided by using suitable adduct forming ligands. For example, the oligomerization of Cu(btsa) (btsa = bis(trimethylsilyl)amide) has been prevented by adducting the precursor with a carbene ligand.[39] In theory, the reactivity is increased by adding electron donating ligands, such as amino or amido functionalities. M–N linkages are typically more reactive than M–O, M–C, or M–X bonds (X = F, Br, Cl, I). Examples of precursors where the ligand is coordinated through a nitrogen atom include amidinates and diazadienyls.[40,41] The reactivity of the diazadienyls is further improved by the complex radical nature of the ligand. Heteroleptic systems may, in some cases, provide higher reactivity than their homoleptic counterparts.[42] Heteroleptic precursors comprise a metal atom bonded to two or more dissimilar ligands. Because of the different ligands, the use of heteroleptic precursors allows careful tailoring of both the reacting group and of the ligand remaining on the metal center. The thermal stability can also be influenced by the addition of stabilizing ligands, such as cyclopentadienyls. In reality, it is difficult to predict the properties of a heteroleptic precursor; instead of having the targeted properties, the precursor may exhibit the undesired properties of the homoleptic analogues.

Reactivity is often a trade-off with thermal stability. By increasing the reactivity, the precursor may become less stable and decompose in the gas phase or at the surface, destroying the self-limiting growth mechanism. If the precursor decomposes cleanly and CVD growth is of no concern, the limited stability can be exploited to afford metal films with increased growth rates. Many of the ALD processes for Co, Ni, and Cu have been carried out at temperatures above the decomposition temperature of the precursor. Such precursors include, but are not limited to, β-diketonates,[43,44] amidinates,[45] and amino alkoxides.[46,47] In some cases, compromised stability on certain substrates, such as metals, may be used to enhance or even initiate deposition.[48–52] A more detailed discussion on the substrate effects is provided in Sections 3.2–3.4 and Section 3.6.

Based on the standard reduction potentials of the Cu ions, Cu(I) precursors [$E°(Cu^{+}/Cu^{0})$ = +0.52 V] are easier to reduce to elemental Cu than Cu(II) compounds [$E°(Cu^{2+}/Cu^{0})$ = +0.34 V].[27] The Cu(I) precursors are, however, prone to disproportionation in which a compound of an intermediate oxidation state forms two new compounds, one of lower and one of higher oxidation state. Although the Cu(I) precursors often provide higher reactivity, this risk of spontaneous metal growth makes them better suited for CVD than ALD.[53]

Getting the metal film deposited is one thing, but the integration of an ALD process to an actual device is a whole other story. Depending on the targeted application, certain impurities may be detrimental, which should be taken into account when selecting a metal precursor. $Cu(hfac)_2$ (hfac = hexafluoroacetylacetonate), for example, is a widely studied precursor for Cu ALD and exhibits the highest volatility within the Cu(II) β-diketonate family. Although $Cu(hfac)_2$ is a suitable precursor for Cu deposition, a fear of fluorine impurities precludes the precursor from being applied to the preparation of Cu interconnects.[54,55] Fluorine contamination at the bottom of the via leads to poor interface stability and film adhesion which, in turn, cause necking and void formation (Figure 13).[55] The Cu voids at the via bottom result in increased electromigration and, ultimately, malfunctioning of the interconnect.

In addition to fluorine, oxygen is also on the list of unwanted impurities in the fabrication of Cu interconnects.[56,57] Konishi et al. observed that traces of oxygen in Cu induce crack and pore formation at grain boundaries after annealing in H_2 atmosphere.[56] The defects are formed when the oxygen impurities react with H_2 to form water vapor. Oxygen can be incorporated into the film from the metal precursor (β-diketonates, carbonyls, and alkoxides) or from the ALD process if intermediate water pulses or certain reducing agents (alcohols and acids) are used. Therefore, oxygen-free precursors, such as cyclopentadienyls, amidinates, and diazadienyls, are generally favored in metal ALD.

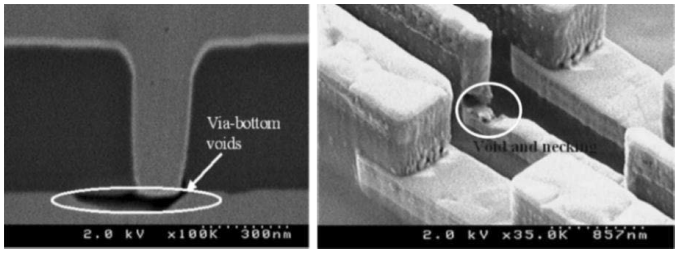

Figure 13. SEM images showing voids and necking in Cu interconnects.[55] Reproduced with permission from ref. 55. Copyright © 2004 The Electrochemical Society.

Reducing agents

Functional and scalable thermal ALD processes are mainly found for noble metals, such as Ru,[58] Pt,[59] and Ir.[60] These metals are typically deposited in oxidizing conditions where molecular oxygen (O_2) is used to combust the ligands of the organometallic precursors. Noble metal oxides are unstable at elevated temperatures even if an oxidizing agent is used in the process.[61] The oxidizing approach is not, however, applicable to the ALD of the late first-row transition metals, as their oxides are stable up to high temperatures. Instead, the ALD of Co, Ni, and Cu requires efficient reducing agents. The most commonly employed reducing agents are H_2 and NH_3, but these can be considered as only moderately reactive, as they typically require deposition temperatures well above 200 °C. The lack of efficient

reducing agents is the main hindrance of the development, not to mention utilization, of Co, Ni, and Cu ALD. In the majority of cases, the low reactivity has been compensated for by using plasma-enhanced ALD (PEALD).[62–64] Instead of using mere thermal activation, PEALD relies on highly reactive species, such as radicals, ions, and electrons, generated from the reactant in a plasma discharge. Owing to this high reactivity, PEALD expands the material selection achievable by ALD. Other advantages of PEALD include lower deposition temperatures, improved film properties due to more complete reactions, and reduced nucleation times. On the downside, PEALD involves complex reaction chemistry and demanding reactor design. Because of the high recombination propensity of the energetic plasma species, PEALD may compromise the film conformality in high aspect ratio structures and is difficult to apply in batch mode. The reactive plasma species may also cause damage to the underlying substrates.

Although the selection of reducing agents for ALD is still quite limited, alternatives to H_2 and NH_3 have been suggested, especially during the past five years. Silanes and boranes have been paired with WF_6 to deposit W thin films.[65–70] Despite being safer to handle and use, the alkyl-substituted variants of these have proven to be quite inefficient in ALD. Borane dimethylamine or $BH_3(NHMe_2)$ has recently gained interest as a suitable reducing agent for the ALD of Cu,[48] Au,[71] and Ag films.[72] The reactant was first introduced for depositing Cr, Fe, Co, and Ni films on Ru,[73] but the process was self-terminating and could be used to deposit films of only 10 nm in thickness. The film growth ceased after the catalyzing Ru substrate was fully covered. Different organic compounds, such as alcohols, aldehydes, and carboxylic acids, have been tested with a variety of metal precursors but seemingly with limited success.[74–80] Formic acid, when combined with $Co(^{tBu2}dad)_2$ (^{tBu2}dad = 1,4-di-tert-butyl-1,4-diaza-1,3-butadiene) on a metal substrate, is one of the few reducing agents allowing the thermal ALD of Co at low temperatures.[49,50] This precursor combination gave some promising results, but the corrosiveness of formic acid makes process integration challenging. The integration problem could be circumvented by changing the reducing agent to tert-butylamine, giving almost identical results as formic acid.[51] The same approach was also applied to the ALD of Ni metal.[52] Other nitrogen-based reducing agents include hydrazine and its alkyl derivatives used, for example, in the ALD of Cu,[81,I] Co,[82] Ag,[83] Ni,[84] and several transition metal nitrides.[85–90,IV]

Out of the metal alkyls explored as reducing agents for ALD, the most promising results have been obtained with diethylzinc (DEZ). The use of Zn metal and trimethylaluminum (TMA) typically results in heavily contaminated films.[91,92] Although no Zn was detected in the Cu films deposited with $Cu(dmap)_2$ (dmap = dimethylamino-2-propoxide) and DEZ at 120 °C,[93] the risk of Zn incorporation precludes any of the ALD processes employing Zn or DEZ as the reducing agent from being employed in microelectronics. Zn atoms may diffuse into the Si structures and generate deep level defects.[94–96] These defects may trap and serve as recombination centers for free electrons and holes, disturbing the electrical properties of Si and ultimately leading to device malfunction. Nevertheless, Zn-based processes could be used for applications where Zn contamination is less critical or as a starting point for analogous processes with more suitable reagents.

Recently, metal hydrides have been in the focal point of developing new ALD chemistry; first, to deposit Al metal at low temperatures[97] and next in the ALD of intermetallic Co_3Sn_2 and Ni_3Sn_2 thin films.[III] A Ge hydride was used for depositing Ni_xGe_y films by ALD.[V] Finally, density functional theory calculations predict that Cu(I) carbene hydrides may serve as both the metal precursor and the reducing agent for Cu ALD.[98] The ALD of electropositive metals such as Ti and Ta is particularly challenging by mere thermal activation. The thermal ALD of Ti has been reported using $TiCl_4$ with 1,4-bis(trimethylsilyl)-1,4-dihydropyrazine or 2-methyl-1,4-bis(trimethylsilyl)-2,5-cyclohexadiene as reducing agents.[99] The former has also been employed in the ALD of metallic Sn films.[100] Both reducing agents resulted in the formation of heavily contaminated films.

3.1.3 Challenges with metal thin films

The greatest challenge in depositing Co, Ni, and Cu metals by ALD is getting the films to grow in the first place. Even if a reactive precursor combination is found and a film is deposited, other challenges may complicate the integration of the process to an actual device. Applicable metal films should be highly conductive but still be limited to sub-10 nm thicknesses. Conductivity in metal thin films is observed only if the film is continuous, that is, a connected network across the substrate or, ideally, a fully closed layer of material. When deposited on a surface, however, metal atoms do not necessarily form monolayers or wet the surface but instead grow as islands. Figure 14 shows the possible growth modes of thin films.[101] The modes are determined by the adsorption energy, surface tension, and mobility of the adsorbates. Metals often follow the Volmer-Weber growth mode, especially if deposited on insulating substrates. Films grow as islands when the cohesive force between the deposited atoms is stronger than the adhesive force to the surface. Continuous films in the Volmer-Weber mode are realized only after the individual islands grow large enough to coalesce. To obtain continuous films that are also thin, the Frank-van der Merwe mode is preferred. The growth mode of a thin film may be manipulated by using adhesion layers, such as Cr, which modify the surface energy of the substrate and thus promote the wetting of the film being deposited.

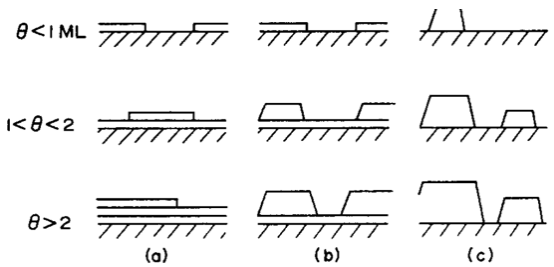

Figure 14. Thin film growth modes: a) layer-by-layer Frank-van der Merwe mode, b) Stranski-Krastanov mode, and c) island-like Volmer-Weber mode.[101] Reproduced with permission from ref. 101. Copyright © 1988 Elsevier.

Regardless of the growth mode, voids may appear in a thin film during the growth, postdeposition treatments, or even after integration into device structures. The atomic movement on a substrate is restricted, resulting in the growth of an unstable or metastable film.[102,103] Because of the non-equilibrated state, the as-deposited films are susceptible to island formation well below the melting point of the material. The exposure of the substrate or dewetting of a continuous film is defined as agglomeration.[102–105] Agglomeration is a thermally activated process driven by the minimization of surface energy or by film stress. The process comprises two steps, void nucleation and void growth, both governed by surface and interfacial diffusion. The void formation often initiates at film edges or defects, such as grain boundary triple points, pinholes, trapped bubbles, and impurities (Figure 15).[104,105] Very thin films with high surface-to-volume ratios are more prone to agglomeration than thicker films. The probability toward agglomeration is higher also for films having weak chemical interactions with the underlying substrate. Agglomeration is minimized by ensuring low process and device operating temperatures as well as careful substrate selection. A thick encapsulation layer reduces grain boundary grooving and thus helps maintain a film intact. According to Hagen et al., island formation is an intrinsic property of Cu ALD and cannot be avoided even at 30 ºC.[106] Because of the low growth rates in metal ALD, the growing metal islands have time to diffuse and form larger islands instead of creating a thin, continuous film. For the deposition of conductive metal films in the sub-5 nm thickness range, processes with high growth rates should be developed.

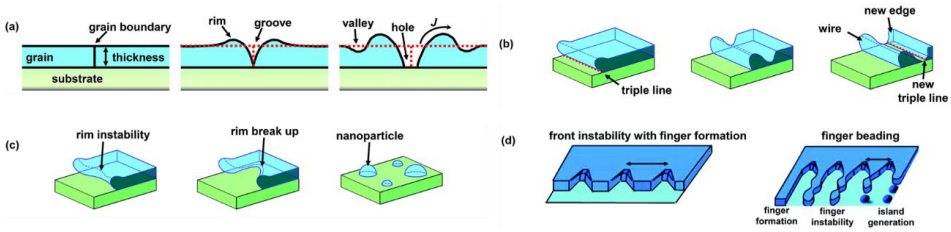

Figure 15. Mechanisms of agglomeration in metal thin films: a) grain boundary grooving and voiding, b) edge retraction and wire formation, c) rim instability and break up into nanoparticles, and d) finger formation and beading into islands.[104,105] a–c) Reproduced with permission from ref. 104. Copyright © 2016 The Royal Society of Chemistry. d) Reproduced with permission from ref. 105. Copyright © 2016 Elsevier.

The most desired property of a metal film is low resistivity. The resistivity of a thin film is generally many times higher than the bulk value, which is the case especially at thicknesses below 10 nm when the film is barely if at all continuous. The first requisite for conductivity is that the film forms a continuous network or a closed layer of material on the substrate. The better the film coverage, the lower the resistivity. If the material is prone to agglomeration, good coverage at small thicknesses is obtained by using low deposition temperatures.[102,103] In some cases, the situation is reversed, and the nucleation density is higher at higher temperatures. Grain size, impurities, morphological defects, surface scattering, and grain boundary scattering are all factors that increase resistivity.[107] For optimal resistivity, thin films should be pure, uniform, and smooth. Impurities are eliminated by careful precursor selection and protection against postdeposition oxidation.

Roughening is dictated by temperature through various diffusion-related processes. High roughness causes electron scattering, leading to increased resistivity. Film roughness can be minimized by using low deposition temperatures and ALD processes with high growth rates.[108] Slow processes allow more time for diffusion, ultimately resulting in increased agglomeration and film roughness.

Sections 3.2 through 3.4 give a literature review on the ALD of the late first-row transition metals. None of the processes can be considered universal but instead require compromises. High growth rate, for instance, is often a trade-off with low deposition temperature. High purity and low resistivity, on the other hand, typically require plasma-enhancement that compromises film conformality. By putting more effort into finding reactive precursor combinations, especially efficient reducing agents, universal processes enabling the facile integration of Co, Ni, and Cu may someday become reality.

3.2 Cobalt

Ever since cobalt was first considered as part of the interconnect stack, there has been a growing interest toward Co ALD. The different aspects of Co ALD were recently reviewed by Kaloyeros et al.[109] The selection of ALD processes for Co is limited, with most of the existing processes relying on plasma-enhancement. The main advantage of using plasma is the lowering of the deposition temperature, making it easier to deposit very thin and continuous films. Unfortunately, many of the PEALD processes for Co have been studied at temperatures above 300 °C. Plasma-enhancement often provides higher growth rates compared to mere thermal activation. A major problem with many of the PEALD Co processes is the inclusion of carbon impurities. Out of the Co PEALD processes, the lowest resistivity films were obtained with a combination of $Co(Cp)_2$ (Cp = cyclopentadienyl) and NH_3 plasma.[110–113]

The conformality provided by PEALD might be sufficient for the preparation of Co caps and even liners, but for the uniform fill of nanoscale interconnect structures, thermal ALD is needed. Despite numerous efforts, the number of thermal processes for Co has remained low. The thermal ALD of Co is challenging because of the negative reduction potential of the Co(II) ion ($E° = -0.28$ V).[27] The reduction of the Co(II) precursors to Co metal requires efficient reducing agents that are, in turn, difficult to find. The major drawbacks of the reported thermal processes are high deposition temperature, low growth rate, and substrate dependent growth. Table 5 lists all the different Co ALD processes reported in the literature. A more in-depth discussion on the most promising thermal processes is provided below. Figure 16 shows the schematic structures of the metal precursors used in the ALD of Co.

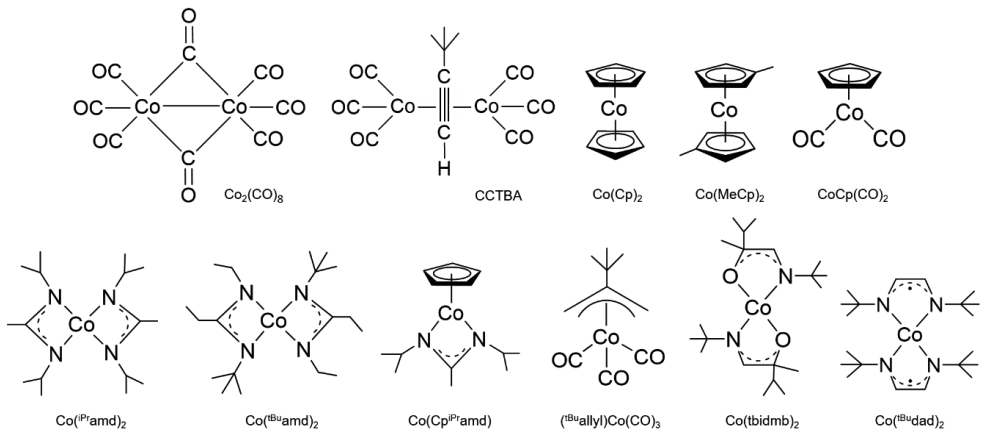

Figure 16. Co precursors and their abbreviations used to deposit Co metal by direct ALD.

Table 5. ALD processes for Co. PEALD processes and one hot wire process are highlighted with gray. '*' after a reactant stands for plasma species.

Precursors	Substrates	T_{range}; T_{ALD} (°C)	Growth rate (Å/cycle)	Resistivity (μΩcm)	Ref.
$Co_2(CO)_8 + H_2*/N_2*$	Si	50–250; 75–110	1.2	-	114,115
CCTBA + H_2*	TaN_x, MnAl	100–250; 150	0.8	90 (20 nm)	116,117
$Co(Cp)_2 + NH_3$*	Si, SiO_2	300	0.94, 0.48	10	110–113
$Co(Cp)_2 + NH_3*/SiH_4$*	Si, SiO_2	300	0.94	-	118
$Co(Cp)_2 + H_2*/N_2$*	Si, SiO_2, Ru, Ta	150–450; 300	0.42	20–35	119,120
$Co(Cp)_2 + NH_3$ (hot wire)	-	100–350; 300	0.38	-	121
$Co(MeCp)_2 + NH_3$*	Si, SiO_2	100–350; 300	0.50	31 (350 °C)	122
$CoCp(CO)_2 + H_2*/N_2$*	Si	50–220; 125–175	1.1	-	115,123,124
$CoCp(CO)_2 + NH_3$*	Si, SiO_2	300	1.6	20	33,110,125
$Co(^{iPr}amd)_2 + H_2$	Si, glass, C, WN	260–350; 300/350	0.04/0.12, 0.43	200	40,45,125,126
$Co(^{iPr}amd)_2 + NH_3$	Si, SiO_2	350	0.26	50	125–128
$Co(^{iPr}amd)_2 + NH_3$*	Si, SiO_2	350	0.33	50	127
$Co(Cp^{iPr}amd) + NH_3$*	Si, SiO_2	100–300; 200–250	0.5	140	129
$Co(^{tBu}amd)_2 + H_2$	Cu, SiO_2, CDO	215–290; 265	0.053 (Cu)	-	130,131
$Co(tbidmb)_2 + BH_3(NHMe_2)$	Ru	180	0.07	-	73
$(^{tBu}allyl)Co(CO)_3 + Me_2NNH_2$	Si	140	0.5	6 (40 nm)	82
$Co(^{tBu2}dad)_2$ + HCOOH	Ru, Pt, Cu	140–220; 180	0.95	13–19	49,50
$Co(^{tBu2}dad)_2$ + $tBuNH_2/Et_2NH$	Ru, Pt, Cu	140–220; 180	0.98	14 (50 nm)	51

3.2.1 $Co(^{iPr}amd)_2$

In the amide-type precursors, the ligands are bonded to the metal center through nitrogen atoms making them more reactive than their M–Cl and M–O counterparts and thus better suited for ALD.[40] As there are no M–C bonds, the amide derivatives afford thin films with low carbon contamination. Finally, the system is free from corrosive byproducts unlike with

the metal halide precursors. Alkylsilylamides have been widely studied for CVD and ALD, but they generally exhibit poor thermal stability and lead to silicon impurities in the films. Dialkylamides, on the other hand, are volatile only for metals with high oxidation states of 4 and above. To benefit from the properties of the amide-type precursors also in the ALD of low valent metals, a set of N,N'-dialkyl-2-alkyl-amidinates were designed.[40] Owing to the bidentate chelating ligand, the compounds have good thermal stability. Furthermore, the volatility of the compounds can be tuned by substitution of the alkyl groups; bulky R and R' inhibit oligomerization, thus increasing the volatility. Volatile, thermally stable compounds were synthesized for metals with oxidation states of +1 (Cu, Ag), +2 (Mn, Fe, Co, Ni), and +3 (Ti, V, La). The precursors have been used in the ALD of both pure metals and metal oxides.[45]

Co(^{iPr}amd)$_2$ (^{iPr}amd = N,N'-diisopropylacetamidinate) was combined with H_2 to deposit Co metal films by ALD within a temperature range of 260–350 °C.[40,45,125,126] No deposition was observed below 260 °C or without H_2 at any of the studied temperatures. A very low growth rate of only 0.04 Å/cycle was measured at 300 °C. By increasing the temperature to 350 °C, the growth rate was increased to 0.12 Å/cycle. A 40 nm thick film exhibited a resistivity of 46 μΩcm, that is, approximately eight times the bulk resistivity of Co. It was also claimed that a 0.8 nm Co film on glass was conductive, but considering the high deposition temperature inevitably causing agglomeration, the film is unlikely to cover the substrate fully but rather forms a continuous Co network across the substrate.

Lee et al. developed an alternative process with Co(^{iPr}amd)$_2$ using NH_3 as the reducing agent at a temperature of 350 °C.[125–128] Co films were also deposited with H_2 under similar conditions to allow comparison of the processes. The growth rate was higher when H_2 was used as the reducing agent (0.43 vs. 0.26 Å/cycle). Interestingly, the growth rate with H_2 was also much higher than reported by Lim et al.[45] Despite the lower growth rate, the films deposited with NH_3 were denser and contained less oxygen after the deposition as observed by X-ray photoelectron spectroscopy (XPS). The films were also of better quality in terms of resistivity; a film deposited with NH_3 exhibited a resistivity of 50 μΩcm, whereas with H_2 the resistivity was 200 μΩcm (thicknesses not reported). Both processes could be used to deposit conformal Co metal films in high aspect ratio structures.

Co(^{iPr}amd)$_2$ shows good thermal properties for ALD, but the precursor should be studied with reactants with more reducing power than H_2 or NH_3. By doing so, higher growth rates at lower temperatures might be reached. The high deposition temperatures of 300–350 °C are the biggest issue with the Co(^{iPr}amd)$_2$ processes, as they lead to agglomeration, thus making the deposition of thin yet continuous films challenging. Furthermore, a separate study showed that a set of slightly modified Co amidinates decompose already below 200 °C,[132] questioning whether the studied thermal amidinate processes are truly self-limiting at all. Elko-Hansen and Ekerdt showed that by switching from Co(^{iPr}amd)$_2$ to bis(N-tert-butyl-N'-ethylpropionamidinato) [Co(^{tBu}amd)$_2$], Co was deposited on Cu surfaces at a temperature of 215 °C.[130,131] Due to partial dissociation of the Co precursor, nucleation was favored on Cu over the SiO_2 and carbon-doped oxide (CDO) substrates. Despite the

dissociation, the reactions on Cu were self-limiting. Out of the dielectric substrates, SiO_2 was preferred for its higher concentration of hydroxyl moieties on the surface. During the H_2 pulse, the ligand fragments are desorbed, and the reduction process is completed. According to Lim et al., the hydrogenation of the surface is required also to cleave the M–L bond and thus enable the chemisorption of the amidinates; in situ studies showed no reaction on clean metal surfaces.[45]

3.2.2 $Co(tbidmb)_2$

Kalutarage et al. designed a set of α-imino alkoxides for all the mid to late first-row transition metals.[73] The complexes were volatile, thermally stable, and susceptible toward reducing agents; thus, ideal for metal ALD. The α-imino alkoxides resemble the β-amino alkoxides that have been employed, for example, to deposit high-purity Cu at temperatures as low as 80 °C.[I] Similar complexes exist also for Ni but not for the other first-row transition metals; the ligands are incapable of saturating the coordination spheres of the larger Co(II), Fe(II), Mn(II), and Cr(II) ions. Although the α-imino alkoxides have not yet been extensively studied in ALD, they are the closest alternative to the well-behaved Cu and Ni β-amino alkoxides.

To study the ALD of Co, bis(1-(tert-butylimino)-2,3-dimethylbutan-2-olate)cobalt(II) [$Co(tbidmb)_2$] was combined with $BH_3(NHMe_2)$.[73] Since Co, Fe, Mn, and Cr, subsequent studies with $BH_3(NHMe_2)$ have been published for the ALD of Cu,[48] Au,[71] and Ag.[72] To avoid the decomposition of the Co precursor at 234 °C, a much lower temperature of 180 °C was chosen for the deposition studies. The tests were carried out on various substrates, but Co film was deposited only on Ru metal. Furthermore, to initiate film growth, a separate nucleation step comprising 50 cycles of 20 s Co precursor pulses was needed. During this step, the Co precursor most likely slowly decomposes and forms the initial Co nuclei on the Ru surface. After the nucleation process, film growth proceeded with a low rate of 0.07 Å/cycle until a thickness of 7 nm was reached, and the growth ceased. Similar self-termination was observed also for Fe, Mn, and Cr, and it was ascribed to the Ru substrate getting fully covered. Ru was hypothesized to activate $BH_3(NHMe_2)$ and thus enable the film growth but only until the substrate was still exposed. Mäkelä et al. showed, however, that the activation could also be done remotely with the activated species being transported through the gas phase.[72] By placing Ru pieces in the source tube of $BH_3(NHMe_2)$, Ag films were deposited even on dielectric substrates.

With the substrate sensitivity, nucleation step, and self-terminating growth, the Co process can hardly be referred to as conventional ALD. However, if $Co(tbidmb)_2$ was combined with another reducing agent, a more general ALD process might be developed. The process also provides valuable insight into the use of $BH_3(NHMe_2)$ in ALD; insight that helped develop, for example, the ALD of Cu,[48] Au,[71] and Ag.[72]

3.2.3 (^{tBu}allyl)Co(CO)$_3$

Thermal ALD of Co metal has also been claimed using tert-butylallylcobalttricarbonyl [(^{tBu}allyl)Co(CO)$_3$] and dimethylhydrazine, though no ALD characteristics, such as a self-limiting growth mechanism, were shown.[82] At 140 °C, a chemical reaction occurred only between the Co precursor and a hydrogen-terminated Si surface. There was no chemical reaction between (^{tBu}allyl)Co(CO)$_3$ and a SiO_2 substrate. Generally, hydroxyl groups have been thought to promote the nucleation of ALD materials. In the case of metals, however, nucleation often requires a metal substrate. The reactions on metals usually arise from partial decomposition of the metal precursor on the substrate or generation of more reactive reducing species by the substrate rather than selective precursor adsorption.

Based on computational studies, the selectivity of the (^{tBu}allyl)Co(CO)$_3$ system was attributed to differences in the hydrogen donor capability of the Si–H and SiO_2 substrates. The Si–H species act as neutral hydrogen or hydride donors, whereas the hydroxyl groups donate bare protons. Surface hydrogen is needed for the formation of the Si–Co linkage through a reaction intermediate where the hydrogen is first transferred back and forth between the allyl ligand and the metal center, eventually producing R$_3$Si–Co(allylH)(CO)$_3$ surface species. The reaction between the Co precursor and Si–H is exothermic by 0.58 eV; thus, the reaction is thermodynamically favorable, albeit with a high barrier for activation. Due to the lack of hydrogen, the reaction on SiO_2 follows a different pathway that is endothermic by 0.65 eV, thus being thermodynamically less favorable. The reaction pathways and enthalpies are shown in Figure 17.[82]

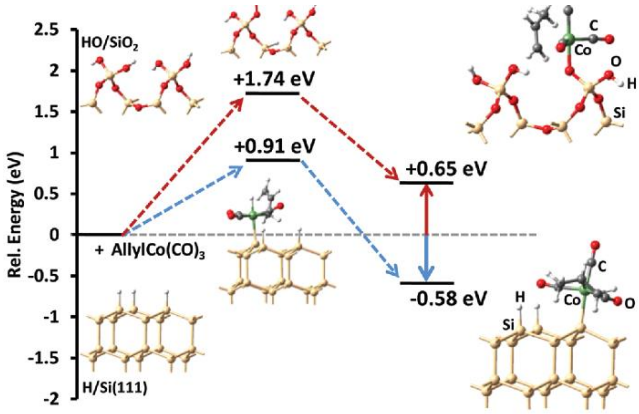

Figure 17. Reaction mechanisms and enthalpies for the adsorption of (^{tBu}allyl)Co(CO)$_3$ on SiO_2 and Si–H.[82] Reproduced with permission from ref. 82. Copyright © 2012 American Chemical Society.

As stated above, the characterization of the process in terms of growth and film properties was minimal, and the article focused mainly on the selective adsorption of (^{tBu}allyl)Co(CO)$_3$. It was demonstrated, however, that after a short nucleation delay within the first ten ALD cycles, the growth rate of Co on Si–H was 0.5 Å/cycle. XPS showed that

the films were, indeed, Co metal. The resistivity of a 40 nm thick film was said to be below the detection limit of the four-point probe, corresponding to the bulk Co resistivity (6.2 μΩcm). Despite the somewhat inconclusive ALD characteristics of the process, (^{tBu}allyl)Co(CO)$_3$ is an interesting example of a precursor with tailored surface selectivity. By applying the same approach to other metals, ALD processes with inherent area-selectivity could be developed.

3.2.4 Co(^{tBu2}dad)$_2$

Metal diazadienyl complexes were introduced as precursor candidates for ALD in 2011,[41] and they have been explored in several ALD processes ever since. Analogous complexes were designed for Cr, Mn, Fe, Co, and Ni, but only the latter two have been used in ALD so far. All the complexes are highly volatile and sublime at low temperatures between 85 and 120 °C. The precursors exhibit high thermal stability, and the stability increases toward the metal ion with the most negative reduction potential. Owing to the reactive M–N bonds, the precursors are also expected to show high reactivity. Finally, the precursors form metals upon decomposition, which is one of the key factors in the Co and Ni metal ALD processes as will be described below.

Out of the metal diazadienyl complexes, Co(^{tBu2}dad)$_2$ has been of the utmost interest because of the urgent need for new Co ALD processes in the microelectronics industry. Co(^{tBu2}dad)$_2$ was first combined with formic acid to deposit Co metal at low temperatures of 140–220 °C.[49] A saturative growth rate of 0.95 Å/cycle was measured at 180 °C. The Co content was 92 at.%. The most interesting feature of the process is that the films grew only on metal substrates. Although the selective growth on metals narrows down the applicability of the process to some extent, the area-selectivity can be leveraged to deposit Co caps and liners on Cu conductors directly without additional patterning steps.

The substrate selectivity of the Co(^{tBu2}dad)$_2$ + formic acid process was scrutinized in a separate study.[50] Film growth was observed only on metal substrates including Ru, Pt, and Cu. No metal deposition occurred on SiO_2, Si(100), Si–H, or CDO. Growth on SiO_2 gave a 35 nm thick film of Co(II) formate. The selective growth on metals was attributed to the catalytic decomposition of formic acid to H_2 and other reducing species by the metal surfaces. No decomposition occurs on insulating substrates. It was also proposed that Co(^{tBu2}dad)$_2$ might not adsorb on insulators, but this is not possible as the precursor affords Co_3O_4 by ALD on Si(100) and soda lime glass when combined with ozone.[133]

When depositing Co on Pt and Cu using Co(^{tBu2}dad)$_2$ and formic acid, the film thickness increased linearly throughout the process, and the growth rate was 0.98 Å/cycle at 180 °C.[50] In contrast, on Ru there was a nucleation delay, and no film growth was observed during the first 50 cycles. After the delay, the film growth proceeded rapidly with a rate of 1.6 Å/cycle between 100 and 150 cycles. The growth rate of 0.95 Å/cycle ensued only after 250 cycles. The nucleation delay on Ru was explained by the oxidation of the substrate

surface. Interestingly, surface oxidation had no effect on nucleation on Pt or Cu due to interfacial mixing of the substrate and the growing film.

Formic acid is mildly corrosive and may cause damage to the substrates as well as the metal parts of the ALD reactor. To overcome this issue, Kerrigan et al. developed a Co ALD process by combining $Co(^{tBu2}dad)_2$ with tert-butylamine.[51] Diethylamine was confirmed to behave similarly to tert-butylamine, but no deposition was obtained with triethylamine. Similar to formic acid, the use of tert-butylamine resulted in high purity Co films (98.0 at.%) at low temperatures ranging from 140 to 220 °C. At 180 °C, a saturative growth rate of 0.98 Å/cycle was observed. Again, the films were grown only on metals, and no deposition occurred on SiO_2, Si–H, or CDO. It was hypothesized that the alkylamines most likely form an adduct with $Co(^{tBu2}dad)_2$, leading to changes in the geometry and the d orbital energies of the Co precursor. The changes in the orbital energies cause electron transfer from the radical-like diazadienyl ligands to the Co(II) ion, resulting in the formation of Co metal.

Since the two processes employing different reducing agents afforded similar growth rates (0.95 and 0.98 Å/cycle) and growth only on metal substrates, it is likely that the role of the reducing agents is quite small. $Co(^{tBu2}dad)_2$ was found to produce 13–15 nm Co metal films on Ru even without an accompanying reducing agent. Clearly, the Co precursor undergoes decomposition on metals at temperatures below the reported solid-state decomposition temperature (235 °C). At 180 °C, the decomposition rate is relatively low, and only a fraction of the precursor molecules decomposes. It is possible that the decomposition of the remaining molecules is imperfect and completed only upon the addition of a suitable reducing agent. Thus, rather than reducing a Co(II) precursor all the way to Co(0), the reducing agent might have more of a purifying role in the process. In any case, the competitive edge of $Co(^{tBu2}dad)_2$ is the fact that it forms pure Co metal upon decomposition. The controlled decomposition of precursors to metals not only facilitates nucleation but also enhances film growth at later stages of the deposition. The appropriate decomposition of a metal precursor can be an asset that should be explored more when designing new precursors for ALD.

3.3 Nickel

Out of the late first-row transition metals, Ni has received the least attention in ALD. Although Ni is an essential material for microelectronics, especially NiSi contacts but also magnetic devices, there has been significantly stronger market pull for Cu and Co ALD because of their criticality in interconnects. As with the other metals, most Ni ALD processes (Table 6) require activation by energetic plasma species, high deposition temperatures, or sometimes both to afford the metal deposition. With Ni, the selection of reducing agents is even narrower than with Cu and Co, and most processes employ H_2, NH_3, or their plasma variants as the reducing agent. The only low temperature thermal processes for Ni require a catalytic metal substrate to initiate the film growth.[52,73] $Ni(dmap)_2$ and

$NiCl_2$(tmpda) (tmpda = N,N,N',N',-tetramethyl-1,3-propanediamine) can also be used at low temperatures, but the films were nitrides with varying stoichiometry rather than pure Ni metal.[89,IV]

On the grounds of their standard reduction potentials, Ni(II) should be slightly easier to reduce to metal than Co(II) ($E° = -0.26$ versus -0.28 V).[27] However, the deposition of pure metal films has proven to be even more of a challenge for Ni than for Co. The so-called Ni ALD films often exhibit high carbon or nitrogen contents often seen as separate Ni_3C and Ni_3N phases in X-ray diffraction (XRD) and XPS. Because of the high impurity levels, the resistivity values of the Ni films have generally been much higher than the bulk resistivity. The best-quality films in terms of purity and resistivity have been obtained with $Ni(acac)_2$(tmeda) + hydrazine (acac = acetylacetonate, tmeda = N,N,N',N'-tetramethyl-ethylenediamine),[84] Ni(^{tBu2}dad)$_2$ + tert-butylamine,[52] Ni(dmamb)$_2$ + NH_3 (dmamb = dimethyl-amino-2-methyl-2-butoxide),[46,47] and $Ni(acac)_2$ + methanol[79]. There are many processes for the ALD of NiO that can be readily reduced to Ni metal by postdeposition reduction.[134,135] Therefore, many of the ALD processes for Ni rely on the indirect approach. The purity of the Ni_3C and Ni_3N films has also been improved by postdeposition reduction or rapid thermal annealing.[136,137] The literature on the indirect approaches to metals will be reviewed in Section 3.4.

All the ALD processes for Ni are listed in Table 6. Figure 18 illustrates the schematic structures of the studied Ni precursors. A more thorough discussion on the thermal Ni ALD processes is given below. The processes employing Ni(^{iPr}amd)$_2$[45] and Ni(tbidmb)$_2$[73] as precursors are excluded from the discussion because of their similarity with the analogous Co processes (Sections 3.2.1 and 3.2.2). The results concerning the $NiCl_2$(tmpda) + tert-butylhydrazine (TBH) process will be covered in Section 5.2.1.

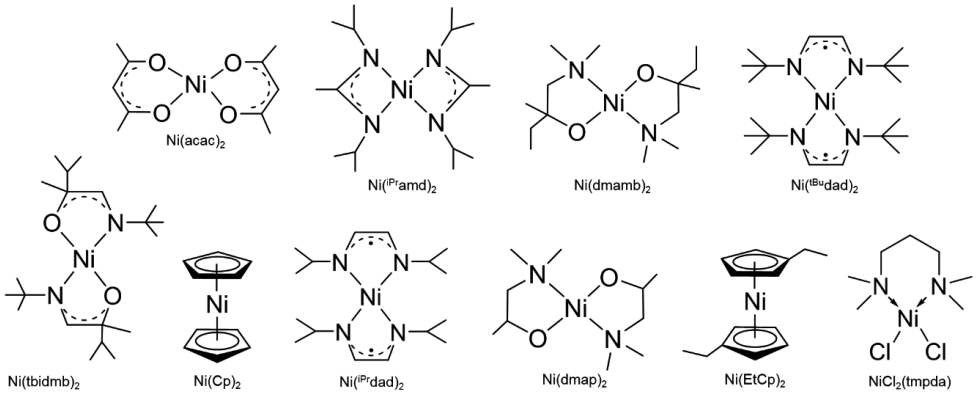

Figure 18. Schematic structures and abbreviations for Ni precursors used in the ALD of Ni and NiN_x.

Table 6. ALD processes for Ni metal or NiN_x. PEALD processes and one hot wire process are highlighted with gray. '*' after a reactant stands for plasma species.

Precursors	Substrate	T_{range}; T_{ALD} (°C)	Growth rate (Å/cycle)	Resistivity (μΩcm)	Ref.
$Ni(acac)_2 + H_2$	Ti, Al, Si	250	-	-	134
$Ni(acac)_2$ + MeOH	SiO_2	250–300	0.07	27 (10–60 nm)	79
$Ni(acac)_2(tmeda) + N_2H_4$	Si, SiO_2	220–300; 240–280	2.1	18 (105 nm)	84
$Ni(acac)_2(py)_2 + N_2H_4$	Si, SiO_2	200–300; 225–250	0.8	26–31	84
$Ni(^{iPr}amd)_2 + H_2$	Si, glass, C, WN	250	0.04	-	45
$Ni(dmamb)_2 + H_2$	Si	175–300; 200–250	1.25	-	138
$Ni(dmamb)_2 + H_2$ & C_2H_5I	Si	225	1.48	20 (24 nm)	139
$Ni(dmamb)_2 + NH_3$	SiO_2, Si–H, C	300	0.64	25	46,47
$Ni(dmamb)_2 + NH_3$*	SiO_2, Si–H, C	150–300; 250	2.0	43	47,140
$Ni(dmamb)_2 + NH_3$*/SiH_4*	Si, SiO_2	300	-	-	118
$Ni(dmamb)_2 + H_2$*	SiO_2, Si–H	150–300; 250	0.8	75	140
$Ni(dmap)_2 + N_2H_4$	Ru	100–200; 140–180	0.25	-	89
$Ni(dmap)_2$ + HCOOH/N_2H_4	Ru	100–200;120–180	0.35	-	89
$Ni(hfip)_2 + H_2$*	Si–H	175–300; 200–250	1.25	5–18 Ω/□	141,142
$Ni(tbidmb)_2 + BH_3(NHMe_2)$	Ru	180	0.09	-	73
$Ni(^{tBu2}dad)_2 + Me_2NNH_2$	SiO_2	200–250; 225–240	0.70	-	88
$Ni(^{tBu2}dad)_2 + tBuNH_2$	Pt, Ru, Cu	160–220; 180–195	0.60	22 (60 nm)	52
$Ni(^{iPr2}dad)_2 + NH_3$*	Si–H	150–300; 250/150	2.2/2.0	33/146	137,143
$Ni(Cp)_2 + NH_3$*	SiO_2, Al_2O_3, ZnO	160–320; 260–280	0.2	71	127,135, 136
$Ni(Cp)_2 + NH_3$ (hot wire)	SiO_2, Si–H	175–350; 250	0.63	28 (25 nm)	146,147
$Ni(EtCp)_2 + H_2$*/N_2*	sapphire	200–360; 320>	0.3	200 (20 nm)	148
$NiCl_2(tmpda)$ + TBH	Al_2O_3, Si, TiN, Cu, Au, Ru	190–250; 220/250	0.08/1.13	9.8 (35 nm)	IV

3.3.1 $Ni(acac)_2$

The first direct ALD process for Ni metal was published in 2000 using $Ni(acac)_2$ and H_2 as precursors.[134] Although no self-limiting growth was shown, the process had an important role in paving the way for the work on Ni ALD that followed. The Ni films were deposited at 250 °C, but the growth rate was not provided. The Ni deposition was preferred on metal substrates (Al and Ti). No film growth was observed on glass at 250 °C. Film growth on Si, on the other hand, was impeded by the interdiffusion of the Ni atoms into the substrate as well as silicide formation. Above the decomposition temperature of $Ni(acac)_2$ (280 °C), CVD-type growth was obtained on all substrates even without the reducing agent. The selective growth on Al and Ti at 250 °C was ascribed to the electron transfer from the metal substrate to the adsorbed $Ni(acac)_2$ molecule, promoting the reduction of the precursor. The metal substrate may also activate H_2, further catalyzing the reaction. As was already seen with many of the Co processes, the role of the substrate is significant when depositing metals and should always be considered when designing and studying a new ALD process.

$Ni(acac)_2$ has also been combined with primary alcohols to deposit Ni and Ni_3C by ALD.[79] Upon adsorption, the Ni precursor loses one acac ligand, and the remaining Ni(acac) surface species is reduced by a dehydrogenation reaction of the alcohol. At 250–300 °C, reasonably

pure Ni metal films (95 at.%) were deposited with methanol, while ethanol and propanol afforded carbon–Ni_3C composite films with 70–80 at.% carbon incorporation. The films were deposited on 50 nm SiO_2 to prevent silicide formation. The growth rate increased with increasing alkyl chain length of the alcohol. The longer the alkyl chain, the more carbon was incorporated into the film, consequently leading to a greater film mass and higher growth rate. Because of its higher propensity of donating a hydrogen atom, propanol afforded the highest growth rate, though the carbon content of the film was the same whether ethanol or propanol was used. The Ni metal process with methanol as the reducing agent showed a saturative growth rate of 0.07 Å/cycle. The low growth rate may be explained by the low reactivity of $Ni(acac)_2$ combined with the use of an insulating substrate. Similar growth rates were measured for the $Ni(^{iPr}amd)_2$ + H_2 and the $NiCl_2$(tmpda) + TBH processes,[45,IV] also studied on insulators.

Owing to the high purity of the Ni metal films, a fairly low resistivity of 27 μΩcm was measured for 15–60 nm films.[79] This is one of the lowest resistivity values ever obtained for Ni metal by ALD, though the bulk value is as low as 6.9 μΩcm.[27] The films also exhibited ferromagnetic behavior; a coercivity of 18 Oe was measured for a 60 nm film. The crystal structure of the films was dependent on the deposition temperature; below 300 °C, the films exhibited a metastable hexagonal phase, and above 300 °C the films crystallized in the fcc lattice.

Zhang et al. increased the volatility and reactivity of $Ni(acac)_2$ by adducting either with a tmeda ligand or two pyridine (py) ligands.[84] Both processes employed hydrazine as the reducing agent and were studied at temperatures below 300 °C. The growth rates were 2.1 Å/cycle with $Ni(acac)_2$(tmeda) at 240–280 °C and 0.8 Å/cycle with $Ni(acac)_2(py)_2$ at 225–250 °C. According to XPS, a 105 nm thick film deposited with $Ni(acac)_2$(tmeda) had a Ni content of 95.1 at.% and, consequently, a low resistivity of 18 μΩcm. This is the lowest resistivity ever reported for ALD Ni films. Low resistivities of 26–31 μΩcm were also measured for the films grown with $Ni(acac)_2(py)_2$.

3.3.2 Ni(II) amino alkoxides

$Ni(dmamb)_2$ has been the most studied Ni precursor in the ALD of Ni metal, and it has been combined with either H_2 and NH_3 in both thermal and plasma ALD.[46,47,138,140] The thermal process with H_2 was studied between temperatures of 175 and 300 °C.[138] A saturative growth rate of 1.25 Å/cycle was measured at 200–250 °C. Above 250 °C, the growth rate increased rapidly likely due to precursor decomposition. Saturation was not determined as a function of precursor pulse time but incorrectly from the linear dependence of the film thickness on the increasing number of cycles. The Ni content of the films was approximately 75 at.%, with the rest being mostly carbon. According to XRD, the carbon was incorporated as Ni_3C. The sheet resistance of the Ni_3C films was low (18.6 Ω/□ at 220 °C) but increased rapidly at temperatures above 250 °C because in addition to the Ni_3C phase, high amounts

of carbon were then incorporated as an impurity. Kang et al. were able to promote the deposition of smooth Ni films by catalyzing the process with ethyl iodide.[139] A 24 nm thick film was reported to exhibit a low resistivity of 20 μΩcm. The iodine treatment improved not only the surface morphology but also the interface quality of NiSi obtained after postdeposition annealing.

The film purity was improved when NH_3 was used as the reducing agent for $Ni(dmamb)_2$ instead of H_2.[46,47] The films were deposited at a high temperature of 300 °C. Based on the studies by Do et al., $Ni(dmamb)_2$ starts to decompose at temperatures above 250 °C.[138] Therefore, the process reported by Kim et al. might involve some CVD-type growth.[46] Nevertheless, a saturative growth rate of 0.64 Å/cycle was reported for the process at 300 °C. The saturation was verified only with respect to the NH_3 pulse length, which is why the decomposition of $Ni(dmamb)_2$ is not conveyed through the results. Similar film growth was observed on both SiO_2 and Si–H regarded as an absence of substrate sensitivity possibly deriving from the decomposition of $Ni(dmamb)_2$. Whichever the growth mechanism, the $Ni(dmamb)_2 + NH_3$ process afforded high-purity films, with the resistivity being 25 μΩcm at the lowest. The process showed good conformality in 5:1 aspect ratio structures and was applied to area-selective ALD for making narrow Ni lines using octadecyl-trichlorosilane-based self-assembled monolayers (OTS SAMs) to prevent deposition on certain areas.

Similar to $Ni(dmamb)_2$, $Ni(dmap)_2$ is also an amino alkoxide and analogous to the commonly used Cu ALD precursor, $Cu(dmap)_2$. $Ni(dmap)_2$ has been used to deposit a mixture of Ni metal and Ni_3N by a two-step process with hydrazine and by a three-step process with formic acid and hydrazine as the reducing agents.[89] Both processes were studied on Ru substrates, and no deposition was observed on insulators.

3.3.3 $Ni(^{tBu2}dad)_2$

As mentioned in Section 3.2.4, analogous metal diazadienyl complexes have been developed for Mn, Fe, Co, and Ni. Similar to $Co(^{tBu2}dad)_2$, the Ni complex has a monomeric structure and tetrahedral coordination at the Ni atom, affording thermal properties compatible with ALD. The ALD of Ni was first attempted with formic acid.[49] Surprisingly, no deposition was observed by a simple two-step process. Ni metal was grown only when an intermediate pulse of 1,4-bis(trimethylsilyl)-1,4-dihydropyrazine was added between the $Ni(^{tBu2}dad)_2$ and formic acid pulses. Ni metal was deposited on Ru with a growth rate of 0.32 Å/cycle, but the process was not studied further.

After establishing a comparable process to Co, $Ni(^{tBu2}dad)_2$ was also combined with tert-butylamine to deposit Ni metal films at low temperatures of 160–220 °C.[52] At 180 °C, a saturative growth rate of 0.60 Å/cycle was measured on Pt. This is markedly lower than reported for the analogous Co process (0.98 Å/cycle).[51] The decomposition temperature of $Ni(^{tBu2}dad)_2$ was estimated to be 230 °C. In the ALD experiments, however, CVD-type growth was observed already at temperatures above 200 °C. As with the Co process,

deposition was observed only on metal substrates, and no films were grown on insulators within the studied temperature range. On Pt, the film thickness showed a linear dependence on the cycle count without any noteworthy delay in nucleation. On Ru substrates, on the other hand, no growth occurred within the first 150 cycles. A similar trend was observed with Co, and it was attributed to the oxidation of the Ru surface that hinders the formation of active sites and thus inhibits the nucleation. Surface oxidation also inhibited nucleation on Cu substrates; only island-like growth was obtained. The Co process was not as sensitive to the oxidation of the substrate, and continuous films were deposited also on Cu.

According to XPS depth profiling, it was proposed that an alloy of Ni and Pt forms at the interface of the Pt substrate and the growing film, explaining the efficient nucleation of Ni on Pt. In the film bulk, a Ni content of 97.3 at.% was measured. Accordingly, a relatively low resistivity of 22 μΩcm was measured for a 60 nm Ni film deposited on Pt. Higher values ranging from 32 to 45 μΩcm were observed for thinner films. Although these values are 4–6 times higher than the bulk Ni resistivity, they correlate well with the other ALD reports.

The reaction mechanism of the $Ni(^{tBu2}dad)_2$ + tert-butylamine process was proposed to resemble the mechanism of the analogous Co process; upon interaction on the surface, the precursors form an unstable adduct that decomposes to the desired metal. Most likely, partial decomposition of the metal precursor on the metal substrate again plays a role in initiating nucleation and enabling further film growth. Because of the similarity of Ni and Co metals, the two processes were much alike but also showed some differences. For example, the Ni process had a lower growth rate (0.60 Å/cycle) and afforded poor nucleation on Cu, whereas the Co process had a growth rate of 0.98 Å/cycle and nucleated well on Cu. Furthermore, $Ni(^{tBu2}dad)_2$ showed no reactivity toward diethylamine, while $Co(^{tBu2}dad)_2$ and diethylamine resulted in Co metal films, albeit with a lower growth rate than with tert-butylamine. Neither of the precursors reacted with triethylamine. The differences in the reactivity of the metal precursors were ascribed to the small differences in the ionic radii; the radius of the Ni(II) ion is 0.69 Å and that of Co(II) 0.72 Å. Both diethylamine and triethylamine were proposed to be too bulky to bond to the Ni(II) ion and initiate a reaction.

3.4 Copper

Out of the three metals discussed in this thesis, Cu is by far the most studied one in ALD. The first ALD processes for Cu were published some twenty years ago in 1997.[91,149–151] Ever since, the quest for new Cu ALD processes has been incessant. Due to the new winds of the microelectronics industry, the focus has recently started to shift from Cu toward Co. Despite this shift, Cu remains as the dominant interconnect material; thus, there is still a demand for improved Cu ALD processes. The ALD precursors for Cu are shown in Figure 19, and the processes are listed in Table 7. As with Co and Ni, many processes require either plasma-enhancement or high deposition temperatures. The most common reducing agent in Cu ALD has been H_2. Owing to the positive reduction potential of Cu ions, there are also

ALD processes employing unconventional reducing agents that afford high-quality Cu thin films at low temperatures. The best quality Cu ALD films have been obtained by using the amino alkoxide precursors with different reducing agents at low temperatures.[81,93,I] The details regarding the thermal Cu ALD processes are scrutinized below.

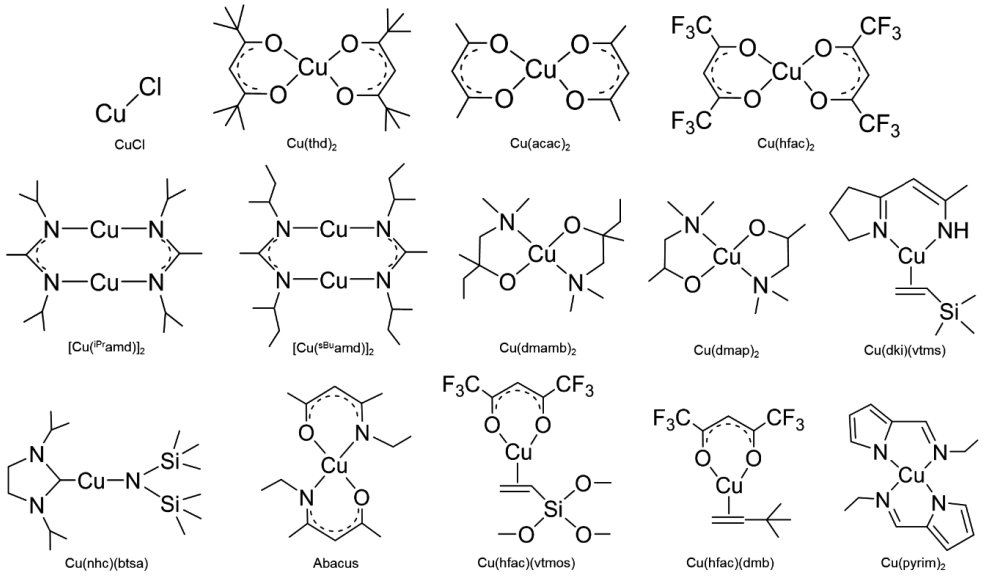

Figure 19. Schematic structures of precursors used in Cu ALD.

Table 7. ALD processes for Cu metal. PEALD processes are highlighted with gray. '*' after a reactant stands for plasma species.

Precursors	**Substrate**	**T_{range}; T_{ALD}** (°C)	**Growth rate** (Å/cycle)	**Resistivity** (μΩcm)	**Ref.**
CuCl + Zn	Al_2O_3	440–500; 500	1–5.5	-	91
CuCl + H_2	Ta	360–410; 410	0.8	-	149–152
CuCl + H_2O +H_2	SiO_2, Al_2O_3	375–475; 400	1.2	-	153–155
Cu(thd)$_2$ + H_2	Pt/Pd Pd Si, glass, TiN	150–350; 190–260 235 350	0.36 0.6 2.1	8 (60 nm) - -	156–158 159–161 43,44
Cu(thd)$_2$ + H_2*	SiO_2, Au, TaN, Pt	60–425; 90–250	0.11	-	162
Cu(acac)$_2$ + H_2	Al, Ti, glass	250	-	-	134
Cu(acac)$_2$ + H_2*	Si, SiO_2, Si–H, glass, SiLK,[163] Cu, Ru, TaN, TiN	140 50–220; 85–135	0.18 0.23	15 (25 nm) 5.3 (30 nm, Ru)	164 165–167
Cu(acac)$_2$ + H_2O + HQ	Si, glass	160–250; 210	2.0	2–5 (75–94 nm)	168
Cu(hfac)$_2$·$x$$H_2O$ + MeOH/EtOH/HCHO	Si	300	-	1.8 (120 nm)	74
Cu(hfac)$_2$ + H_2 & pyridine	TiN	25–175; 25–100	0.19	19 (15 nm)	169
Cu(hfac)$_2$ + DEZ	glass	140–220; 180–200	1.4	2.2 (42 nm)	170
[Cu(^{iPr}amd)]$_2$ + H_2	Si, glass, C, Co	180–300; 250	0.34	-	45
[Cu(^{iPr}amd)]$_2$ + H_2*	Si, glass	50–140; 50–100	0.71	5.6 (33 nm)	171

[Cu(^{sBu}amd)]$_2$ + H_2	SiO_2, Al_2O_3, glass, Si_3N_4, WN, Ru, Co, Cu	185	0.11–1.9	2.9 (80 nm)	172–176
Cu(nhc)(btsa) + H_2*	Si	225	0.2	11.2 (35 nm)	39
Cu(nhc)(btsa) + H_2	Ru, Pd	170–320; 220	0.4 (Pd)	-	177
AbaCus + H_2*	Si, TaN, CDO, Ru, Pd	30–100; 60	0.3 (TaN)	50 (38 nm) 19 (12 nm, Ru)	178,179
AbaCus + H_2	Ru	120–200; 140	1.2	18 (36 nm)	180
Super AbaCus + H_2*	TaN	30–80; 40–80	0.47	75 (20 nm)	178
Cuprum + H_2*	SiO_2, Ta, Ru	100	0.2	20 (42 nm)	181
Cu(hfac)(vtmos) + H_2*	TiN, TaN	150–350; 200	0.5	2.0 (40 nm)	182
Cu(hfac)(dmb) + H_2	Ru	110–230; 170–230	8.0	2 Ω/□ (160 nm)	183
Cu(dki)(vtms) + Et_2SiH_2	-	120	-	-	184
Cu(pyrim)$_2$ + DEZ	SiO_2, Ta, Ru	120–150; 130	0.1	89 (12 nm)	92
Cu(dmamb)$_2$ + H_2*	Ta	100–220; 150	0.65, 0.5	5.2 (10 nm)	185,186
Cu(dmap)$_2$ + HCOOH + H_2NNH	Si	80–200; 120	0.5	9.6–16.4 (45–50 nm)	81
Cu(dmap)$_2$ + HCOOH + $BH_3(NHMe_2)$	Pd, Pt	110–175; 150	0.2 (Pd)	6.4–9.2 (20 nm) 15.6–21.4 (Pt)	48
Cu(dmap)$_2$ + $BH_3(NHMe_2)$	Ru	110–175; 150	0.13	400–500 Ω/□	48
Cu(dmap)$_2$ + DEZ	Si	80–200; 100–120	0.2	2.8 (50 nm)	93
Cu(dmap)$_2$ + TBH	Si, glass, Al_2O_3, Si–H, TiN, Ru	80–140; 120	0.15 (Si)	1.9 (54 nm)	I
CTA-1 + H_2*	Si, TaN, CDO, Ru, Pd	30–100	0.2 (Ru)	5.9 (450 nm)	179

3.4.1 CuCl

The very first attempt for the ALD of Cu thin films was published in 1997 using CuCl and Zn as precursors.[91] Although self-limiting growth was not observed, the process is unique for being the only pulsed deposition method for Cu using pure metal as the reducing agent. Because of the poor volatility of the precursors, the films were deposited at high temperatures between 440 and 500 °C. Excess Zn was dissolved into the Cu film forming an alloy and destroying the self-limiting growth mechanism. At 500 °C, the outdiffusion of Zn was enhanced minimizing dissolution, and the films contained only 3 at.% Zn.

Along with Zn, CuCl has also been combined with H_2 to deposit Cu films by ALD.[152] Although the Zn contamination was eliminated, the films were still grown at a high temperature of 350 °C and above, leading to severe agglomeration of the films. The process was examined on Ta substrates catalyzing the CuCl reduction. Nucleation on insulators was improved by adding an intermediate water pulse to the process.[153] However, the only real solution to the deposition of thin yet continuous films is to lower the process temperature, which is impossible when CuCl is used as the precursor. To resolve this issue, precursors with higher volatility were designed and tested as described in Sections 3.4.2–3.4.5.

3.4.2 Cu(II) β-diketonates

$Cu(thd)_2$

Cu(II) β-diketonates serve as more volatile alternatives to CuCl and, in theory, make it possible to deposit Cu films by low-temperature ALD. In practice, however, the Cu(II) β-diketonates exhibit quite low reactivity and thus require deposition temperatures above 200 °C. Furthermore, the so-called ALD processes have often been studied above the decomposition temperatures of the precursors, implying CVD-type growth in addition to ALD. $Cu(thd)_2$ (thd = 2,2,6,6-tetramethylheptane-3,5-dionate), for example, has been reported to decompose around 190 °C.[173] Mårtensson and Carlsson switched from CuCl to $Cu(thd)_2$ to lower the Cu ALD temperature from 350 to 150–350 °C.[156] H_2 was used as the reducing agent. Self-limiting growth was observed within the temperature range of 190–260 °C. A saturative growth rate of 0.36 Å/cycle was obtained at 230 °C. A relatively high resistivity of 8 μΩcm was measured even for a film as thick as 60 nm. Considering the high resistivity, the films were surprisingly pure as measured by XPS. The films were deposited on mixtures of sputtered Pd and Pt. In contrast, no film was grown on insulators or even on Ta, Fe, TiN, Ni, or indium tin oxide (ITO) despite them being conductive. The selectivity of the process was lost at temperatures above 300 °C due to precursor decomposition. Mane et al. were able to deposit Cu also on oxidized Si and glass because they used a temperature of 350 °C, meaning that the deposition proceeded through CVD rather than ALD.[43,44]

Mårtensson and Carlsson explained the inherent selectivity of the $Cu(thd)_2 + H_2$ process on Pd and Pt by the incomplete dissociation of the $Cu(thd)_2$ molecule on hydroxyl-terminated oxide and oxidized metal substrates.[156] On these surfaces, the film growth is ceased after the adsorption of one monolayer of $Cu(thd)_2$, whereas on metals electron transfer between the substrate and the adsorbate allows full ligand removal, thus enabling the deposition of Cu metal. Willis and co-workers have performed extensive studies on the selectivity of the $Cu(thd)_2 + H_2$ process and report somewhat conflicting results regarding the reaction mechanism.[157–160] According to their mechanistic investigations, Pd is capable of dissociating hydrogen to stable surface species that, in turn, react with the $Cu(thd)_2$ molecules and produce Cu metal and Hthd. Because of the reversible adsorption of $Cu(thd)_2$ as well as steric hindrance, the growth rate of the process was speculated to be much lower than the observed 0.36 Å/cycle if the growth proceeded through the $Cu(thd)_2$ adsorbates. Intermixing of Cu and Pd enables the production of the hydrogen intermediates even after the initial stages of the ALD process. In contrast, Pt did not segregate through the Cu film to the surface like Pd did but still allowed Cu deposition, albeit with different surface morphology. Selective Cu ALD on Pd and Pt substrates has also been reported by Winter and co-workers, as will be discussed in Section 3.4.4.[48]

Cu(acac)$_2$

The idea of using Cu(acac)$_2$ as a precursor for Cu ALD was introduced simultaneously with the Ni(acac)$_2$ + H$_2$ process in the year 2000.[134] As with Ni, no ALD characteristics were shown for the process. Nevertheless, the process can be considered as a starting point for all the research on Cu(acac)$_2$ that followed. Cu(acac)$_2$ has mostly been used in PEALD[164–167] and only once in thermal mode where it was combined with an organic reducing agent, hydroquinone (HQ).[168] Cu films were deposited by a three-step process comprising the metal precursor pulse, water, and the reducing agent at relatively low temperatures of 170–230 °C. The films were deposited on native oxide-terminated Si and soda lime glass substrates. It was speculated that Cu(acac)$_2$ and water first form Cu$_2$O and Cu–OH surface groups. In the second phase, the Cu$_2$O film is reduced to Cu metal by H$_2$ produced through oxidation reactions between HQ and the –OH groups. The process exhibited a saturative growth rate of 2 Å/cycle that is almost an order of magnitude higher than what has been reported for the majority of Cu ALD processes. The use of the intermediate water pulse led to the formation of a parasitic Cu$_2$O phase detected by XRD. As no compositional data was provided, it is impossible to assess the extent of oxygen incorporation. Nevertheless, the film resistivity was low (2–5 μΩcm), indicating a low impurity level. Because of the good electrical properties of the films, the process was marketed for the development of interconnect applications. The use of water, however, makes the integration of the process difficult, as the microelectronics industry is aiming at an oxygen-free production scheme.

Cu(hfac)$_2$

Owing to the fluorinated methyl groups, Cu(hfac)$_2$ (hfac = hexafluoroacetylacetonate) exhibits the highest volatility among the Cu(II) β-diketonates and has thus been studied more for ALD than Cu(thd)$_2$ or Cu(acac)$_2$. Although Cu(hfac)$_2$ can be used to deposit high-quality Cu films at relatively low temperatures, its use in the production of interconnects is precluded by a fear of fluorine incorporation. Solanki and Pathangey combined Cu(hfac)$_2$·*x*H$_2$O with three reducing agents: methanol, ethanol, and formalin at 230–300 °C.[74] The depositions were performed on glass and 6 nm thick Ta, TaN, and TiN barrier layers. At 300 °C, the use of methanol afforded a resisitivity of 5.3 μΩcm (200 nm Cu thickness), and with ethanol resistivities of 1.9–2.4 μΩcm were observed for 120 nm thick Cu films. The carbon content was lowered from 5 to 3 at.% when ethanol was used instead of methanol. The best-quality Cu films were obtained when formalin was used as the reducing agent; a 120 nm thick film exhibited a carbon content below the detection limit of XPS and a resistivity of only 1.8 μΩcm. A resistivity of 4.3 μΩcm was measured for a 20 nm thick film. Although the films were of low resistivity, they were most likely grown by CVD rather than ALD, as the authors provided no data on the growth characteristics and the deposition temperature was as high as 300 °C. Cu deposition using Cu(hfac)$_2$ was also studied by bubbling the carrier gas through water to produce Cu$_2$O that was reduced to Cu

metal with isopropanol at 260 °C or formaldehyde at 300 °C.[75] The films were of higher purity than the ones deposited with methanol or ethanol without the oxide intermediate, but the growth mechanism is closer to CVD than ALD.

Kang et al. were able to deposit Cu films from $Cu(hfac)_2$ and H_2 at room temperature by using a pyridine catalyst.[169] The reaction is catalyzed either by the direct interaction of the pyridine N lone-pair electrons with the Cu atoms or by the weakening of the Cu–O bonds via interactions between the N lone-pair electrons and the hydrogens in the hfac ligands. The schematics for these mechanisms are shown in Figure 20.[169] The Cu films were grown on TiN substrates. A growth rate of 0.19 Å/cycle was measured from room temperature to 100 °C. The growth rate increased to 0.25 Å/cycle when the temperature was raised to 175 °C. No data on the growth properties was provided, leaving the growth mechanism an open question. The carbon content in the films deposited at room temperature was as high as 15 at.% but by raising the temperature to 100 °C, the carbon content was lowered to 5 at.%. Regardless of the deposition temperature (room temperature or 100 °C) and consequent carbon incorporation, the resistivities of 15 nm thick films were 19 μΩcm. This is a rather good value for a film as thin as 15 nm. Although the carbon content was lower at 100 °C, the increase of the deposition temperature enhances film agglomeration, which is why the resistivity was not improved by the improved film purity.

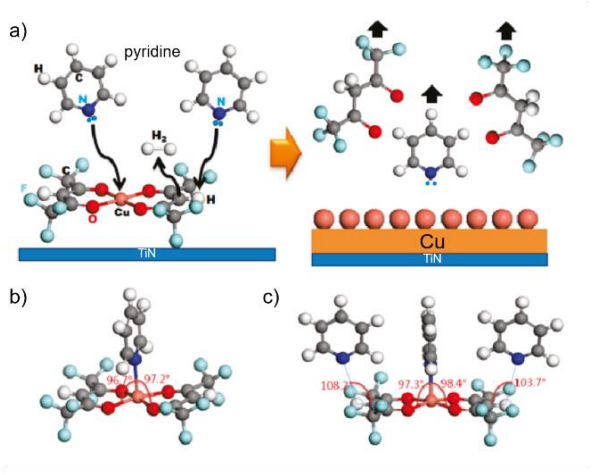

Figure 20. a) Proposed reaction mechanism for pyridine-catalyzed Cu ALD. Bond angles for b) Cu in $Cu(hfac)_2$–pyridine and c) both Cu and H in $Cu(hfac)_2$–pyridine.[169] Reproduced with permission from ref. 170. Copyright © 2010 American Chemical Society.

$Cu(hfac)_2$ has also been combined with DEZ to deposit Cu films on glass substrates at 140–220 °C.[170] The saturation of the growth rate was confirmed as a function of both precursor pulse times. A surprisingly high growth rate of 1.4 Å/cycle was reported at 180–200 °C. Apart from the $Cu(acac)_2$ + HQ process, the Cu growth rates with the Cu(II) β-diketonates are usually below 0.4 Å/cycle. According to XPS, the Zn level in the films deposited at 180–200 °C was low (0.3 at.%). The Zn content was higher outside these temperatures due to

either slow desorption or the decomposition of Zn compounds. As is expected for temperatures as high as these, the Cu films grew as islands that coalesced only after a certain number of ALD cycles. A 42 nm thick Cu film exhibited a low resistivity of 2.2 μΩcm. At the critical thickness of 8 nm, the resistivity was 150 μΩcm that was decreased to 80 μΩcm by annealing at 350 °C. Annealing at 400 °C resulted in a higher resistivity because of extensive film agglomeration. The critical thickness (the lowest film thickness required for conductivity) is rarely reported, despite it being valuable information for device fabrication. Therefore, it is useful that Zhong and co-workers have studied the resistivity of the thin Cu films, although 150 μΩcm is a fairly high value. In comparison, the resistivity of a 10 nm thick Cu film deposited by the $Cu(dmap)_2$ + TBH process was only 6.4 μΩcm.[I]

3.4.3 Cu(I) amidinates

As discussed in Section 3.2.1, amidinate-type precursors were designed not only for Co and Ni but also for Cu. To study the ALD of Cu, Lim et al. combined $[Cu(^{iPr}amd)]_2$ with H_2 at 180–300 °C.[45] The films were deposited on Si, glass, glassy carbon, and ALD Co. The use of Co seed layers helped circumvent the issue with poor adhesion of the Cu films to the substrate. At 250 °C, a saturative growth rate of 0.34 Å/cycle was measured on Si with the native oxide as a function of both precursor pulse lengths. The growth rate increased with increasing temperature, and no plateau was observed within the studied temperature range. Although an ALD window is not a requisite for ALD, the increase of the growth rate in the case of $[Cu(^{iPr}amd)]_2$ is most likely a result of increased precursor decomposition. Despite $[Cu(^{iPr}amd)]_2$ being a dimer, it is still a Cu(I) precursor and thus prone to undergo disproportionation. A later study showed that $[Cu(^{iPr}amd)]_2$ starts to decompose already at 140 °C,[187] which certainly indicates a CVD-type mechanism for the $[Cu(^{iPr}amd)]_2$ + H_2 process when employed at 180–300 °C.

$[Cu(^{sBu}amd)]_2$ is a solid at room temperature but evaporates from liquid state, which is why it has been studied more for ALD than its isopropyl analogue with a high melting point. $[Cu(^{sBu}amd)]_2$ also shows higher reactivity at lower temperatures, minimizing film agglomeration. The compound has been shown to exhibit a half-life of 33 days at 190 °C, indicating good thermal stability.[173] Li et al. were able to deposit Cu films as low as 190 °C by combining $[Cu(^{sBu}amd)]_2$ with H_2.[172,173] This precursor combination exhibited a saturative growth rate of 0.9 Å/cycle with respect to both precursor doses on Al_2O_3 at 185 °C. Similar to the $Cu(dmap)_2$ + TBH process,[I] the growth rate on insulating substrates slowed down to 0.5 Å/cycle after all the –OH groups were occupied, and the film started to grow on itself. The Cu growth rate was 0.1 Å/cycle on Ru and 0.4 Å/cycle on Co substrates. The higher growth rate on oxides was explained by fast diffusion and self-agglomeration of Cu atoms and chemisorbed precursor molecules on the surface, opening access to more reactive sites (–OH) onto which additional $[Cu(^{sBu}amd)]_2$ molecules may chemisorb during the next pulse (Figure 21e).[176] The strong adhesion of Cu atoms to metal surfaces restrains diffusion; thus, the sparsely spread adsorbates block access to the neighboring reactive sites,

limiting the amount of chemisorbed precursor per half cycle. The chemisorption of $[Cu(^{sBu}amd)]_2$ on SiO_2 occurs through a displacement of one of the ligands and a consequent formation of a Si–O–Cu–(^{sBu}amd) surface species. H_2 dissociates the rest of the amidinate groups, producing Cu metal and amidine vapor. A schematic representation of the reaction mechanism is shown in Figure 21a–d.[176] Despite the lower growth rate, the films deposited on metals were of excellent uniformity and showed denser nucleation as opposed to the films grown on insulators.[173] Furthermore, the adhesion of the Cu films was improved when deposited on a Co/WN/SiO_2 structure instead of using insulating substrates or the traditional Ta/TaN_x/SiO_2 stack.[172] Because of severe island-like growth on insulators, conductive films were obtained only at thicknesses of 40 nm and above.[173] The resistivity of an 80 nm thick film was as low as 2.9 μΩcm, corroborating with the low impurity levels (1.0 at.% carbon) measured by Rutherford backscattering spectrometry.

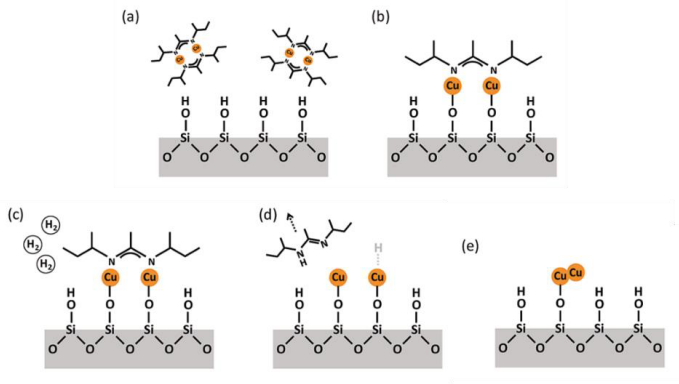

Figure 21. Schematic views of a–d) reactions between $[Cu(^{sBu}amd)]_2$ and H_2 and e) self-agglomeration of Cu on SiO_2.[176] Reproduced with permission from ref. 177. Copyright © 2010 American Chemical Society.

The $[Cu(^{sBu}amd)]_2$ + H_2 process could be used to conformally cover structures with an aspect ratio of over 35:1.[173] Kucheyev et al. demonstrated the conformality of the process further on nanoporous silica aerogel monoliths with ultrahigh aspect ratios.[174] The penetration depth of Cu atoms was limited by deviation from the ideal ALD behavior most likely caused by some irreversible reactions between the Cu atoms and the reactive N,N'-di-sec-butylacetamidine byproducts or partial decomposition of the $[Cu(^{sBu}amd)]_2$ molecules after multiple collisions inside the narrow pores. In their mechanistic studies, Dai et al. postulated that the amidine may also react with the –OH groups on the SiO_2 surface, inhibiting chemisorption of the precursor molecules.[176] Finally, Seitz and co-workers have shown that the $[Cu(^{sBu}amd)]_2$ + H_2 process can be applied to deposit Cu onto carboxyl-terminated SAMs without damaging the Si/SAM interface.[175] This successful deposition shows promise for integrating the process, and ALD in general, into making top contact electrodes in molecular electronic devices.

3.4.4 Cu(II) amino alkoxides

$Cu(dmamb)_2$ is an amino alkoxide precursor that has been used to deposit Cu thin films by PEALD with H_2 plasma[185,186] and also indirectly by first depositing Cu_3N that was subsequently reduced to Cu metal with H_2 at temperatures above 200 °C.[188] Although $Cu(dmamb)_2$ was the first amino alkoxide to be introduced in ALD, more work has been put into the use of another compound from the same family, $Cu(dmap)_2$. To study the ALD of Cu, $Cu(dmap)_2$ has been combined with several reducing agents, including formic acid, hydrazine, $BH_3(NHMe_2)$, DEZ, and TBH. This set of processes provides interesting insight into the role of the reducing agent; both the growth characteristics and film properties varied significantly depending on the choice of reactant.

One of the best qualities of $Cu(dmap)_2$ is its high reactivity even at temperatures below 150 °C. Most of the $Cu(dmap)_2$ processes result in film deposition as low as 80 °C. The lower temperature limit is dictated by the evaporation temperature of the precursor (65 °C in an F-120 ALD reactor). Low deposition temperatures are critical in Cu ALD because of the high mobility of the Cu atoms. Lee et al. combined $Cu(dmap)_2$ with DEZ to deposit metallic Cu films at low temperatures of 80–200 °C.[93] The growth rate of the $Cu(dmap)_2$ + DEZ process increased rapidly above 140 °C, most likely due to the onset of $Cu(dmap)_2$ decomposition. Corroborating results were seen with the $Cu(dmap)_2$ + TBH process.[I] Other studies show, however, that the growth rate stays constant until a temperature of 160 or 170 °C. The differences may originate from differences in reactor designs.

A saturative growth rate of 0.2 Å/cycle (100–120 °C) was observed for the $Cu(dmap)_2$ + DEZ process.[93] This growth rate is similar to the processes employing formic acid and $BH_3(NHMe_2)$ (in a three-step process)[48] or TBH as the reducing agent.[I] The film thickness increased linearly with respect to the increasing number of ALD cycles. Considering the granular appearance of a 50 nm Cu film in SEM, a surprisingly low resistivity of 2.78 μΩcm was measured. The low resistivity can be ascribed to the high purity of the films deposited at 100–120 °C; no contaminants, including Zn, were seen in XPS. At lower and higher temperatures, peaks corresponding to Zn, C, and O were observed. The proposed mechanism behind the $Cu(dmap)_2$ + DEZ process is that $Cu(dmap)_2$ is first adsorbed on the substrate via dipole–dipole interactions. Upon reaction with DEZ, the Cu metal centers are reduced from +II to 0, releasing volatile $Zn(dmap)_2$ and butane as byproducts. The inclusion of impurities is explained by either the decomposition of $Zn(dmap)_2$ and DEZ (above 120 °C) or incomplete evaporation of the two (below 100 °C).

Knisley et al. developed a three-step process for Cu ALD using $Cu(dmap)_2$, formic acid, and hydrazine as precursors.[81] The role of hydrazine was to reduce the Cu(II) formate formed by the $Cu(dmap)_2$ and formic acid pulses. The Cu films were deposited on native oxide-terminated Si, and no Cu metal was deposited without the intermediate formic acid pulse or without hydrazine. The process was studied at temperatures of 80–200 °C, and a saturative growth rate of 0.5 Å/cycle was measured at 120 °C. The growth rate stayed constant up to a temperature of 170 °C, though some precursor decomposition was observed

at 140 °C when $Cu(dmap)_2$ was used with TBH.[I] The films exhibited high purity (95.9–98.8 at.%) and relatively low resistivities (9.6–16.4 μΩcm for 45–50 nm thick Cu films). Surprisingly, all the films passed the Scotch tape test, even though continuous Cu films typically suffer from poor adhesion and delamination on insulators.

Winter's group also investigated Cu ALD using $BH_3(NHMe_2)$ as the reducing agent.[48] A two-step process combining $Cu(dmap)_2$ with $BH_3(NHMe_2)$ was studied only on Ru substrates. A nucleation period of 50 cycles was required to initiate film growth. To deposit Cu films on Pd and Pt substrates, an intermediate formic acid pulse was applied. The growth rates of both processes were somewhat lower (0.13 Å/cycle for the two-step and 0.20 Å/cycle for the three-step process) than with formic acid and hydrazine (0.5 Å/cycle). In the three-step process, the Cu film thickness on Pd increased linearly as a function of increasing cycle count because of intermixing of the two metals. On Pt, there was less intermixing, and the growth rate dropped from 0.4 to 0.03 Å/cycle after the first 500 cycles. At 120–160 °C, the two-step process afforded particulate, nonconductive Cu films with a modest Cu content of 85.0 to 89.2 at.%. The films were amorphous most likely due to the high impurity content. In general, ALD Cu films are polycrystalline even when deposited at low temperatures. The three-step process deposited high-purity Cu films, with the Cu content exceeding 97.5 at.% at 140 °C. Resistivities ranging from 6.4 to 9.2 μΩcm and 15.6 to 21.4 μΩcm were measured for 20 nm thick Cu films grown on Pd and Pt, respectively. It was claimed that a film of only 2 nm thickness formed a fully closed layer of Cu on Pd and Pt at 150 °C.

The latest results concerning Cu ALD with $Cu(dmap)_2$ have been obtained by using TBH as the reducing agent.[I] Different from the previous processes with $Cu(dmap)_2$, the growth rate was lower with TBH, especially after the substrate surface was covered. These differences can be ascribed to the reducing agent, as the Cu processes published by Winter's group afforded deposition with a higher rate despite the same metal precursor.[48,81] Unlike the other processes, the $Cu(dmap)_2$ + TBH process was also strongly dependent on the deposition temperature. This anomaly may arise from the differences in reactor designs. It is also possible that the reducing power of TBH is increased at higher temperatures. Nevertheless, the use of TBH as the reducing agent had significant improvement on the Cu film quality; the Cu content in the bulk of a 50 nm film exceeded 99.4 at.%, and the resistivity was as low as 1.9 μΩcm. The process will be discussed more thoroughly in Section 5.2.1.

3.4.5 Other Cu precursors

In addition to the traditional, homoleptic, and well-researched Cu precursors described in the previous sections, more complex molecules with specifically tuned thermal properties have also been proposed for the ALD of Cu. Most of these have been tested only with H_2, with or without plasma-enhancement. Furthermore, not many of the processes have been

studied for their growth characteristics, making it impossible to say whether the films are grown in a self-limiting manner. The use of Cu(hfac)(dmb) (dmb = 3,3-dimethyl-1-butene), for example, afforded Cu films with a rate of 8 Å/cycle, indicating CVD-type growth instead of ALD.[183] Being a Cu(I) compound, Cu(hfac)(dmb) is likely prone to disproportionation, which may result in spontaneous metal deposition. The CVD mechanism of this process is further corroborated by the fact that there was no mention of a reducing agent in the article.

Hagen and co-workers combined a carbene-stabilized Cu(I) silylamide (1,3-diisopropyl-imidazolin-2-ylidene-Cu-bis(trimethylsilyl)amide) together with H_2 in thermal ALD.[177] The precursor was first introduced for Cu PEALD.[179] The Cu precursor is favorable from the industry viewpoint, as it lacks both oxygen and halogen-containing species. $Cu(btsa)_2$ does not exist in the linear form but forms a poorly volatile tetramer instead. The formation of the tetrameric byproduct was prevented by the carbene ligand serving as a strong σ donor. The proposed mechanism is the adsorption of the Cu precursor by breaking of the Cu–carbene bond, dissociative adsorption of hydrogen, and the formation of Cu metal and Hhmds (hmds = hexamethyldisilazane). The Cu depositions were carried out on Ru and Pd substrates at 170–320 °C. The substrate had a significant effect on the film structure; on Pd continuous films were formed, whereas on Ru the films were island-like and coalesced only after a thick enough film was formed. The differences were ascribed to the differences in Cu solubility in to the two metals; Cu and Pd are soluble, whereas Cu and Ru are insoluble in each other. Corroborating results were obtained also with the $Cu(thd)_2$ + H_2 and $Cu(dmap)_2$ + $BH_3(NHMe_2)$ processes.[48,156] The Cu(I) silylamide process exhibited a constant growth rate of 0.45 Å/cycle on Pd at 190–250 °C. Saturation of the growth rate with respect to the Cu precursor pulse time was verified at 220 °C. Due to the island-like structure, a lower growth rate (0.13–0.27 Å/cycle) was observed on Ru.

Abacus is a Cu(II) ketoiminate precursor supplied by Air Liquide. It has been studied mainly in PEALD.[178,179,181] Park et al. used Abacus in thermal ALD by combining it with H_2 at 120–200 °C.[180] Ru was selected as the substrate for its potential use in next-generation Cu interconnects. A growth rate of 1.2 Å/cycle was reported for the process, but no additional results on the growth characteristics were provided. Because of agglomeration, the films were rough and therefore exhibited high resistivity. At the lowest, a resistivity of 18 μΩcm was obtained. Marshall's group examined the possibility of using a Cu(I) diketiminate as a precursor for low-temperature Cu ALD.[184] The precursor was combined with diethylsilane at 120 °C. Although no deposition results were given, the process was said to produce "a clean, conformal Cu film". A separate study showed, however, that the growth proceeded through CVD rather than ALD.[189]

Vidjayacoumar et al. carried out extensive solution screening studies to identify suitable combinations of Cu precursors and metal alkyl compounds for Cu ALD.[92] The Cu precursors were tested with $AlMe_3$, BEt_3, $ZnEt_2$, Si_2Me_6, Sn_2Me_6, and $B_2(Pin)_2$ as reducing agents. Although solution studies give a first indication of the reactivity of two precursors and information about potential reaction routes during ALD, what happens in the solution and in the gas phase, let alone on the surface, are three quite different things. For instance,

the species taking part in the reaction as well as the reaction kinetics change when a system is transferred from a solution to the surface. Although promising results were obtained for almost all the combinations, only one of the Cu precursors, $Cu(PyrIm^{Et})_2$ ($PyrIm^{Et}$ = N-ethyl-2-pyrrolylaldiminate), was tested in ALD conditions. The depositions were carried out on SiO_2, Ta, and Ru at 120–150 °C. Nonconductive films with high levels of Al and O impurities were deposited using TMA, and no films were deposited with BEt_3 as the reducing agent. The use of DEZ, on the other hand, led to the formation of conductive Cu films, albeit with a high resistivity of 89 μΩcm. Zn incorporation into the films was inevitable, and the Cu content after sputtering was only about 70 at.% as measured by XPS.

3.5 Indirect approaches to metal ALD

The indirect approach to metal ALD, in this case, means the ALD of a film comprising a metal-containing compound, such as a metal nitride or oxide, subsequently converted to elemental metal by some postdeposition treatment. The conversion can be done, for example, by annealing the film at high temperature or by reducing it with H_2 or NH_3 at a lower temperature. The indirect approach is also used to remove contaminants from the films, thus improving film purity.

The indirect approach is a convenient way to circumvent the low reactivity of common metal precursors and reducing agents in the ALD of the late first-row transition metals; the compounds of these metals are much easier to deposit than the pure elements. Furthermore, the indirect approach often yields metal films with higher growth rates and can be applied on a variety of substrates, whereas many of the direct ALD processes are slow and substrate sensitive. Other benefits include, for example, decreased surface roughness and denser nucleation, as was observed in the case of Cu when prepared indirectly through the reduction of Cu_3N.[190] The use of a nitride intermediate instead of an oxide is beneficial when the target is to deposit metals for microelectronics. The integration of an oxide process into microelectronic manufacturing is problematic when making, for example, seed layers for Cu electroplating, as the process would also oxidize the underlying barrier layer. Also, the film density is not changed as drastically when reducing a nitride instead of an oxide, which helps minimize shrinkage of the films. The shrinkage contributes to agglomeration and void formation that depends not only on the density change but also on the substrate and temperature used in the postdeposition treatment. For some applications, void formation and the resulting particulate film morphology may be useful. Alburquenque et al. observed higher coercivities for Co nanoparticles than for films with better continuity.[191] Film agglomeration also gives a higher surface area that can be exploited, for example, in catalysis. In interconnects, however, conductivity is needed, which is why metal films should be continuous even when prepared by the indirect approach. For minimizing film agglomeration, metal substrates and low reduction temperatures should be used.

Co, Ni, and Cu have all been prepared by the indirect approach. The research has mostly focused on Ni and Cu, but a couple of reports also exist on the reduction of CoO_x. Most studies have been carried out on metal oxides because they are easier to make by ALD than the nitrides of Co, Ni, and Cu. The reduction of NiO, in particular, has been under scrutiny in the past. Further insight into the indirect ALD of the late first-row transition metals is provided in Sections 3.5.1–3.5.3.

3.5.1 Cobalt

Although Co precursors are difficult to reduce to elemental Co in ALD, there are only a couple of reports showing the deposition of Co through postdeposition treatment of some Co compound ALD films. CoN_x is unstable at high temperatures and would be easy to convert to Co metal by heating; Alexander et al. reported complete denitridation of CoN_x in a mixture of H_2 and Ar at 250 °C.[192] Unfortunately, no reports on the ALD of CoN_x exist to date. Instead, Co metal has been obtained by using ALD CoO_x as the starting material. Alburquenque and co-workers studied the reduction of Co_3O_4 films deposited with $Co(Cp)_2$ and ozone at 250 °C.[191] The films were reduced to Co metal in H_2/Ar at 430 °C. Because of the high reduction temperature, the films consisted of separate agglomerates instead of being continuous layers of metal. The particulate morphology is problematic when conductivity is needed but not necessarily in the case of magnetic applications. Alburquenque et al. measured a maximum coercivity of 510 Oe for a ~25 nm thick Co film and observed a decreasing trend in coercivity as a function of increasing film thickness. Daub et al. employed the indirect approach for the preparation of ferromagnetic nanotubes.[193] The Co_3O_4 films were grown with the $Co(Cp)_2$ + ozone process and reduced in H_2/Ar at 400 °C.

Due to the lower oxidation state of cobalt, CoO is easier to reduce to elemental Co than Co_3O_4. In ALD, CoO is typically formed only when water is used as the oxygen source, but not many of the existing Co precursors are reactive toward water. Instead, they are combined with ozone, which results in ligand combustion and loss of control over the oxidation state.[133,194–197] The only precursors shown to react with water to produce ALD CoO films are: $Co(^{iPr}amd)_2$,[45,198] $Co(^{tBuEt}amd)_2$,[199,200] $Co(btsa)_2$,[201] and $CoCl_2(tmeda)$[II] (though no verification of saturation was given for the amidinates). The reduction of the CoO films deposited with the first three precursors required high temperatures above 400 °C when performed under H_2. Zhang et al. reached a low reduction temperature of 200 °C by switching the H_2 to either deuterium atoms or an oxygen-scavenging Al overlayer.[199] When $CoCl_2$(tmeda) was used, the reduction temperature even with forming gas was as low as 250 °C.[II] Owing to the low temperature, the film agglomeration was minimized, and a film of only 16 nm thickness formed a continuous network of metal over a TiN substrate. Full coverage of the substrate was not, however, reached even with a film thickness of 50 nm. Details regarding these results are further discussed in Section 5.3.

3.5.2 Nickel

NiN_x

There are only two actual reports on the ALD of NiN_x, though some of the Ni ALD processes produce films with high nitrogen contents and are thus closer to nitride than Ni metal processes. In her PhD thesis, Ariyasena described an ALD process for NiN_x using $Ni(dmap)_2$ with hydrazine or a combination of formic acid and hydrazine.[89] No attempts were made to lower the nitrogen content in the films. Ni_3N films have also been deposited with $NiCl_2$(tmpda) and TBH.[IV] The nitrogen content was lowered by treating the films in 10% forming gas at 150 °C. The results on this process are presented in Chapter 5.

Wang et al. deposited Ni films by PEALD using $Ni(Cp)_2$ and NH_3 as precursors.[136] Depending on the deposition temperature, the nitrogen and carbon contents varied between 7 and 13 at.%. By annealing in hydrogen at 400 °C, all the nitrogen was removed, and the carbon content was lowered to 5–6 at.%. Accordingly, the resistivities were lowered from 71–127 μΩcm to 11.8–13.6 μΩcm. As a result of annealing, Park and co-workers were also able to lower the resistivity of Ni films deposited with $Ni(^{iPr2}dad)_2$ and NH_3 plasma from 146 to 13.3 μΩcm.[137]

NiO

The reduction of ALD grown NiO to Ni metal was first reported by Utriainen and co-workers.[134] Thick NiO films (130–230 nm) were deposited on glass substrates with $Ni(acac)_2$ and ozone at 250 °C. The resulting oxide films were reduced in a H_2/Ar mixture (5% H_2) at 230–500 °C. At a reduction temperature of 230 °C, the films suffered from void formation caused by the density changes upon reduction. Chae et al. were able to avoid the void formation by performing the reduction studies on thinner NiO films on TiN substrates at a lower temperature of 165 °C.[135] The NiO films were grown with the $Ni(Cp)_2$ + water process and reduced by H_2 plasma. A Ni thickness of 15 nm was enough to form a continuous metal film. The resistivity of this film was between 25 and 30 μΩcm. The carbon content in the oxide film was as high as 16 at.% but was lowered to 6 at.% upon reduction.

Lindahl et al. were able to lower the reduction temperature of NiO in H_2 from 230 to 200 °C by growing a Ni_3N film on top of the oxide.[202] The NiO films were grown by $Ni(thd)_2$ and water. Without the nitride layer, no reduction occurred. It was proposed that the Ni metal, formed upon the decomposition of Ni_3N, dissociates H_2 into atomic hydrogen capable of reducing the underlying oxide layer. For the preparation of NiO/Ni dual layers, a lower temperature of 180 °C was used to inhibit the reduction of the NiO film.

The indirect approach for obtaining Ni metal through NiO reduction offers an easy and robust alternative to the slow and often substrate sensitive direct ALD processes. The

approach is particularly useful for applications where the pinhole formation is not of major concern, such as the preparation of Ni nanoparticles and nanotubes.[193,203–210]

3.5.3 Copper

Cu_3N

Similar to CoN_x and NiN_x, the nitrides of Cu are also unstable at elevated temperatures and have been used as intermediates for subsequent reduction to Cu metal. Törndahl et al. deposited Cu_3N thin films by ALD using $Cu(hfac)_2 \cdot xH_2O$, water, and NH_3 at 210–302 °C.[211] The intermediate water pulse was a requisite for initiating film growth on the SiO_2 and Al_2O_3 substrates. The addition of water into the process also decreased contamination from carbon impurities. Although no saturation with respect to the Cu precursor pulse lengths was achieved, film thickness was linearly dependent on the number of deposition cycles at 247 °C. At a deposition temperature of 283 °C, the films were a mixture of Cu_3N and Cu metal, and at 302 °C the films were phase pure cubic Cu.

Li and Gordon deposited Cu_3N thin films by combining $[Cu(^{sBu}amd)]_2$ with NH_3 and reduced the films to Cu metal using H_2 at 225 °C.[190] The amount of nitrogen in the Cu_3N films was dependent on the deposition temperature. At low temperatures (160 °C), there was no precursor decomposition, which allowed the deposition of pure, stoichiometric Cu_3N films. The reduction temperature to metallic Cu could be lowered by increasing either the partial pressure of H_2 or the reduction time. As reported in Section 3.4.3, $[Cu(^{sBu}amd)]_2$ has also been used with H_2 to deposit Cu metal directly by ALD.[173] The resulting films exhibited high surface roughness, especially when deposited on insulating substrates. By using the indirect approach via nitride reduction, smoother films were obtained. Cu films as thin as 0.8 nm were claimed to be conductive, and thicker films exhibited resistivities similar to that of bulk Cu. Furthermore, the films were uniform over large areas and could be deposited conformally inside holes with aspect ratios of over 40:1.

Park and co-workers prepared ALD Cu_3N films using $Cu(dmamb)_2$ and NH_3 at 100–140 °C and were able to reduce the films to Cu metal at 200 °C in 10% forming gas.[188] The nitride films were grown with a high rate of 1.0 Å/cycle on both Ru and SiO_2 substrates at 120–140 °C. Similar to the $[Cu(^{iPr}amd)]_2$ processes, film roughness was decreased by using the indirect approach instead of direct ALD with H_2 as the reducing agent. A resistivity of 30 μΩcm was measured for a film as thin as 4.2 nm.

CuO_x

Although less studied, Cu metal films can also be made by the postdeposition reduction of CuO_x. Soininen et al. compared the reduction efficiency of different alcohols, aldehydes, and carboxylic acids below 400 °C.[212] The CuO_x films were prepared by oxidizing

electrochemically deposited Cu metal films, but the approach could just as well be applied to ALD CuO_x films. Ethanol and formic acid allowed fast and complete reduction at 310 °C. The other reagents required higher temperatures and/or longer reduction times, but even then, complete reduction was not always achieved.

Waechtler et al. were able to reduce Cu_2O films at low temperatures between 110 and 120 °C.[213] The oxide films were grown by ALD using $(^nBu_3P)_2Cu(acac)$ ($^nBu_3P$ = tri-n-butylphosphane) and wet oxygen as precursors. The films were deposited on Ru and TaN substrates and reduced by exposure to formic acid vapor. The Ru substrate enhanced the reduction process through catalytic dissociation of formic acid. The reduced Cu films were tested as seed layers for Cu electroplating. The ALD Cu seed on Ru outperformed the ALD Cu seed on TaN and even PVD Cu in terms of film morphology and resistivity.

3.6 Substrate effects

As seen in Sections 3.2 through 3.5, the substrate plays a critical role in many thermal ALD metal processes. The processes are often studied on only a couple of different substrates, but for facile device integration it is important to span a wide variety of substrates. In interconnects, Cu is combined with a diffusion barrier, an adhesion layer, and caps. These materials include but are not limited to TaN, Ta, Co, and Ru. For efficient silicide formation, the ALD of Ni and Co should be studied on hydrogen-terminated Si. The ferromagnetic metal films in a magnetic tunnel junction, on the other hand, require an insulating tunnel barrier, such as MgO. The metal films need not only to be grown on these substrates, but the processes themselves must be compatible with the underlying materials. In the case of interconnects, for example, oxidative processes should be avoided to prevent oxidation of the diffusion barrier and adhesion layer. It is also important to select the precursors so that any undesirable impurities or corrosion can be prevented.

Some of the thermal processes are inherently selective, meaning that film is grown only on certain substrates. The selectivity can stem from selective precursor adsorption, partial decomposition of the metal precursor, or activation of the reducing agent by certain surfaces. The selectivity is typically lost when operating at high enough temperatures, that is, if the precursor decomposes or when enhancing the system with plasma. $(^{tBu}allyl)Co(CO)_3$, for example, was found to chemisorb only on hydrogen-terminated Si surfaces and not on SiO_2.[82] The diazadienyl precursors, on the other hand, afford film only on metal substrates most likely due to partial precursor decomposition caused by interactions between the complex radical structure of the precursor and a catalytic metal surface.[49–52] The combination of $Cu(thd)_2$ and H_2 also required a metal substrate either to remove the thd ligands through electron transfer or to dissociate H_2 to reactive hydrogen surface species.[156–161] Metal substrates are also needed to catalyze other reducing agents, such as $BH_3(NHMe_2)$ and formic acid. Sometimes a metal substrate (for example, Pd) enhances nucleation

through the formation of an interfacial alloy between the substrate and the film that is being deposited. [48,156,177]

Many metal ALD processes can be applied on a variety of substrates but often with different growth rates. The growth rate may also vary between different metal substrates. When combining $Cu(dmap)_2$ with TBH, Cu deposition was faster on insulators than on conductive substrates.[I] The growth on insulators can also be slowed down once the initial substrate surface is covered. Similar results were obtained with the $[Cu(^{sBu}amd)]_2 + H_2$ process.[173] In contrast, the growth of Co from $Co(^{tBuEt}amd)_2$ was more favorable on Cu than on SiO_2 or CDO.[130] Corroborating results were also obtained for $Cu(acac)_2$ and $Ni(acac)_2$.[134] When using $NiCl_2(tmpda)$ and TBH, the growth rate of Ni_3N was almost doubled on Cu and Au as opposed to Si, Al_2O_3, TiN, and Ru.[IV] Li et al. also observed variation in Cu growth rate on different metal substrates; the growth rate was 0.5 Å/cycle on Cu itself, 0.1 Å/cycle on Ru, and 0.4 Å/cycle on Co.[173]

In metal ALD, the substrate typically has a significant impact on film morphology. In most cases, deposition on insulators leads to film agglomeration and island-like growth. The resulting film is particulate unless the deposition is carried out for enough cycles. The deposition of conductive films in the sub-10 nm thickness range is challenging and possible only at low temperatures and with the right reducing agent, such as TBH. When TBH was used to reduce $Cu(dmap)_2$ at 80 °C, a film of only 10 nm thickness exhibited full substrate coverage and a resistivity of 6.4 μΩcm.[I] Hagen et al, on the other hand, were unable to obtain conductivity for sub-10 nm Cu PEALD films on Si, TaN, and CDO substrates even at a temperature as low as 30 °C.[179] The combination of $Cu(hfac)_2$, H_2, and a pyridine catalyst at 100 °C afforded conductive Cu films at a thickness of 15 nm.[169] With the $[Cu(^{sBu}amd)]_2 + H_2$ process, conductivity on insulators was observed only at thicknesses of 40 nm and above.[173] On conductive substrates, nucleation is typically denser and film agglomeration is minimized. Several groups have reported the deposition of conductive Cu films in the sub-10 nm thickness range on metals like Ru or Pd.[48,188] In general, the films deposited on metals are smoother than those grown on insulators.

In addition to the growth characteristics, the substrate may also have an impact on the film properties. Film adhesion, for example, is largely determined by the underlying substrate material. Metals usually adhere strongly to other metals, whereas metal films deposited on insulators are often peeled off in the Scotch tape test. In some cases, the crystal structure of the substrate affects the structure of the film. Kerrigan et al. deposited cubic Ni films on top of cubic Pt substrates at a low temperature of 180 °C.[52] The Pt substrate likely affected the crystallization through lattice templating, as thermally grown ALD Ni often exhibits the metastable hexagonal phase when deposited below 300 °C.[79,148]

4 Experimental methods

This chapter describes the experimental methods used to obtain the results presented in publications I–V and Chapter 5. More details related to each ALD process can be found from the publications themselves. This chapter is divided into two sections: 4.1 Film deposition and 4.2 Film characterization. The synthesis and characterization of the precursors are described in the publications.

4.1 Film deposition

All the films through publications I–V were deposited in a hot-wall, cross-flow F-120 ALD reactor (ASM Microchemistry Oy, Helsinki, Finland). The reactor was operated under a pressure of ~10 mbar using nitrogen (N_2, AGA, 99.999%; H_2O, ≤ 3 ppm; O_2, ≤ 3 ppm) as both the carrier and purge gas.

The films were, in most cases, deposited on 5 cm × 5 cm native oxide-terminated Si(100) and soda lime glass substrates. To improve the nucleation of the Ni_3N films in publication IV, the depositions were performed on 10 nm thick Al_2O_3 films grown in situ from $AlCl_3$ and water. In the case of the Ni_xGe_y films in paper V, TMA was used instead of $AlCl_3$ for growing the Al_2O_3 films. Most of the characterization was done on the films deposited on Si (with or without in situ Al_2O_3), whereas the films on soda lime glass were used to evaluate, for example, film resistivity. The adhesion of Cu in publication I was investigated on Si, glass, hydrogen-terminated Si, Al_2O_3, TiN, and Ru as substrates. The reduction behavior of CoO in publication II was studied on TiN to suppress agglomeration of the reduced Co metal films. The growth rate and adhesion of the Ni_3N films were studied on several substrates: in situ Al_2O_3, Si with the native oxide, TiN, Cu, Au, and Ru. In addition to Al_2O_3-coated Si and glass, Ni_xGe_y growth was also evaluated on Ge treated with HCl and a pulse of TMA. The conformality of Cu and Co_3Sn_2 in publications I and III was assessed using a structured Si substrate with trenches of varying aspect ratios.

Most precursors were heated to their target temperatures and sublimed from open glass boats inside the reactor. The sublimation temperatures for $Cu(dmap)_2$, $CoCl_2(tmeda)$, and $NiCl_2(tmpda)$ were 65, 170, and 157 °C, respectively. Both tributyltin hydride (TBTH) and tributylgermanium hydride (TBGH) were evaporated at 30 °C. Deionized water and TBH held in external sources at room temperature and 15 °C, respectively, were delivered into the reaction chamber by vacuum draw. The pulse and purge durations were controlled by inert gas valving. $Cu(dmap)_2$ was synthesized at Ruhr-University Bochum according to the procedure in the literature,[214] while the diamine adducts of metal(II) halides were synthesized in-house by Dr. Timo Hatanpää. Tert-butylhydrazine (TBH) was purchased from EpiValence, TBTH from Alfa Aesar, and TBGH from either Gelest or Sigma-Aldrich. Apart from deionized water, all the precursors were air and moisture sensitive and thus handled in a glovebox.

4.2 Film characterization

The thicknesses of metal thin films were determined by energy dispersive X-ray spectrometry (EDS) using an Oxford INCA 350 instrument connected to a Hitachi S-4800 SEM. The thicknesses were calculated with the GMRFILM program assuming bulk density for each material. Due to deviations from bulk density evident especially for discontinuous films, each result comprised an uncertainty of about 5%. The thicknesses of the CoO films were measured by a Film Sense FS-1 Multi-Wavelength ellipsometer.

Either a PANalytical X'Pert Pro MPD or a Rigaku SmartLab X-ray diffractometer was used to identify the crystal structure of the films by grazing incidence XRD. The preferred orientation of selected samples was analyzed with the θ–2θ geometry. The same tools were used to analyze film density by X-ray reflectivity (XRR). The high temperature XRD (HTXRD) studies in publication II and IV were carried out in an Anton-Paar HTK1200 oven in 10% forming gas at atmospheric pressure. The oven was connected to the PANalytical X'Pert Pro MPD instrument.

Nucleation of the films as well as morphology and conformality were evaluated by SEM. In publications II–V, the film morphology was studied further by atomic force microscopy (AFM). The images were recorded in tapping mode in air using a Veeco Multimode V microscope equipped with Si probes (NTESP or RTESP from Bruker). The adhesion of the Cu and Ni_3N films was tested on the many substrates by the Scotch tape test.

The elemental compositions of all materials were determined by time-of-flight elastic recoil detection analysis (ToF-ERDA) using a setup described in the literature.[215] The samples were bombarded with 40 or 50 MeV $^{79}Br^{7+}$ ions at a 16° angle. A 40 MeV $^{127}I^{8+}$ beam was used to analyze the composition of the Ni_3N films. The angle between the film surface and the detector was 24°.

The chemical states of Co and O as well as Co, Ni, and Sn in publications II and III, respectively, were analyzed by XPS using an Omicron Argus instrument with a pass energy of 20 eV. Mg Kα X-rays at a photon energy of 1253.6 eV were emitted from an Omicron DAR 400 source. A different system (PHI Quantum 2000, ESCA Microprobe) operated at an energy of 23.5 eV was employed for the analysis of the Ni_3N films. The films were exposed to 1486.6 eV X-rays (Al source, Kα line) with and without sputtering.

The resistivities of the Cu, Co_3Sn_2, Ni_3N, and Ni_xGe_y films deposited on soda lime glass substrates were measured using a four-point probe (CPS Probe Station, Cascade Microtech connected to a Keithley 2400 SourceMeter). The film resistivities were obtained by multiplying the measured sheet resistances by the film thicknesses.

The magnetic properties of the Co_3Sn_2 and reduced Ni films were characterized by the vibrating sample magnetometer (VSM) option of a Quantum Design PPMS. The measurements were done at room temperature and in two orientations: in-plane and out-of-plane with respect to the film surface. The mass of the substrate was included in the analysis.

5 Results and discussion

This chapter summarizes the key results obtained in the course of this PhD project. Section 5.1 is an introduction to the diamine adducts of metal(II) halides that form the basis for publications II–V. The properties of $CoCl_2$(tmeda) were evaluated by combining it with water to deposit ALD CoO films (II); an overview of the results is given in Section 5.1.1. In addition to different metal precursors, many reducing agents and reactants were also studied. The focus was on testing unconventional, potentially more powerful reducing agents than traditional H_2 and NH_3. The most relevant reducing agents from the viewpoint of this thesis are tert-butylhydrazine (TBH; I, IV) and the tributyl hydrides of Sn and Ge (III, V). The key points of the processes developed using these reactants are reviewed in Section 5.2. Section 5.3 concentrates on the postdeposition reduction of CoO to Co and Ni_3N to Ni metal films. Finally, all unpublished results and figures of related metal precursors and reducing agents not reported in publications I–V are provided in Section 5.4.

5.1 New metal precursors

During this PhD project, several metal precursors were explored for the ALD of Co, Ni, and Cu metals. In some cases, known ALD precursors were combined with new reducing agents, and in other cases, new metal precursors were tested with a variety of reactants. Out of all of the new metal precursors studied, only the diamine adducts of Co(II) and Ni(II) chlorides proved to be suitable for ALD, at least with the reactants that were tested in this work. $CoCl_2$(tmeda) (Figure 22 left) could be used to deposit both Co(II) oxide[II] and intermetallic Co_3Sn_2 thin films.[III] The CoO films were converted to Co metal by postdeposition reduction. $NiCl_2$(tmpda) (Figure 22 right) was suitable for the ALD of Ni_3Sn_2,[III] Ni_3N,[IV] and Ni_xGe_y films.[V] The Ni_3N films could be reduced to Ni metal by postdeposition annealing at 150 °C in 10% forming gas.

The diamine adducts of metal(II) halides were known compounds but had not been studied for their volatility, let alone used in ALD before. The halides of both Co and Ni are polymeric compounds with low volatility. By adducting the halides with proper amines, monomeric structures were created, improving the volatility of the compounds. $CoCl_2$(tmeda) and $NiCl_2$(tmpda) are volatile and withstand quite high temperatures, providing a wide processing window for ALD. Furthermore, the precursors are inexpensive and easy to synthesize, making them also applicable on an industrial scale.

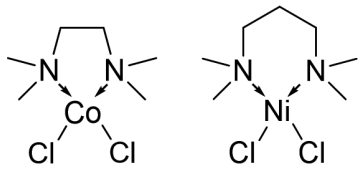

Figure 22. Schematic structures of $CoCl_2$(tmeda) and $NiCl_2$(tmpda).

5.1.1 $CoCl_2$(tmeda)

$CoCl_2$(tmeda) is a monomeric compound where the Co atom is tetrahedrally coordinated to the two nitrogen and two chlorine atoms. In its simplicity, the precursor was synthesized by adding a stoichiometric amount of the adduct ligand to a dichloromethane solution of $CoCl_2$. The solution was then stirred, evaporated, and the residue was sublimed, producing $CoCl_2$(tmeda) with a yield of 99.4%. Thermogravimetric analysis (TGA) conducted under dynamic vacuum showed a residue of only 2.5% at the end of the measurement, indicating clean and nearly complete evaporation of the precursor (Figure 23).[II] No decomposition was observed in the ALD experiments below 300 °C. $CoCl_2$(tmeda) melted around its ALD source temperature (170 °C), ensuring a homogenous flux of precursor.

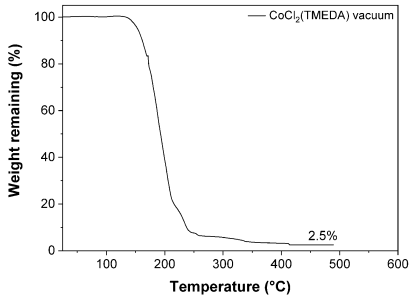

Figure 23. Vacuum TG curve for $CoCl_2$(tmeda).

To study the behavior of $CoCl_2$(tmeda) in ALD, the precursor was combined with water to deposit CoO thin films.[II] $CoCl_2$(tmeda) is one of the four known Co precursors that are reactive toward water. The other three are $Co(^{iPr}amd)_2$,[45,198] $Co(^{tBuEt}amd)_2$,[199,200] and $Co(btsa)_2$.[201] The advantage of using water as the oxygen source instead of ozone is the control over the oxidation state of Co. The use of ozone leads to combustion type reactions that typically produce Co_3O_4 and, in some cases, a mixture of both Co_3O_4 and CoO. The combination of $CoCl_2$(tmeda) and water produced stoichiometric Co(II) oxide films at 275 °C. The films deposited on soda lime glass exhibited the characteristic light green color of CoO as can be seen in Figure 24a.[II] XPS showed that the amount of Co_3O_4 in a 50 nm film is, indeed, negligible and Co is mostly in an oxidation state of +II (Figure 24b).[II] The

X-ray diffractograms depicted in Figure 24c verify that the films consist of two phases of CoO, the hexagonal and the cubic phase, and that no Co_3O_4 is observed.[II] A weak reflection corresponding to Co metal is seen at $2\theta = 44.2°$ when the film was deposited at 300 °C. The formation of Co was also demonstrated in the higher Co:O ratio of 1.3 as measured by ToF-ERDA. Otherwise the films were of high purity, with the film deposited at 275 °C having the least impurities; the H, C, N, and Cl contents were 0.5, 0.5, 0.2, and 0.8 at.%, respectively. This high purity is one of the major advantages of using $CoCl_2$(tmeda) as the precursor; the CoO films deposited with $Co(btsa)_2$, for example, contained a high level of both Si and H impurities.[201]

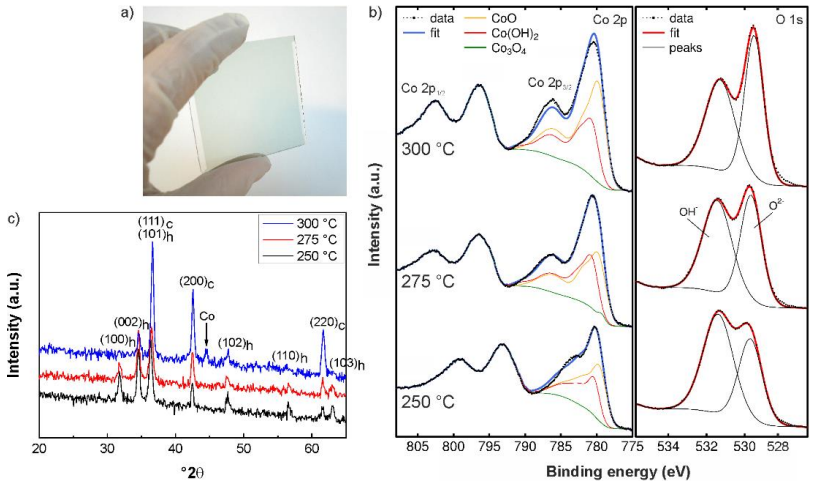

Figure 24. a) CoO film deposited on glass, b) Co 2p and O 1s XPS spectra, and c) XRD patterns of 50 nm CoO films deposited at 250–300 °C.[II]

The $CoCl_2$(tmeda) + water process was studied within a temperature range of 225−300 °C. A very low growth rate of only 0.06 Å/cycle was measured at 225 °C, which is why lower temperatures were excluded from the study. The upper limit of 300 °C was dictated by the onset of $CoCl_2$(tmeda) decomposition. The highest growth rate and the best film quality were obtained at 275 °C, making it the most important temperature for studying the growth characteristics of the process. The saturation curves for both precursors are shown in Figure 25.[II] Long pulses exceeding 4.5 s were required to reach saturation with water, indicating a slow reaction between the precursors. The growth rate saturated at 0.4 Å/cycle. This rate is similar to what was observed using $Co(^{iPr}amd)_2$ and water at 250 °C.[45] Saturation as a function of the $CoCl_2$(tmeda) pulse was seen already with 0.5 s pulses. The saturation was verified with both 1.0 and 4.5 s water pulses. The film thickness increased linearly with the increasing number of cycles, further proving an ALD-type growth mechanism of the process (Figure 25c).[II]

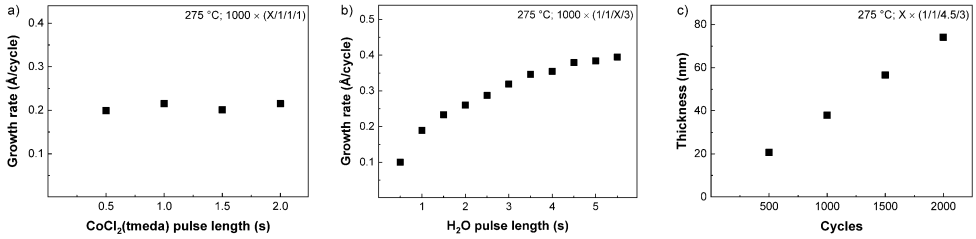

Figure 25. CoO growth rate as a function a) $CoCl_2$(tmeda) and b) water pulse lengths. c) CoO film thickness as a function of cycle count.[II]

The CoO thin films could be reduced to Co metal by postdeposition reduction. This type of indirect approach is a good alternative for metal deposition in cases where no suitable reducing agents are found. The results of the reduction studies are presented in Section 5.3.

In addition to the CoO films, $CoCl_2$(tmeda) was combined with tributyltin hydride (TBTH) to deposit intermetallic Co_3Sn_2 films by ALD.[III] These results are discussed in more detail in Section 5.2.2. Cobalt in the precursor was reduced by the hydride, even though Sn was incorporated into the films. $CoCl_2$(tmeda) appears to be a potential precursor also for the direct deposition of Co metal, though no suitable reducing agent was found during this PhD project. The studied reducing agents included H_2, tert-butylhydrazine, $BH_3(NHMe_2)$, triethylsilane, and hexa-n-butylditin. PEALD with H_2 or NH_3 plasma is one viable option for the reduction of $CoCl_2$(tmeda) but was unavailable to us in the course of this project.

5.1.2 $NiCl_2$(tmpda)

$NiCl_2$(tmpda) is a Ni analogue to $CoCl_2$(tmeda) but with a slightly different adduct forming ligand. The tmeda ligand was found to be unsuitable for Ni, as it led to the formation of ion pair and cluster compounds, hindering the volatility of the precursor. $NiCl_2$(tmpda), on the other hand, exhibited high volatility and good thermal stability, thus being suitable for ALD. The TG curve measured for $NiCl_2$(tmpda) in vacuum is presented in Figure 26.[IV] The synthesis for $NiCl_2$(tmpda) was slightly more complicated than that of $CoCl_2$(tmeda); the compound was prepared by using a threefold excess of the amine, and the solution had to be refluxed for three hours. Still, the synthesis of $NiCl_2$(tmpda) can be considered to be easy and fast. Given the easy synthesis, the low cost of the constituents, and a high synthetic yield of 92.3%, $NiCl_2$(tmpda) is also an inexpensive and highly attractive precursor also for large-scale production.

Since $NiCl_2$(tmpda) is almost analogous to $CoCl_2$(tmeda), it was first combined with water to deposit NiO at 200–280 °C. Surprisingly, no film was deposited within the studied temperature range. The dissociation energy is slightly higher for the Ni–Cl bond than for Co–Cl, possibly explaining the difference in the reactivity of the two precursors toward water. $NiCl_2$(tmpda) could, however, be employed to deposit Ni_3N, Ni_3Sn_2, and Ni_xGe_y

films when combined with tert-butyhydrazine and the tributyl hydrides of Sn and Ge, respectively.[IV,III,V] The main results of these processes are summarized in Section 5.2.

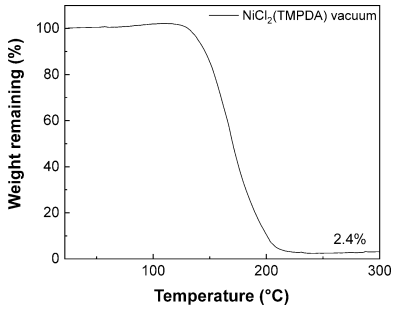

Figure 26. Vacuum TG curve for $NiCl_2$(tmpda).[IV]

5.2 New reducing agents

As could be seen from the literature survey in Chapter 3, ALD research on the late first-row transition metals has mainly focused on the development of new metal precursors. In these ALD experiments, the precursors have typically been combined with the rather inert H_2 or NH_3 gases. To supply more energy into the system, high temperatures well above 200 °C have been used. In many cases, the poor reducing power of the reactants has been compensated with plasma-enhancement.

High temperatures and plasma-enhancement make it difficult to deposit conductive sub-10 nm metal films on 3D structures. To resolve this issue, more efficient reducing agents are needed. In the past five years, many alternatives for the conventional H_2 and NH_3 have been introduced. Finding new reducing agents was also one of the key objectives of this PhD project. Tert-butylhydrazine (TBH) had been used once in Ag ALD[83] and was, in this work, employed for depositing Cu and Ni_3N films by ALD.[I,IV] Tributyltin hydride (TBTH) turned out to be highly efficient for the ALD of intermetallic Co_3Sn_2 and Ni_3Sn_2 thin films.[III] A Ge analogue, tributylgermanium hydride (TBGH), was employed in the ALD of Ni_xGe_y thin films.[V] The schematic structures of these reducing agents are displayed in Figure 27.

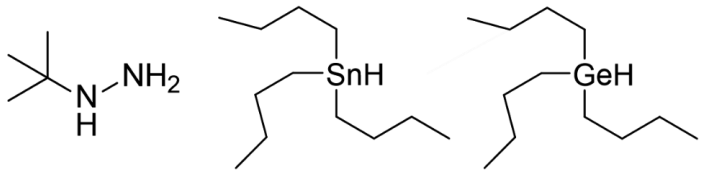

Figure 27. Schematic structures of tert-butylhydrazine, tributyltin hydride, and tributylgermanium hydride.

5.2.1 Tert-butylhydrazine

TBH was first introduced as a reducing agent in metal ALD by combining it with (hfac)Ag(1,5-cod) (cod = 1,5-cyclooctadiene) to deposit Ag thin films.[83] The use of TBH allowed low process temperatures of 100–135 °C, with a growth rate of 0.18 Å/cycle at 105–128 °C. The most significant improvement provided by TBH was the deposition of continuous, conductive Ag films. Other reducing agents used in Ag ALD, such as propan-1-ol and $BH_3(NHMe_2)$, result in the deposition of particulate, nonconductive films.[72,80,83]

In publication I, TBH was selected as the reducing agent for the ALD of Cu thin films. $Cu(dmap)_2$ was employed as the metal precursor for its high volatility. Publication IV describes the use of TBH with a new Ni precursor, $NiCl_2$(tmpda), to deposit Ni_3N films by ALD. The Ni_3N films could be reduced to Ni metal by postdeposition annealing at 150 °C in 10% forming gas. With the Cu process, pure Cu metal films were deposited, whereas with Ni the resulting films had the structure and composition of an interstitial nitride. This difference is most likely due to the difference in the reduction potentials of the two metals (Cu^{2+}/Cu^0 = +0.34 V, Ni^{2+}/Ni^0 = -0.26 V).[27] Because of its positive reduction potential, Cu(II) is easier to reduce to metal than Ni(II). The formation of a nitride is more favorable with Ni than with Cu. Accordingly, Cu_3N is more readily decomposed to metal at elevated temperatures than Ni_3N.[216] The Ni_3N process was also studied at a higher temperature as opposed to Cu. The Ni_3N films were deposited at 190–250 °C, whereas the Cu films were deposited between 80 and 140 °C. It is possible that TBH decomposes at the higher temperatures leading to the incorporation of nitrogen into the growing Ni films.

Although the Cu and Ni_3N processes were studied at quite different temperature ranges, both processes exhibited increasing growth rates with increasing temperature (Figures 28a and b).[I,IV] The growth rate of the nitride process remained constant from 200 to 210 ºC. The absence of the so-called ALD temperature window is common in metal ALD and is not necessarily an indication of inferiority of the process. Constant growth rate regimes have been obtained for other Cu processes using $Cu(dmap)_2$ and also for the Ag process employing TBH as the reducing agent.[48,81,83,93] The differences may arise from different reactor designs; the substrates in an F-120 reactor are facing each other only a few millimeters apart, allowing multiple collisions between the precursors and the substrate surfaces. At higher temperatures, the number of collisions increases, resulting in more surface reactions and possibly a higher growth rate.

Saturation of the growth rate was observed in both processes with respect to the metal precursor as well as the reducing agent pulse times (Figures 28c and d).[I,IV] A saturative growth rate of 0.15 Å/cycle was measured for Cu at 120 °C, and 0.075 Å/cycle for Ni_3N at 200 °C. For higher Ni_3N growth rates, higher deposition temperatures are needed. At 250 °C, for example, the growth rate was 0.12 Å/cycle. At this temperature, complete saturation as a function of the $NiCl_2$(tmpda) pulse time was not achieved due to partial precursor decomposition. Still, the film thickness exhibited linear dependence on the number of cycles at both temperatures (Figure 28e).[I,IV]

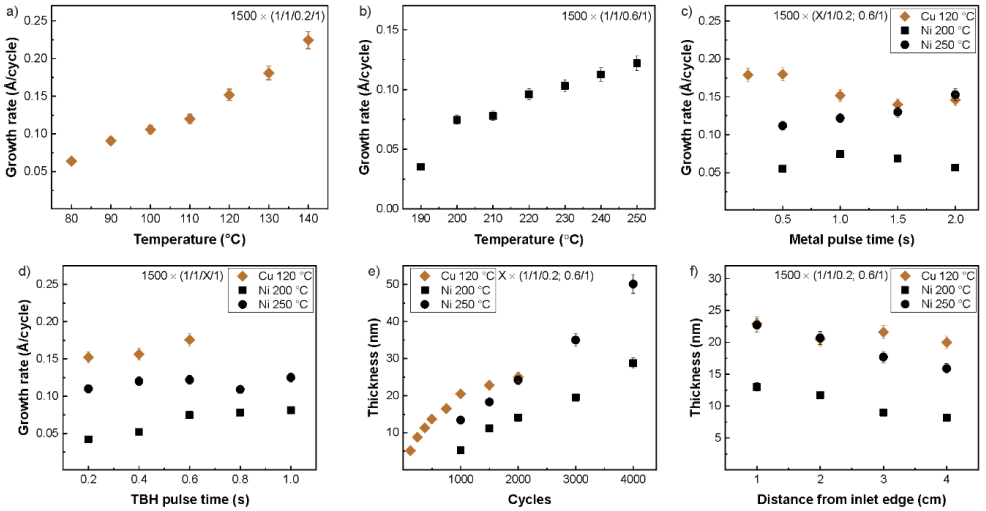

Figure 28. Growth properties of the Cu and Ni_3N processes: a) Cu and b) Ni_3N growth rate as a function of temperature, c) growth rate as a function of metal precursor and d) reducing agent pulse time, e) film thickness as a function of cycle count, and f) film thickness across the 5 cm × 5 cm substrate. The pulsing sequences in seconds are labeled in the following order: cycle count × (metal precursor pulse, purge, reducing agent pulse, and purge).[I,IV]

The Cu process showed two linear regions instead of one; the film thickness increased linearly up to 1000 cycles (0.2 Å/cycle), after which the initial substrate surface was covered, and the film growth continued with a lower growth rate (0.05 Å/cycle). When depositing on metal substrates, the growth rate of the Cu process was low throughout the deposition. A similar trend was observed also in the $[Cu(^{sBu}amd)]_2$ and H_2 process.[173] Despite the same reducing agent, the Ni_3N thickness was linearly dependent on the increasing number of cycles at 200 and 250 °C.

The Cu films deposited with $Cu(dmap)_2$ and TBH were uniform across the 5 cm × 5 cm substrates as shown in Figure 28f.[I,IV] The Ni_3N films, on the other hand, were thicker at the inlet edge and thinner at the exhaust edge of the substrate. It is typical in an F-120 ALD reactor to get a thickness profile within the first centimeter from the inlet edge. Apart from the first centimeter, the rest of the film is usually uniform. With the Ni_3N process, however, a thickness gradient was observed across the entire substrate. The nonuniformity may stem from HCl which forms when $NiCl_2$(tmpda) reacts with TBH and surface –NH groups, readsorbs downstream, and blocks surface sites from the Ni precursor. It is also possible that some surface sites are occupied by free tmpda ligands, causing the lower growth rate closer to the exhaust. Yet another possibility is that part of the $NiCl_2$ species on the surface react with the free tmpda ligands and are lost as volatile $NiCl_2$(tmpda).

Both processes produced polycrystalline films, even at the lowest deposition temperatures and with thicknesses of only a few nanometers. The Cu films were cubic, while the Ni_3N films exhibited the hcp crystal structure. The reflections of the hexagonal Ni and Ni_6N_2 are at roughly the same positions; the crystal structure of the nitride is similar to that of the

metal, apart from minor distortion caused by the interstitial nitrogen atoms.[217] With the thicker films (over 15 nm), a weak reflection corresponding solely to the nitride phase could be observed at $2\theta = 30.5°$.

The compositions of the Cu and Ni_3N films were determined by ToF-ERDA (Table 8). The impurity levels in all films were extremely low. The Cu films, in particular, were of excellent purity; the Cu content in the film bulk was as high as 99.4 at.%. Interestingly, the nitrogen content in the Cu films was below the detection limit of the ToF-ERDA instrument. Thus, the reducing power of TBH is enough to reduce the Cu precursor to pure Cu metal, but with the Ni precursor nitride films are grown instead.

Table 8. ToF-ERDA results of Cu and Ni_3N films. Surface oxidation and oxidized interfaces have been excluded from the analysis.

Element	Cu 120 °C (at.%)	Ni_3N 200 °C (at.%)	Ni_3N 250 °C (at.%)
M	99.4	73.6	75.2
N	-	23.3	21.7
H	0.3	1.5	0.8
C	0.08	0.8	1.4
O	0.2	0.7	0.9
Cl	-	0.07	0.04

Owing to the high purity of the Cu films, a remarkably low resistivity of 1.9 μΩcm was measured for a 54 nm thick film. This is the lowest resistivity reported for a true Cu ALD process. The bulk value for Cu resistivity is 1.7 μΩcm. Solanki et al. also measured low resistivity values (1.78 μΩcm) for their films deposited using $Cu(hfac)_2$ and formaldehyde but showed no ALD characteristics for the process.[74] In spite of the nitride component, the Ni_3N films were also highly conductive, and the lowest resistivity obtained was 37 μΩcm (30 nm). The resistivity is lower than what has been obtained for NiN_x films deposited with CVD or PVD methods.[218,219] Although the result is far from the bulk resistivity of Ni metal, it is only a factor of two higher than the lowest value reported for ALD Ni metal films (18 μΩcm) achived by using $Ni(acac)_2$(tmeda) and hydrazine.[84] A low resistivity of 22 μΩcm (60 nm) was reported for the $Ni(^{tBu2}dad)_2$ + tert-butylamine process, but the measurements were done on metal substrates, possibly distorting the result.[52] In our case, critical thicknesses of 10 and 13 nm were needed for the Cu and Ni_3N films to cover the substrate surface. The Cu film was deposited at 80 °C and the Ni_3N film at 250 °C. At the critical thickness, the resistivity of Cu was 6.4 μΩcm, and that of Ni_3N was 57 μΩcm. Despite the low temperature in the Cu process, film agglomeration could not be avoided completely. In the early stages of the deposition, the films grew as separate islands that coalesced after a sufficient number of cycles. The agglomeration could, to some extent, be minimized by using metallic substrates instead of oxides.

To summarize, TBH is a highly suitable reducing agent for the ALD of Cu and Ni_3N thin films. Owing to its high reducing power, the films could be deposited at low temperatures

and on assorted substrates. Most importantly, TBH afforded low-resistivity ALD Cu and Ni_3N films, and conductive films were achieved already at thicknesses of around 10 nm.

5.2.2 Tributyltin hydride

The use of metal hydrides as reducing agents in metal ALD has been scarce, and they have not been of great interest until recently. Winter's group introduced the very first thermal ALD process for Al metal by combining $AlCl_3$ and N,N-dimethylamine ethylen N'-tertbutylamido-aluminumdihydride [AlH_2(dmetda)] at low temperatures of 100–180 °C.[97] It was speculated that the precursors undergo a ligand exchange reaction, producing a chloride analogue of the reducing agent and Al–H surface species that further decompose to Al and H_2. However, because of the high growth rate of the process (3.5 Å/cycle at 140 °C), it is more plausible that Al is obtained from both $AlCl_3$ and AlH_2(dmetda). This hypothesis is better in line with our results described in publications III and V where we combined the diamine adducts of Co(II) and Ni(II) chlorides with the tributyl hydrides of Sn and Ge to deposit intermetallic Co_3Sn_2, Ni_3Sn_2, and Ni_xGe_y films by ALD. The initial idea was to use tributyltin hydride (TBTH) to reduce the metals and scavenge the chlorine atoms from the adsorbed precursor molecules and thus deposit Co and Ni metal films. The chlorines were removed as suspected but, to our surprise, the Sn atoms remained in the films and formed intermetallic compounds with the Co and Ni atoms. This finding revealed a whole new area of ALD: the ALD of intermetallics. This same approach was then applied to the ALD of Ni_xGe_y covered in Section 5.2.3. By combining different metal hydrides with different metal precursors, processes for other types of intermetallic compounds or even pure elements, such as Sn or Ge, may be developed. The use of metal hydrides as reducing agents is definitely one of the most intriguing, growing trends in the field of metal ALD.

Intermetallic compounds are formed between two or more metals whose bonds are stronger than the bonds between the atoms of the same element.[220,221] In intermetallics, the atoms are arranged with a defined stoichiometry and crystal structure that differs from the structures of the individual metal components. In contrast, metal alloys are random mixtures of different metal atoms, typically exhibiting the crystal structure of one of the components. The films deposited using $CoCl_2$(tmeda) and TBTH had the hexagonal Co_3Sn_2 crystal structure (Figure 29a).[III] Similarly, the combination of $NiCl_2$(tmpda) and TBTH also produced the hexagonal phase of Ni_3Sn_2 (Figure 29b).[III] As can be seen from the X-ray diffractograms, both materials show reflections that cannot be attributed to either Co, Ni, or Sn. The reflection at 44.2° could correspond to Co metal and the ones at 30.6 and 43.9° to tetragonal Sn, but the rest of the characteristic reflections are missing, thus proving the intermetallic crystal structure.

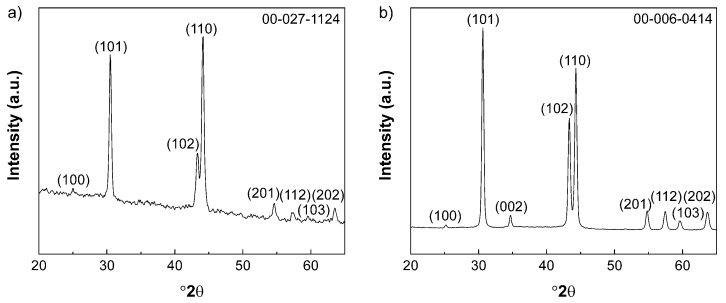

Figure 29. X-ray diffractograms for the hexagonal a) Co_3Sn_2 (87 nm) and b) Ni_3Sn_2 (127 nm) thin films deposited at 180 and 160 °C, respectively.[III]

Owing to their unique crystal structures, intermetallic compounds often exhibit unusual chemical and physical properties, such as magnetoresistance,[222,223] superconductivity,[224–226] and high catalytic activity.[227,228] Intermetallic compounds of Co–Sn and Ni–Sn with varying stoichiometry have been explored mostly for Li- and Na-ion battery anodes[229–232] but also for magnetic applications[233,234] and catalysis.[235,236] The Co_3Sn_2 films deposited using $CoCl_2$(tmeda) and TBTH were tested for their magnetic performance. Three films of different thicknesses (15, 37, and 87 nm) all showed magnetic hysteresis, the coercivity values being 320, 485, and 510 Oe in the order of increasing film thickness (Figure 30a).[III] The coercivity values shown here are much higher than what had previously been reported for Co_3Sn_2. Yi et al., for example, reported a coercivity of only 131 Oe for Co_3Sn_2 nanoparticles.[237] In our case, the high coercivity values most likely stem from the fact that the samples are in thin film form and highly crystalline as well as highly pure. According to the electrical characterization, the Co_3Sn_2 films were conductive, with the resistivity increasing with increasing film thickness (Figure 30b).[III] This somewhat contradictory behavior is caused by changes in the film composition; the Co:Sn ratio was closer to 70:30 in thinner films and 60:40 in thicker films. Based on the good magnetic and electrical performance, our Co_3Sn_2 films show promise for memory and battery applications; however, no device integration was undertaken in the course of this PhD project.

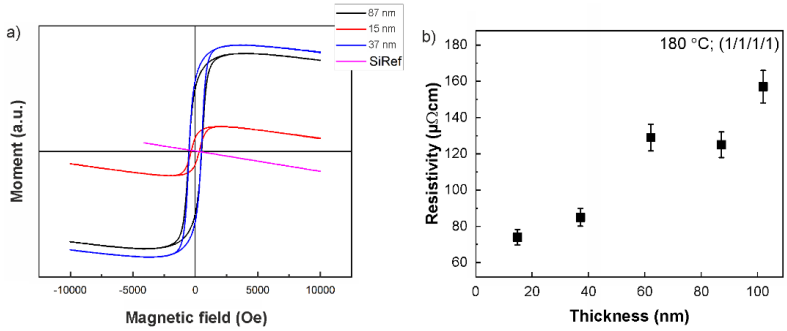

Figure 30. a) Magnetic and b) electrical properties of Co_3Sn_2 films deposited at 180 °C.[III]

TBTH turned out to be an efficient reducing agent allowing low deposition temperatures and high growth rates for both Co_3Sn_2 and Ni_3Sn_2 processes. The Co_3Sn_2 process was studied at 170–200 °C. $CoCl_2$(tmeda) is thermally stable up to a temperature of ~300 °C, but the upper limit of 200 °C was chosen to minimize agglomeration of the films and to prevent TBTH from decomposing. Because of the lower source temperature of $NiCl_2$(tmpda), the Ni_3Sn_2 films could be grown as low as 160 °C. Both processes exhibited fast deposition; the growth rates of Co_3Sn_2 at 180 °C and Ni_3Sn_2 at 160 °C were 0.9 and 1.3 Å/cycle, respectively. The growth rate of Co_3Sn_2 was shown to saturate as a function of both precursors (Figures 31a and b).[III] The process also fulfilled the other requirements for an ideal ALD process; the film thickness was uniform across the 5 cm × 5 cm substrates, and the Co_3Sn_2 films showed uniform trench fill when deposited on a textured structure.

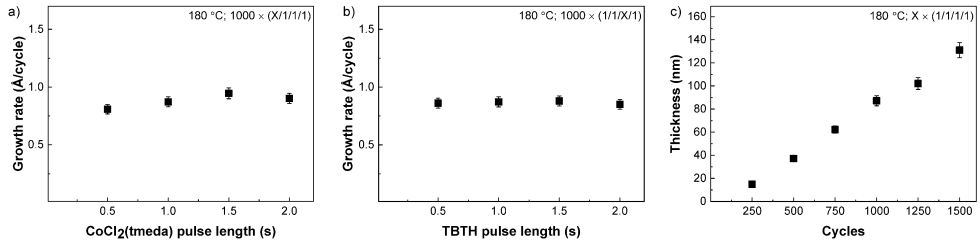

Figure 31. Growth rate of Co_3Sn_2 as a function of a) $CoCl_2$(tmeda) and b) TBTH pulse lengths. c) Co_3Sn_2 film thickness with respect to the number of deposition cycles.[III]

Figure 31c depicts how the Co_3Sn_2 film thickness increased linearly with the increasing number of ALD cycles.[III] Top-view SEM images of the films are shown in Figure 32.[III] Some nucleation delay could be observed within the first 250 cycles when the films were not yet continuous. As is often the case with metals, nucleation of the film started off as islands. Nevertheless, a continuous network of film was formed at a thickness of only 15 nm. The grain size increased with increasing thickness. Accordingly, the surface roughness also increased with increasing thickness; the R_q (root-mean-square) values of 15, 37, and 87 nm films were 4.8, 5.5, and 7.1 nm, respectively.

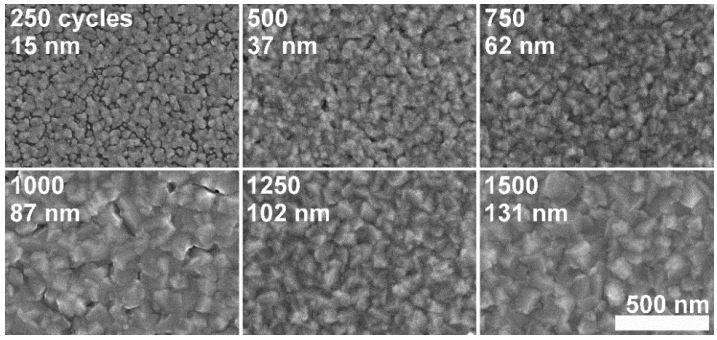

Figure 32. Top-view SEM images of Co_3Sn_2 films of different thicknesses deposited at 180 °C.[III]

Both Co_3Sn_2 and Ni_3Sn_2 films exhibited very high purity (Table 9). Interestingly, neither of the analyzed films contained any chlorine, although it was a constituent of the precursors. The high film purity indicates fast and complete reactions between the precursors. We believe that the neutral adduct forming ligands are lost upon chemisorption of the Co and Ni precursors, and only the chlorine ligands take part in the surface chemical reactions. It is expected that the chlorine atoms are removed by the butyl groups of TBTH, and volatile 1-chlorobutane and H_2 are released as byproducts. Because of the strong interaction of Co and Ni with the Sn atoms, Sn is incorporated into the film, and the intermetallic compounds are formed. Even though Co_3Sn_2 and Ni_3Sn_2 are compounds, all the metals are in a zero oxidation state as verified by XPS. Thus, TBTH indeed serves as the reducing agent in the process, though Sn is incorporated in the final product. If TBTH was combined with a metal where the M–M bonds are stronger than the M–Sn bonds, TBTH might work as a reducing agent also for the deposition of a pure metal.

Table 9. ToF-ERDA results of 131 nm Co_3Sn_2 and 127 nm Ni_3Sn_2 films.

Element	Co_3Sn_2 180 °C (at.%)	Ni_3Sn_2 160 °C (at.%)
M	64.6	59.4
Sn	33.9	38.9
H	0.41	0.6
C	0.14	0.15
N	-	0.07
O	0.85	0.95
Cl	-	-

5.2.3 Tributylgermanium hydride

Similar to tributyltin hydride, the Ge analogue, tributylgermanium hydride (TBGH), could be used to deposit Ni_2Ge thin films when combined with $NiCl_2$(tmpda).[V] The proposed mechanism for the process is the same as for the intermetallic Co_3Sn_2 and Ni_3Sn_2 films. Because of its high charge carrier mobility, Ge is making a strong comeback in microelectronics and has been proposed as an alternative for Si in future transistors.[238,239] Ni_xGe_y is a low-resistivity material potentially suitable for ohmic contacts in Ge-containing devices. Typically, Ni_xGe_y is prepared by annealing Ni films on Ge substrates.[240,241] In our case, we were able to deposit Ni_2Ge directly by low-temperature ALD. The films were deposited at 160–200 °C, and the growth rate increased with increasing temperature. Saturative growth (0.9 Å/cycle) was observed with 1.0 s $NiCl_2$(tmpda) and 1.5 s TBGH pulse lengths at 180 °C (Figures 33a and b).[V] The growth rate was faster during the initial stages of the deposition and slowed down once the Al_2O_3 surface was fully covered (Figure 33c).[V] Similar to the Co_3Sn_2 films, the Ni_2Ge films also exhibited uniform thickness across the 5 cm × 5 cm substrate.

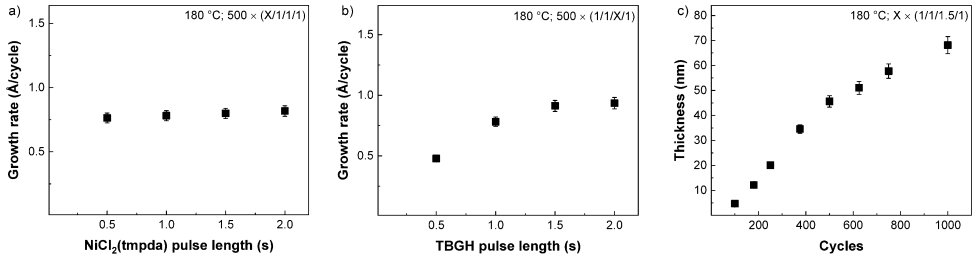

Figure 33. Growth characteristics of the Ni_2Ge ALD process: growth rate with respect to a) Ni precursor and b) TBGH pulse length, and c) film thickness as a function of cycle count.[V]

Low resistivity is a requisite for a material to be used as an electrical contact between a metal and a semiconductor. The Ni_2Ge films deposited by our process exhibited low resistivity; the lowest value was 26 μΩcm (measured for a 68 nm thick film). The result corroborates with the results of other groups; the lowest resistivities reported for Ni_xGe_y films are in the range of 17–24 μΩcm.[240–242] The resistivity of Ni_2Ge films is typically slightly higher compared to the NiGe films obtained by annealing of Ni on Ge substrates.[240] According to AFM, the Ni_2Ge films were rough; the R_q values for 15–58 nm thick films deposited at 180 ºC ranged between 5.3 and 7.9 nm. Figure 34a displays the elemental depth profiles of a 58 nm thick film measured by ToF-ERDA.[V] The total impurity content in the film bulk was only 0.95 at.%. The Ni and Ge contents in the film were 65 and 34 at.%. The Ni:Ge ratio corroborated with XRD showing reflections corresponding to the orthorhombic and hexagonal Ni_2Ge phases. (Figure 34b).[V]

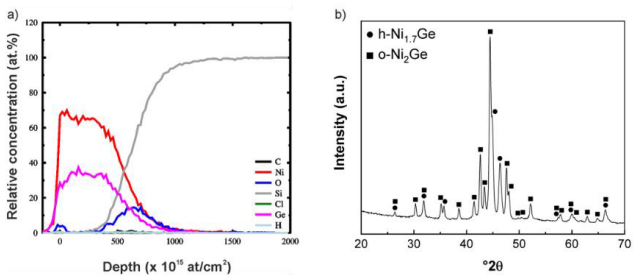

Figure 34. a) ToF-ERDA depth profiles of a 58 nm and b) X-ray diffractogram of an 80 nm Ni_2Ge film grown at 180 °C.[V]

To conclude, the tributyl hydrides of Sn and Ge turned out to be highly reactive reducing agents toward the diamine adducts of Co(II) and Ni(II) chlorides but instead of depositing pure metals, intermetallic films were formed. Co_3Sn_2 showed promising ferromagnetic behavior, but further studies are required to clarify the applicability of the process. To determine whether the Co_3Sn_2 films could be used as anodes in Li- and Na-ion batteries, their capacity should be explored. The performance of the Ni_2Ge films as ohmic contacts is also worth further investigation. It was demonstrated in paper III that Ni_3Sn_2 films could also be deposited using $Ni(dmap)_2$, showing that the reactivity of TBTH is not limited to metal halides only. Further studies using other types of Co and Ni precursors should be

carried out for both hydrides. By combining different metal precursors with new metal hydrides, the approach may be extended from films containing Sn and Ge to the ALD of other intermetallic compounds as well. Metal hydrides form an intriguing group of reducing agents, and their use in the ALD of both intermetallics and pure metals will for sure be one of the future topics in the field of ALD.

5.3 Indirect approach to metal ALD

This work also explored the indirect approach for obtaining Co and Ni metals.[II,IV] Co films were prepared by postdeposition reduction of CoO films deposited using $CoCl_2$(tmeda) and water at 275 °C. The details of the CoO process were summarized in Section 5.1.1 and more explicitly in paper II. The reduction studies were performed in 10% forming gas close to atmospheric pressure. First, the onset temperature for the reduction was determined with HTXRD on a 50 nm CoO film deposited on native oxide-terminated Si. The reduction began at an exceptionally low temperature of 250 °C. Although the reduction temperature in HTXRD (250 °C) was below the deposition temperature of the CoO film (275 °C), Co metal films could not be deposited directly by a three-step ALD process comprising $CoCl_2$(tmeda), water, and H_2. The reason for this is the difference in the partial pressures of H_2; the pressure in the HTXRD studies is about 10% of atmospheric pressure (100 mbar), whereas in the ALD reactor the partial pressure of H_2 is only 0.1 mbar.

To suppress the agglomeration of the resulting Co film, most of the reduction studies were done on TiN substrates. TiN is a relevant material for Co and Cu as it is often used as a barrier layer in interconnects. Furthermore, TiN is metallic, which lowers the interface energy and minimizes agglomeration. The CoO morphology was different on TiN than on Si with the native oxide; the film on TiN was dense and uniform, whereas the film on Si comprised higher pyramid-like grains embedded in a smoother layer (Figure 35).[II] The differences appear to stem from the fact that the film on TiN exhibited only the cubic phase of CoO, while the film on Si was a mixture of both hexagonal and cubic phases. The better uniformity on TiN was expected to facilitate the reduction of the oxide into a continuous metal film.

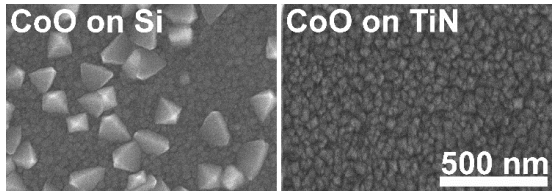

Figure 35. CoO deposited at 275 °C on Si with the native oxide (50 nm) and on TiN (68 nm).[II]

Figure 36 depicts SEM images of reduced Co metal films of different thicknesses on TiN. The thicknesses of the metal films were 50–58% of the original oxide thicknesses. The

thickness differences are a direct result of the shrinkage of the films caused by the density change; the bulk density of CoO is 6.4 and that of Co 8.9 g/cm^3. The thicker the original CoO film, the better the continuity of the reduced Co film was. Full coverage of the TiN substrate was not, however, obtained even with 50 nm Co thickness, as the film still had some voids. A film of only 15 nm thickness formed a continuous network of Co, albeit surrounded by voids. Owing to the high purity of the CoO films (Section 5.1.1), the reduced Co metal films were also of high purity. The Co content of a 50 nm Co film was 95 at.%, with the rest being oxygen (3 at.%) and hydrogen (2 at.%). The oxygen content might have been even lower with a longer reduction time than the 45 minutes used here.

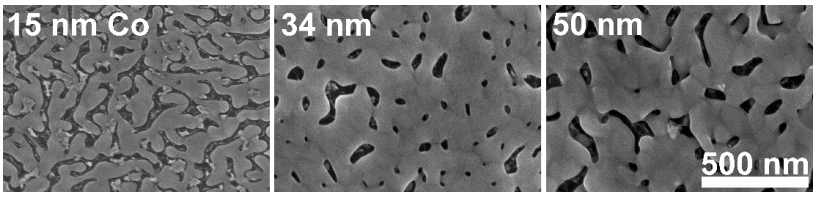

Figure 36. Reduced Co films of different thicknesses on TiN. The original CoO thicknesses were 27, 68, and 89 nm.[II]

In addition to the reduction of CoO to Co metal films, the indirect approach was also applied to reduce Ni_3N films to Ni metal.[IV] The postdeposition reduction was performed at 150 °C in 10% forming gas. Without a reducing agent, a higher temperature of 300 °C was required for decomposing the nitride to a metal. Corroborating results are found in the literature.[216,218,243] After the reduction, the nitrogen content in the film deposited at 200 °C was lowered from 23.3 at.% down to 1.2 at.%. The Ni content was as high as 92.5 at.%. Unlike the diamagnetic Ni_3N films, the reduced Ni metal films exhibited ferromagnetic behavior, with the coercivity being 30 Oe. In the future, it would be interesting to examine whether Ni metal films could be deposited directly by adding a pulse of H_2 after TBH.

5.4 Unpublished results

During this PhD project, a wide range of precursor combinations was tested for Co, Ni, and Cu ALD. Although only a handful of combinations proved to be successful, valuable information can be gained from the other experiments as well. Table 10 lists all the unpublished results obtained in the course of this research. Along with the precursor combinations and relevant experimental details, some comments regarding the outcome are provided. In most cases, no film whatsoever or only a very thin layer of material was deposited. The experiments were typically carried out with 1000 ALD cycles on native oxide-terminated Si and soda lime glass substrates. Initial trials were usually executed with 1.0 s pulse and purge times except when TBH was used as the reducing agent, and the pulse length was 0.2 s. Figure 37 depicts the schematic structures of the metal precursors and reducing agents not shown previously in this thesis. The origin of the precursor is given

below the structure unless considered as a widely available commercial chemical. A precursor is marked as ‘new’ if not employed in ALD before.

Metal precursors

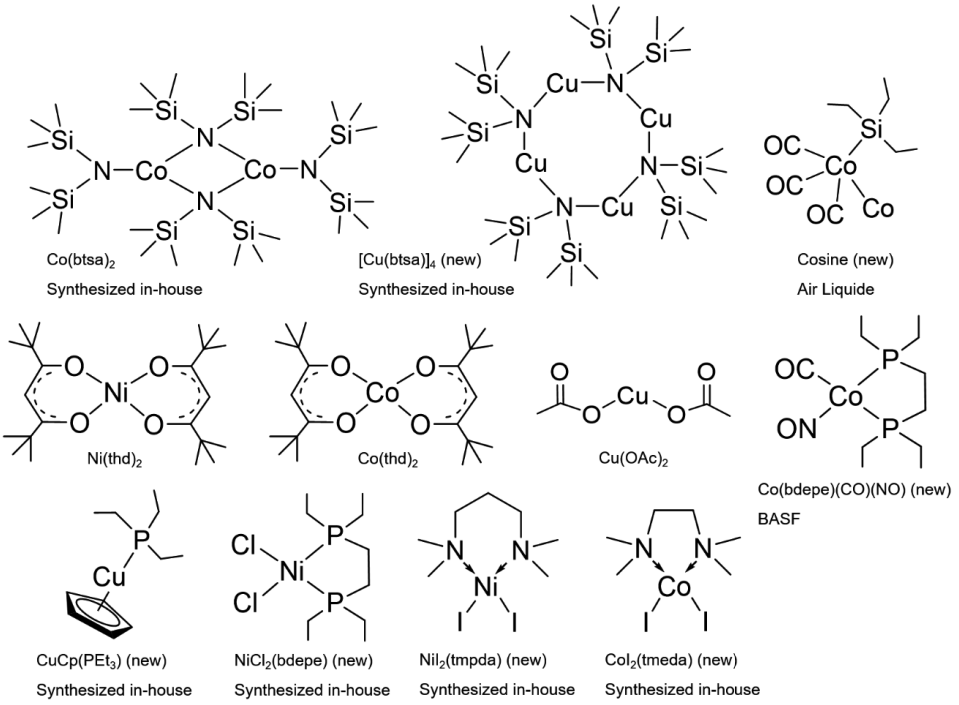

Reducing agents

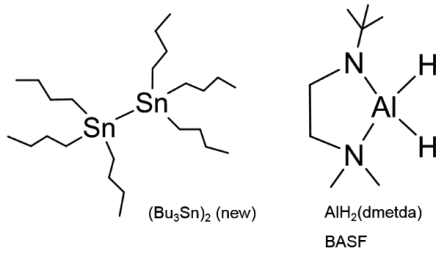

Figure 37. Metal precursors and reducing agents tested but not published during this PhD project.

Table 10. Unpublished results related to Co, Ni, and Cu ALD in chronological order starting from the oldest experiments.

Material	Precursors	Substrates	$T_{dep.}$ (°C)	Comments
Co	$Co(btsa)_2 + BH_3(NHMe_2)$	Si, glass, Al_2O_3, Ru	150–225	Nonmetallic, nonuniform deposit at 225 °C
Co	$Co(btsa)_2 + H_2O + BH_3(NHMe_2)$	Si, glass	150	Only oxide
Co	$Co(btsa)_2$ + HCOOH	Si, glass, Ru	180–225	Very thin metal film
Cu	$[Cu(btsa)]_4 + BH_3(NHMe_2)$	Si, glass, Al_2O_3, Ru	160–200	Thin, nonuniform Cu film
Cu	$[Cu(btsa)]_4$ + HCOOH	Si, glass, Al_2O_3, Ru	200–225	11 nm uniform Cu film on Ru, no deposition without HCOOH
Co	$Co(btsa)_2$ + TBH	Si, glass, Ru	150–200	Uncontrolled, nonuniform rainbow-colored film
Co	$Co(^{tBu2}dad)_2$ + TBH	Si, glass, Ru	150	No deposition
Co	Cosine + TBH	Si, glass, Ru, Cu	120	No deposition
Co	Cosine + $BH_3(NHMe_2)$	Si, glass, Ru, Au	120	No deposition
Co	Cosine + HCOOH	Si, glass, Ru, Au	120–140	Thin Co film with high HCOOH consumption with 1500 cy, metallic inlet edge (10 nm) at 140 °C
Co	$Co(thd)_2$ + TBH	Si, glass	200	No deposition
Ni	$Ni(Cp)_2$ + TBH	Si, glass	160	No deposition
Ni	$Ni(thd)_2$ + TBH	Si, glass	250	6 nm Ni or Ni_3N film with 1000 cy
Ni	$Ni(dmap)_2$ + TBH	Si, glass	120–170	No deposition at 120 °C, 3 nm Ni or Ni_3N at 150 °C and 7 nm at 170 °C with 1000 cy
Co	Co(bdepe)(CO)(NO) + TBH	Si, glass	250–325	Thin, nonconductive Co film with or without TBH; 4 nm at 275 °C, 8 nm at 300 °C and 16 nm at 325 °C with 1000 cy
Co	Co(bdepe)(CO)(NO) + $BH_3(NHMe_2)$	Si, glass, Ru	200–250	No deposition
CoO_x	Co(bdepe)(CO)(NO) + H_2O	Si, glass	250	No deposition
Cu	$Cu(thd)_2$ + TBH	Si, glass	150–220	3 nm Cu film at 150 °C, 9 nm at 180 °C, and 10 nm at 220 °C with 1000 cy
Cu	$Cu(acac)_2$ + TBH	Si, glass	200	Very thin Cu film with 1000 cy
Cu	$Cu(hfac)_2$ + TBH	Si, glass	200	Very thin film
Cu	$Cu(OAc)_2$ + TBH	Si, glass	190	No deposition
Cu	$Cu(OAc)_2 + (H_2O)$ + TBH	Si, glass	190–200	No metal deposition
Cu	$Cu(OAc)_2 + BH_3(NHMe_2)$	Si, glass, Ru	180–200	Strong profile, droplet formation in air; etching verified by pulsing $Cu(OAc)_2$ over Cu metal
Co	$Co(Cp)_2$ + TBH	Si, glass	300	No deposition
Cu	$CuCp(PEt_3)$ + TBH	Si, glass	150	Nanoparticles
Co	$CoCl_2(tmeda) + BH_3(NHMe_2)$	Si, glass, Ru	200–300	Thin Co film with 1000 cy, no improvement with 1500 cy
Co	$CoCl_2(tmeda)$ + TBH	Si, glass	200–300	Thin, nonuniform Co film at 275 and 300 °C (1000 cy)
Co	$CoCl_2(tmeda) + H_2$	Si, glass	275–300	No deposition
Co	$CoCl_2(tmeda) + (Bu_3Sn)_2$	Si, glass	275	Uncontrolled, nonuniform Co–Sn film with 1000 cy
Co	$CoCl_2(tmeda) + H_2O + H_2$/TBH	Si, glass	275	Only oxide
Ni	$NiCl_2(bdepe)$ + TBH	Si, glass	280	No deposition
Ni	$NiCl_2(bdepe) + H_2$	Si, glass	280	No deposition

NiO	$NiCl_2$(bdepe) + H_2O	Si, glass	280–320	No oxide deposition, decomposition at 320 °C
NiO	$NiCl_2$(tmpda) + H_2O	Si, glass	200–280	No deposition
Ni	$NiCl_2$(tmpda) + $BH_3(NHMe_2)$	Si, glass	160–200	Ni_2B deposition (ToF-ERDA), no ALD characteristics
Ni_3Sn_2	$Ni(dmap)_2$ + TBTH	Si, glass	130–160	Deposition with high growth rate, no saturation at 160 °C
Ni	NiI_2(tmpda) + TBH	Al_2O_3	200–220	No deposition
Co	CoI_2(tmeda) + TBH	Al_2O_3	220–280	Metallic inlet edge at 250 °C, XRD showed CoN_x
Co	$CoCl_2$(tmeda) + TBGH	Si, glass	180–250	Milky, nonuniform Co–Ge growth
Ni	$NiCl_2$(tmpda) + AlH_2(dmetda)	Si, glass	180–220	Thin, brownish film. Thicker at 220 °C
Co	$CoCl_2$(tmeda) + AlH_2(dmetda)	Si, glass	180	Thin, nonuniform, brownish film

6 Conclusions

The main motivation behind this PhD project was to find solutions for the challenges facing the microelectronics industry by developing new ALD processes for the late first-row transition metals, namely Co, Ni, and Cu. A myriad of new metal precursors was evaluated to deposit high-quality metal thin films that would match the requirements set for the modern interconnect and memory structures. More efficient alternatives for H_2 and NH_3 were sought to enable reduction at lower temperatures, thus promoting the deposition of thin yet continuous metal films. ALD was selected as the deposition method to ensure film uniformity in terms of thickness, composition, and quality even in the most demanding 3D structures.

This thesis described, for the first time, the use of diamine adducts of metal(II) halides as precursors for the ALD of metals, metal nitrides, metal oxides, and intermetallic compounds. New ALD processes were developed for Ni_3N, CoO, Co_3Sn_2, Ni_3Sn_2, and Ni_2Ge thin films. Ni and Co metal films were obtained by postdeposition reduction of the Ni_3N and CoO films. Both $CoCl_2$(tmeda) and $NiCl_2$(tmpda) are versatile precursors with high volatility and thermal stability. Chlorine was incorporated into the films only in small amounts (below 1.0 at.%) if at all. As simple and inexpensive compounds, the diamine adducts of metal(II) halides would make good precursors for others to test both in the ALD research community and in industry. In addition to the indirect approach, the deposition of Co and Ni metals should still be explored by direct ALD using new reducing agents and conventional H_2 and NH_3 plasmas.

$CoCl_2$(tmeda) is one out of four Co ALD precursors that reacts with water and deposits exclusively Co(II) oxide. When deposited at 275 °C, the films exhibited 1:1 Co:O stoichiometry. On Si with the native oxide, the films were a mixture of cubic and hexagonal CoO, whereas on TiN substrates cubic CoO was deposited. The CoO films could be fully reduced to Co metal at 250 °C in 10% forming gas. The reduced Co films were of high purity but suffered from agglomeration. Further studies should be carried out to improve the continuity of the films. Or even better, more effort should be put on developing a low-temperature ALD process for Co, inherently minimizing the agglomeration. Because oxides were not in the focal point of this thesis, and the CoO process was developed essentially to study the properties of $CoCl_2$(tmeda), no thorough characterization was done in terms of the applicability of the CoO films. In the future, the films could be studied for their performance in photocatalysis and Li-ion batteries.

In addition to new metal precursors, this thesis also focused on finding more efficient reducing agents to, first of all, enable the ALD of metals, and further, to enable growth at low temperatures. TBH, an under-used reducing agent in ALD, was employed to develop new processes for the ALD of Cu and Ni_3N using $Cu(dmap)_2$ and $NiCl_2$(tmpda) as the metal precursors. The Cu films could be deposited at low temperatures of 80–140 °C, and the Ni_3N films at 190–250 °C. Both processes showed saturative growth rates with respect to

both the metal precursor and TBH. The Cu process also exhibited excellent film uniformity and conformality, and the Ni_3N process showed a linear increase of film thickness as a function of increasing cycle count. The Cu films were of remarkably high purity, with the Cu content in the film bulk exceeding 99.4 at.%. The resistivity of a 50 nm film was as low as 1.9 μΩcm. Despite being a nitride instead of a pure metal, the Ni_3N films had a resistivity of 37 μΩcm at the lowest. This is lower than what has been observed for CVD or PVD Ni_3N and only a factor of two higher than the lowest resistivity reported for ALD Ni metal.

Other powerful reducing agents introduced in this thesis were the tributyl hydrides of Sn and Ge. Tributyltin hydride (TBTH) was combined with $CoCl_2$(tmeda) and $NiCl_2$(tmpda) to deposit intermetallic Co_3Sn_2 and Ni_3Sn_2 compounds. This was the first time TBTH was used in ALD, and the first time intermetallics were deposited by a direct ALD process. The processes were studied at low temperatures below 200 °C. A full ALD study on the Co_3Sn_2 process showed saturative growth, film thickness linearity with respect to the number of ALD cycles, excellent uniformity, and conformal coverage of a trench structure. Both processes afforded high-purity films, with the metals having a zero oxidation state. Owing to the specific, intermetallic crystal structure, the Co_3Sn_2 films showed magnetic hysteresis with coercivity values exceeding 500 Oe. An analogous process was developed for Ni_2Ge films using tributylgermanium hydride and $NiCl_2$(tmpda) as precursors. The films exhibited low resistivity (26 μΩcm) and may thus work as ohmic contacts in Ge-containing transistors. By combining volatile metal hydrides with different metal precursors, the approach presented here could potentially be extended from Co_3Sn_2, Ni_3Sn_2, and Ni_2Ge to other materials as well. Metal hydrides could have a significant impact in the field of ALD, not only for depositing intermetallics but also for obtaining pure metal films.

As this thesis mainly focused on the fundamental part of materials research, that is, developing new precursors and processes for the ALD of the late first-row transition metals, the next logical pathway would be to implement the discovered processes into making actual device structures. The performance of the Cu films could be tested in interconnects, for example. Both the reduced Ni and the intermetallic films might be suitable for magnetic applications, including memory devices. The intermetallic Co_3Sn_2 and Ni_3Sn_2 films are also potential candidates as anode materials for Li- and Na-ion batteries. Finally, the Ni_xGe_y films could be studied as ohmic contacts in Ge-containing devices. The processes presented in this thesis cover many of the topical challenges facing the microelectronics industry. Evidently, ALD is in the center of tackling these challenges, but only time will tell whether the processes studied here will provide actual solutions. In the meantime, research on new precursors and processes for the ALD of the late first-row transition metals should be continued.

References

(1) D. Reinsel, J. Gantz, J. Rydning. The Digitization of the World – From Edge to Core. In *IDC's Data Age 2025 whitepaper, sponsored by Seagate*, 2018; https://www.seagate.com/files/www-content/our-story/trends/files/idc-seagate-dataage-whitepaper.pdf (accessed January, 2019).

(2) Computer History: The Storage Engine. http://www.computerhistory.org/storage engine/first-commercial-hard-disk-drive-shipped/ (accessed September, 2018).

(3) P. C. Andricacos, C. Uzoh, J. O. Dukovic, J. Horkans, H. Deligianni, *IBM J. Res. Develop.* **1998**, *42*, 567.

(4) R. C. Johnson. IBM: Copper Interconnects Here to Stay. In *EETimes*, 2017; https://www.eetimes.com/document.asp?doc_id=1332609# (accessed March, 2018).

(5) C. S. Hau-Riege, *Microelectron. Reliab.* **2004**, *44*, 195.

(6) R. Jakkaraju. RC Delay: Bottleneck to Scaling. In *Semiconductor Engineering*, 2016; http://semiengineering.com/rc-delay-bottleneck-to-scaling/ (accessed December, 2018).

(7) S. Jones. IEDM 2018 Imec on Interconnect Metals Beyond Copper. In *SemiWiki.com*, 2018; https://www.semiwiki.com/forum/content/7923-iedm-2018-imec-interconnect-metals-beyond-copper.html (accessed January, 2019).

(8) M. Lapedus. Interconnect Challenges Grow. In *Semiconductor Engineering*, 2015; http://semiengineering.com/interconnect-challenges-grow-2/ (accessed February, 2018).

(9) A. H. Simon, T. Bolom, C. Niu, F. H. Baumann, C.-K. Hu, C. Parks, J. Nag, H. Kim, J. Y. Lee, C.-C. Yang, S. Nguyen, H. K. Shobha, T. Nogami, S. Guggilla, J. Ren, D. Sabens, J. F. AuBuchon. In *Electromigration Comparison of Selective CVD Cobalt Capping with PVD Ta(N) and CVD Cobalt Liners on 22nm-Groundrule Dual-Damascene Cu Interconnects*, Proceedings of the IEEE International Reliability Physics Symposium, Anaheim, CA, USA, 14–18 April, 2013.

(10) T. Nogami, M. He, X. Zhang, K. Tanwar, R. Patlolla, J. Kelly, D. Rath, M. Krishnan, X. Lin, O. Straten, H. Shobha, J. Li, A. Madan, P. Flaitz, C. Parks, C.-K. Hu, C. Penny, A. Simon, T. Bolom, J. Maniscalco, D. Canaperi, T. Spooner, D. Edelstein. In *CVD-Co/Cu(Mn) Integration and Reliability for 10 nm Node*, Proceedings of the IEEE International Interconnect Technology Conference, Kyoto, Japan, 13–15 June, 2013.

(11) W. He, J. Kang, J. Luo, G. Wu, L. Zhang, *ECS Trans.* **2014**, *60*, 471.

(12) D. James. IEDM 2017: Intel's 10nm Platform Process. In *Solid State Technology*, 2017; http://electroiq.com/chipworks_real_chips_blog/2017/12/18/iedm-2017-intels-10nm-platform-process/ (accessed February, 2018).

(13) D. Gall, *J. Appl. Phys.* **2016**, *119*, 085101.

(14) K. Croes, C. Adelmann, C. J. Wilson, H. Zahedmanesh, O. Varela Pedreira, C. Wu,

A. Leśniewska, H. Oprins, S. Beyne, I. Ciofi, D. Kocaay, M. Stucchi, Z. Tőkei. In *Interconnect Metals Beyond Copper: Reliability Challenges and Opportunities*, Proceedings of the IEEE International Electron Devices Meeting, San Francisco, CA, USA, 1–5 Dec., 2018.

(15) J. A. Kittl, A. Lauwers, O. Chamirian, M. Van Dal, A. Akheyar, M. De Potter, R. Lindsay, K. Maex, *Microelectron. Eng.* **2003**, *70*, 158.

(16) S.-L. Zhang, M. Östling, *Crit. Rev. Solid State Mater. Sci.* **2003**, *28*, 1.

(17) P. Kumar, *Nanoscale Res. Lett.* **2010**, *5*, 1596.

(18) D. Chiba, S. Fukami, K. Shimamura, N. Ishiwata, K. Kobayashi, T. Ono, *Nat. Mater.* **2011**, *10*, 853.

(19) F. Tabrizi. The Future of Scalable STT-RAM as a Universal Embedded Memory. In *Embedded*, 2007; https://www.embedded.com/design/real-time-and-performance /4026000/The-future-of-scalable-STT-RAM-as-a-universal-embedded-memory (accessed November, 2018).

(20) STT-MRAM: Introduction and Market Status. https://www.mram-info.com/stt-mram (accessed December, 2018).

(21) T. Suntola, J. Antson, U.S. Patent 4,058,430, 1977.

(22) T. Suntola, *Mater. Sci. Rep.* **1989**, *4*, 261.

(23) M. T. Bohr, R. S. Chau, T. Ghani, K. Mistry, *IEEE Spectrum* **2007**, *44*, 29.

(24) M. Ritala, M. Leskelä. Atomic Layer Deposition. In *Handbook of Thin Film Materials*; H. S. Nalwa, Ed.; Academic Press: San Diego, USA, 2002; pp 103.

(25) M. Ritala, J. Niinistö. Atomic Layer Deposition. In *Chemical Vapour Deposition: Precursors, Processes and Applications*; A. C. Jones, M. L. Hitchman, Eds.; Royal Society of Chemistry: Cambridge, U.K., 2009; pp 158.

(26) S. M. George, *Chem. Rev.* **2010**, *110*, 111.

(27) J. R. Rumble, Ed., *CRC Handbook of Chemistry and Physics*, 99th Edition (Internet Version 2018), CRC Press/Taylor & Francis: Boca Raton, FL, USA.

(28) E. A. Owen, D. M. Jones, *Proc. Phys. Soc.* **1954**, *67*, 456.

(29) C. Auth, A. Aliyarukunju, M. Asoro, D. Bergstrom, V. Bhagwat, J. Birdsall, N. Bisnik, M. Buehler, V. Chikarmane, G. Ding, Q. Fu, H. Gomez, W. Han, D. Hanken, M. Haran, M. Hattendorf, R. Heussner, H. Hiramatsu, B. Ho, S. Jaloviar, I. Jin, S. Joshi, S. Kirby, S. Kosaraju, H. Kothari, G. Leatherman, K. Lee, J. Leib, A. Madhavan, K. Marla, H. Meyer, T. Mule, C. Parker, S. Parthasarathy, C. Pelto, L. Pipes, I. Post, M. Prince, A. Rahman, S. Rajamani, A. Saha, J. Dacuna Santos, M. Sharma, V. Sharma, J. Shin, P. Sinha, P. Smith, M. Sprinkle, A. St. Amour, C. Staus, R. Suri, D. Towner, A. Tripathi, A. Tura, C. Ward, A. Yeoh. In *A 10nm High Performance and Low-Power CMOS Technology Featuring 3rd Generation FinFET Transistors, Self-Aligned Quad Patterning, Contact Over Active Gate and Cobalt Local Interconnects*, Proceedings of the IEEE International Electron Devices Meeting, San Francisco, CA, USA, 2–6 Dec., 2017.

(30) L. Zhao. All About Interconnects. In *Semiconductor Engineering*, 2017; https://semiengineering.com/all-about-interconnects/ (accessed September, 2018).

(31) P. McLellan. IEDM: The World After Copper. In *Breakfast Bytes Blogs*, 2019; https://community.cadence.com/cadence_blogs_8/b/breakfast-bytes/posts/iedm18-interconnect (accessed January, 2019).

(32) J. P. Gambino, E. G. Colgan, *Mater. Chem. Phys.* **1998**, *52*, 99.

(33) H. Kim, *Microelectron. Eng.* **2013**, *106*, 69.

(34) A. Makarov, V. Sverdlov, S. Selberherr. In *New Trends in Microelectronics: Towards an Ultimate Memory Concept*, Proceedings of the 8th International Caribbean Conference on Devices, Circuits and Systems, Playa del Carmen, Mexico, 14–17 March, 2012.

(35) P. Chi, S. Li, Y. Cheng, Y. Lu, S. H. Kang, Y. Xie. In *Architecture Design with STT-RAM: Opportunities and Challenges*, Proceedings of the 21st Asia and South Pacific Design Automation Conference, Macau, China, 25–28 Jan., 2016.

(36) V. Miikkulainen, M. Leskelä, M. Ritala, R. L. Puurunen, *J. Appl. Phys.* **2013**, *113*, 021301.

(37) T. Hatanpää, M. Ritala, M. Leskelä, *Coord. Chem. Rev.* **2013**, *257*, 3297.

(38) S. E. Koponen, P. G. Gordon, S. T. Barry, *Polyhedron* **2016**, *108*, 59.

(39) J. P. Coyle, G. Dey, E. R. Sirianni, M. L. Kemell, G. P. A. Yap, M. Ritala, M. Leskelä, S. D. Elliott, S. T. Barry, *Chem. Mater.* **2013**, *25*, 1132.

(40) B. S. Lim, A. Rahtu, J.-S. Park, R. G. Gordon, *Inorg. Chem.* **2003**, *42*, 7951.

(41) T. J. Knisley, M. J. Saly, M. J. Heeg, J. L. Roberts, C. H. Winter, *Organometallics* **2011**, *30*, 5010.

(42) T. Blanquart, J. Niinistö, M. Ritala, M. Leskelä, *Chem. Vap. Deposition* **2014**, *20*, 189.

(43) A. U. Mane, S. A. Shivashankar, *Mater. Sci. Semicond. Process.* **2004**, *7*, 343.

(44) A. U. Mane, S. A. Shivashankar, *J. Cryst. Growth* **2005**, *275*, e1253.

(45) B. S. Lim, A. Rahtu, R. G. Gordon, *Nat. Mater.* **2003**, *2*, 749.

(46) W.-H. Kim, H.-B.-R. Lee, K. Heo, Y. K. Lee, T.-M. Chung, C.-G. Kim, S. Hong, J. Heo, H. Kim, *J. Electrochem. Soc.* **2011**, *158*, D1.

(47) S. W. Ryu, J. Yoon, H.-S. Moon, B. Shong, H. Kim, H.-B.-R. Lee, *Nanotechnology* **2017**, *28*, 115301.

(48) L. C. Kalutarage, S. B. Clendenning, C. H. Winter, *Chem. Mater.* **2014**, *26*, 3731.

(49) J. P. Klesko, M. M. Kerrigan, C. H. Winter, *Chem. Mater.* **2016**, *28*, 700.

(50) M. M. Kerrigan, J. P. Klesko, S. M. Rupich, C. L. Dezelah, R. K. Kanjolia, Y. J Chabal, C. H. Winter, *J. Chem. Phys.* **2017**, *146*, 052813.

(51) M. M. Kerrigan, J. P. Klesko, C. H. Winter, *Chem. Mater.* **2017**, *29*, 7458.

(52) M. M. Kerrigan, J. P. Klesko, K. J. Blakeney, C. H. Winter, *ACS Appl. Mater. Interfaces* **2018**, *10*, 14200.

(53) A. Jain, K. M. Chi, T. T. Kodas, M. J. Hampden-Smith, J. D. Farr, M. F. Paffett, *Chem. Mater.* **1991**, *3*, 995.

(54) M. T. Mocella, *J. Fluor. Chem.* **2003**, *122*, 87.

(55) T. C. Wang, T. E. Hsieh, M.-T. Wang, D.-S. Su, C.-H. Chang, Y. L. Wang, J. Y. Lee, *J. Electrochem. Soc.* **2005**, *152*, G45.

(56) S. Konishi, M. Moriyama, M. Murakami, *Mater. Trans.* **2002**, *43*, 1624.

(57) L.-A. Cao, X.-P. Qu. In *The Oxygen Barrier Properties of Co_xMo_y Diffusion Barrier for Cu Interconnect*, Proceedings of the IEEE International Interconnect Technology Conference / Advanced Metallization Conference, San Jose, CA, USA, May 23–26, 2016.

(58) T. Aaltonen, P. Alén, M. Ritala, M. Leskelä, *Chem. Vap. Deposition* **2003**, *9*, 45.

(59) T. Aaltonen, M. Ritala, T. Sajavaara, J. Keinonen, M. Leskelä, *Chem. Mater.* **2003**, *15*, 1924.

(60) T. Aaltonen, M. Ritala, V. Sammelselg, M. Leskelä, *J. Electrochem. Soc.* **2004**, *151*, G489.

(61) J. Hämäläinen. Atomic Layer Deposition of Noble Metal Oxide and Noble Metal Thin Films. PhD Thesis. University of Helsinki, 2013.

(62) H. B. Profijt, S. E. Potts, M. C. M. van de Sanden, W. M. M. Kessels, *J. Vac. Sci. Technol. A* **2011**, *29*, 050801.

(63) H. Kim, I.-K. Oh, *Jpn. J. Appl. Phys.* **2014**, *53*, 03DA01.

(64) PEALD Publication Database. https://www.plasma-ald.com/ (accessed October, 2018).

(65) J. W. Klaus, S. J. Ferro, S. M. George, *Appl. Surf. Sci.* **2000**, *162–163*, 479.

(66) J. W. Elam, C. E. Nelson, R. K. Grubbs, S. M. George, *Surf. Sci.* **2001**, *479*, 121.

(67) R. K. Grubbs, C. E. Nelson, N. J. Steinmetz, S. M. George, *Thin Solid Films* **2004**, *467*, 16.

(68) R. K. Grubbs, N. J. Steinmetz, S. M. George, *J. Vac. Sci. Technol. B* **2004**, *22*, 1811.

(69) S.-H. Kim, E.-S. Hwang, B.-M. Kim, J.-W. Lee, H.-J. Sun, T. E. Hong, J.-K. Kim, H. Sohn, J. Kim, T.-S. Yoon, *Electrochem. Solid-State Lett.* **2005**, *8*, C155.

(70) S.-H. Kim, N. Kwak, J. Kim, H. Sohn, *J. Electrochem. Soc.* **2006**, *153*, G887.

(71) M. Mäkelä, T. Hatanpää, M. Ritala, M. Leskelä, K. Mizohata, K. Meinander, J. Räisänen, *J. Vac. Sci. Technol. A* **2017**, *35*, 01B112.

(72) M. Mäkelä, T. Hatanpää, K. Mizohata, K. Meinander, J. Niinistö, J. Räisänen, M. Ritala, M. Leskelä, *Chem. Mater.* **2017**, *29*, 2040.

(73) L. C. Kalutarage, P. D. Martin, M. J. Heeg, C. H. Winter, *J. Am. Chem. Soc.* **2013**,

135, 12588.

(74) R. Solanki, B. Pathangey, *Electrochem. Solid-State Lett.* **2000**, *3*, 479.

(75) J. Huo, R. Solanki, J. McAndrew, *J. Mater. Res.* **2002**, *17*, 2394.

(76) J. W. Elam, A. Zinovev, C. Y. Han, H. H. Wang, U. Welp, J. N. Hryn, M. J. Pellin, *Thin Solid Films* **2006**, *515*, 1664.

(77) H. Feng, J. W. Elam, J. A. Libera, W. Setthapun, P. C. Stair, *Chem. Mater.* **2010**, *22*, 3133.

(78) V. R. Anderson, N. Leick, J. W. Clancey, K. E. Hurst, K. M. Jones, A. C. Dillon, S. M. George, *J. Phys. Chem. C* **2014**, *118*, 8960.

(79) M. Sarr, N. Bahlawane, D. Arl, M. Dossot, E. McRae, D. Lenoble, *J. Phys. Chem. C* **2014**, *118*, 23385.

(80) Z. Golrokhi, S. Chalker, C. J. Sutcliffe, R. J. Potter, *Appl. Surf. Sci.* **2016**, *364*, 789.

(81) T. J. Knisley, T. C. Ariyasena, T. Sajavaara, M. J. Saly, C. H. Winter, *Chem. Mater.* **2011**, *23*, 4417.

(82) J. Kwon, M. Saly, M. D. Halls, R. K. Kanjolia, Y. J. Chabal, *Chem. Mater.* **2012**, *24*, 1025.

(83) Z. Golrokhi, P. A. Marshall, S. Romani, S. Rushworth, P. R. Chalker, R. J. Potter, *Appl. Surf. Sci.* **2017**, *399*, 123.

(84) Y. Zhang, L. Du, X. Liu, Y. Ding, *Nanoscale* **2019**, *11*, 3484.

(85) M. Juppo, M. Ritala, M. Leskelä, *J. Electrochem. Soc.* **2000**, *147*, 3377.

(86) B. B. Burton, A. R. Lavoie, S. M. George, *J. Electrochem. Soc.* **2008**, *155*, D508.

(87) Z. Fang, H. C. Aspinall, R. Odedra, R. J. Potter, *J. Cryst. Growth* **2011**, *331*, 33.

(88) T. J. Knisley. New Precursors and Chemistry for the Growth of Transition Metal Films by Atomic Layer Deposition. PhD Thesis, Wayne State University, 2012.

(89) T. C. Ariyasena. (i) Chromatographic Methods for Solute Descriptor Determinations (ii) Ruthenium Substrate-Catalyzed Growth of Nickel Nitride Thin Films by Atomic Layer Deposition. PhD Thesis, Wayne State University, 2015.

(90) S. Wolf, M. Breeden, I. Kwak, J. H. Park, M. Kavrik, M. Naik, D. Alvarez, J. Spiegelman, A. C. Kummel, *Appl. Surf. Sci.* **2018**, *462*, 1029.

(91) M. Juppo, M. Ritala, M. Leskelä, *J. Vac. Sci. Technol. A* **1997**, *15*, 2330.

(92) B. Vidjayacoumar, D. J. H. Emslie, S. B. Clendenning, J. M. Blackwell, J. F. Britten, A. Rheingold, *Chem. Mater.* **2010**, *22*, 4844.

(93) B. H. Lee, J. K. Hwang, J. W. Nam, S. U. Lee, J. T. Kim, S.-M. Koo, A. Baunemann, R. A. Fischer, M. M. Sung, *Angew. Chem. Int. Ed.* **2009**, *48*, 4536.

(94) A. Prabhakar. Investigations of Deep Level Defects in Semiconductor Material Systems. PhD Thesis, California Institute of Technology, 1985.

(95) S. Weiss, R. Beckmann, R. Kassing, *Appl. Phys. A* **1990**, *50*, 151.

(96) A. Masuhr, H. Bracht, N. A. Stolwijk, H. Overhof, H. Mehrer, *Semicond. Sci. Technol.* **1999**, *14*, 435.

(97) K. J. Blakeney, C. H. Winter, *Chem. Mater.* **2018**, *30*, 1844.

(98) G. Dey, S. D. Elliott, *Theor. Chem. Acc.* **2014**, *133*, 1416.

(99) J. P. Klesko, C. M. Thrush, C. H. Winter, *Chem. Mater.* **2015**, *27*, 4918.

(100) E. C. Stevens, M. B. M. Mousa, G. N. Parsons, *J. Vac. Sci. Technol. A* **2018**, *36*, 06A106.

(101) K. Reichelt, *Vacuum* **1988**, *38*, 1083.

(102) P. R. Gadkari, A. P. Warren, R. M. Todi, R. V. Petrova, K. R. Coffey, *J. Vac. Sci. Technol. A* **2005**, *23*, 1152.

(103) C. V. Thompson, *Annu. Rev. Mater. Res.* **2012**, *42*, 399.

(104) M. Altomare, N. T. Nguyen, P. Schmuki, *Chem. Sci.* **2016**, *7*, 6865.

(105) F. Leroy, Ł. Borowik, F. Cheynis, Y. Almadori, S. Curiotto, M. Trautmann, J. C. Barbé, P. Müller, *Surf. Sci. Rep.* **2016**, *71*, 391.

(106) D. J. Hagen, J. Connolly, I. M. Povey, S. Rushworth, M. E. Pemble, *Adv. Mater. Interfaces* **2017**, *4*, 1700274.

(107) J.-W. Lim, M. Isshiki, *J. Appl. Phys.* **2006**, *99*, 094909.

(108) M. Ohring. *The Materials Science of Thin Films*, 2nd Edition, Academic Press: San Diego, USA, 2001.

(109) A. E. Kaloyeros, Y. Pan, J. Goff, B. Arkles, *ECS J. Solid State Sci. Technol.* **2019**, *8*, P119.

(110) H.-B.-R. Lee, H. Kim, *Electrochem. Solid-State Lett.* **2006**, *9*, G323.

(111) H.-B.-R. Lee, J. Y. Son, H. Kim, *Appl. Phys. Lett.* **2007**, *90*, 213509.

(112) S. K. Kim, S. Hoffmann-Eifert, M. Reiners, R. Waser, *J. Electrochem. Soc.* **2011**, *158*, D6.

(113) H.-B.-R. Lee, Y. J. Park, S. Baik, H. Kim, *Chem. Vap. Deposition* **2012**, *18*, 41.

(114) K. Kim, K. Lee, S. Han, W. Jeong, H. Jeon, *J. Electrochem. Soc.* **2007**, *154*, H177.

(115) K. Kim, K. Lee, S. Han, T. Park, Y. Lee, J. Kim, S. Yeom, H. Jeon, *Jpn. J. Appl. Phys.* **2007**, *46*, L173.

(116) J.-H. Park, D.-Y. Moon, D.-S. Han, Y.-J. Kang, S.-R. Shin, H.-T. Jeon, J.-W. Park, *Surf. Coat. Technol.* **2014**, *259*, 98.

(117) J. You, Y. Guo, *J. Alloys Compd.* **2018**, *758*, 116.

(118) H.-B.-R. Lee, G. H. Gu, J. Y. Son, C. G. Park, H. Kim, *Small* **2008**, *4*, 2247.

(119) J. Yoon, H.-B.-R. Lee, D. Kim, T. Cheon, S.-H. Kim, H. Kim, *J. Electrochem. Soc.*

2011, *158*, H1179.

(120) J. Yoon, J.-G. Song, H. Kim, H.-B.-R. Lee, *Surf. Coat. Technol.* **2015**, *264*, 60.

(121) H. Shimizu, K. Sakoda, T. Momose, M. Koshi, Y. Shimogaki, *J. Vac. Sci. Technol. A* **2012**, *30*, 01A144.

(122) J. Park, H.-B.-R. Lee, D. Kim, J. Yoon, C. Lansalot, J. Gatineau, H. Chevrel, H. Kim, *J. Energy Chem.* **2013**, *22*, 403.

(123) K. Lee, K. Kim, H. Jeon, Y. Lee, J. Kim, S. Yeom, *J. Korean Phys. Soc.* **2007**, *50*, 1141.

(124) K. Lee, K. Kim, T. Park, H. Jeon, Y. Lee, J. Kim, S. Yeom, *J. Electrochem. Soc.* **2007**, *154*, H899.

(125) H. Kim, J. Yoon, H.-B.-R. Lee. In *Atomic Layer Deposition for Nanoscale Contact Applications*, Proceedings of the IEEE International Interconnect Technology Conference, Dresden, Germany, May 8–12, 2011.

(126) H.-B.-R. Lee, W.-H. Kim, J. W. Lee, J.-M. Kim, K. Heo, I. C. Hwang, Y. Park, S. Hong, H. Kim, *J. Electrochem. Soc.* **2010**, *157*, D10.

(127) H.-B.-R. Lee, J. Kim, H. Kim, W.-H. Kim, J. W. Lee, I. Han, *J. Korean Phys. Soc.* **2010**, *56*, 104.

(128) H.-B.-R. Lee, G. H. Gu, C. G. Park, H. Kim, *J. Electrochem. Soc.* **2012**, *159*, K146.

(129) J.-M. Kim, H.-B.-R. Lee, C. Lansalot, C. Dussarrat, J. Gatineau, H. Kim, *Jpn. J. Appl. Phys.* **2010**, *49*, 05FA10.

(130) T. D.-M. Elko-Hansen, J. G. Ekerdt, *Chem. Mater.* **2014**, *26*, 2642.

(131) T. D.-M. Elko-Hansen, A. Dolocan, J. G. Ekerdt, *J. Phys. Chem. Lett.* **2014**, *5*, 1091.

(132) Z. Li, D. K. Lee, M. Coulter, L. N. J. Rodriguez, R. G. Gordon, *Dalton Trans.* **2008**, 2592.

(133) J. Kim, T. Iivonen, J. Hämäläinen, M. Kemell, K. Meinander, K. Mizohata, L. Wang, J. Räisänen, R. Beranek, M. Leskelä, A. Devi, *Chem. Mater.* **2017**, *29*, 5796.

(134) M. Utriainen, M. Kröger-Laukkanen, L.-S. Johansson, L. Niinistö, *Appl. Surf. Sci.* **2000**, *157*, 151.

(135) J. Chae, H.-S. Park, S. Kang, *Electrochem. Solid-State Lett.* **2002**, *5*, C64.

(136) Y.-P. Wang, Z.-J. Ding, Q.-X. Liu, W.-J. Liu, S.-J. Ding, D. W. Zhang, *J. Mater. Chem. C* **2016**, *4*, 11059.

(137) J.-M. Park, S. Kim, J. Hwang, W. S. Han, W. Koh, W.-J. Lee, *J. Vac. Sci. Technol. A* **2018**, *36*, 01A119.

(138) K.-W. Do, C.-M. Yang, I.-S. Kang, K.-M. Kim, K.-H. Back, H.-I. Cho, H.-B. Lee, S.-H. Kong, S.-H. Hahm, D.-H. Kwon, J.-H. Lee, J.-H. Lee, *Jpn. J. Appl. Phys.* **2006**, *45*, 2975.

(139) H.-S. Kang, J.-B. Ha, J.-H. Lee, C. K. Choi, J. Y. Lee, K.-M. Lee, *Thin Solid Films*

2011, *519*, 6658.

(140) H.-B.-R. Lee, S.-H. Bang, W.-H. Kim, G. H. Gu, Y. K. Lee, T.-M. Chung, C. G. Kim, C. G. Park, H. Kim, *Jpn. J. Appl. Phys.* **2010**, *49*, 05FA11.

(141) C.-M. Yang, S.-W. Yun, J.-B. Ha, K.-I. Na, H.-I. Cho, H.-B. Lee, J.-H. Jeong, S.-H. Kong, S.-H. Hahm, J.-H. Lee, *Jpn. J. Appl. Phys.* **2007**, *46*, 1981.

(142) J.-B. Ha, S.-W. Yun, J.-H. Lee, *Curr. Appl. Phys.* **2010**, *10*, 41.

(143) J. Kim, W. Jang, J. Park, H. Jeon, H. Kim, J. Yuh, H. Jeon, *J. Korean Phys. Soc.* **2015**, *66*, 821.

(144) S.-B. Qian, Y.-P. Wang, Y. Shao, W.-J. Liu, S.-J. Ding, *Nanoscale Res. Lett.* **2017**, *12*, 138.

(145) Q.-H. Ren, Y. Zhang, H.-L. Lu, Y.-P. Wang, W.-J. Liu, X.-M. Ji, A. Devi, A.-Q. Jiang, D. W. Zhang, *ACS Appl. Mater. Interfaces* **2018**, *10*, 468.

(146) G. Yuan, H. Shimizu, T. Momose, Y. Shimogaki, *Microelectron. Eng.* **2014**, *120*, 230.

(147) G. Yuan, H. Shimizu, T. Momose, Y. Shimogaki, *J. Vac. Sci. Technol. A* **2014**, *32*, 01A104.

(148) P. Motamedi, K. Bosnick, K. Cui, K. Cadien, J. D. Hogan, *ACS Appl. Mater. Interfaces* **2017**, *9*, 24722.

(149) P. Mårtensson, K. Larsson, J.-O. Carlsson, *Appl. Surf. Sci.* **1998**, *136*, 137.

(150) P. Mårtensson, K. Larsson, J.-O. Carlsson, *Appl. Surf. Sci.* **1999**, *148*, 9.

(151) P. Mårtensson, K. Larsson, J.-O. Carlsson, *Appl. Surf. Sci.* **2000**, *157*, 92.

(152) P. Mårtensson, J.-O. Carlsson, *Chem. Vap. Deposition* **1997**, *3*, 45.

(153) T. Törndahl, M. Ottosson, J.-O. Carlsson, *Thin Solid Films* **2004**, *458*, 129.

(154) A. Johansson, T. Törndahl, L. M. Ottosson, M. Boman, J.-O. Carlsson, *Mater. Sci. Eng. C* **2003**, *23*, 823.

(155) T. Törndahl, J. Lu, M. Ottosson, J.-O. Carlsson, *J. Cryst. Growth* **2005**, *276*, 102.

(156) P. Mårtensson, J.-O. Carlsson, *J. Electrochem. Soc.* **1998**, *145*, 2926.

(157) B. G. Willis, J. Qi, X. Jiang, J. Chen, G. J. Weisel, D. T. Zimmerman, *ECS Trans.* **2014**, *64*, 253.

(158) X. Jiang, H. Wang, J. Qi, B. G. Willis, *J. Vac. Sci. Technol. A* **2014**, *32*, 041513.

(159) R. Gupta, B. G. Willis, *Appl. Phys. Lett.* **2007**, *90*, 253102.

(160) I. J. Hsu, B. E. McCandless, C. Weiland, B. G. Willis, *J. Vac. Sci. Technol. A* **2009**, *27*, 660.

(161) B. G. Willis, R. Gupta, C.-Y. Ni, *ECS Trans.* **2010**, *33*, 25.

(162) C. Jezewski, W. A. Lanford, C. J. Wiegand, J. P. Singh, P. I. Wang, J. J. Senkevich, T.-M. Lu, *J. Electrochem. Soc.* **2005**, *152*, C60.

(163) S. J. Martin, J. P. Godschalx, M. E. Mills, E. O. Shaffer II, P. H. Townsend, *Adv. Mater.* **2000**, *12*, 1769.

(164) A. Niskanen, A. Rahtu, T. Sajavaara, K. Arstila, M. Ritala, M. Leskelä, *J. Electrochem. Soc.* **2005**, *152*, G25.

(165) L. Wu, E. Eisenbraun, *J. Vac. Sci. Technol. B* **2007**, *25*, 2581.

(166) L. Wu, E. Eisenbraun, *Electrochem. Solid-State Lett.* **2008**, *11*, H107.

(167) L. Wu, E. Eisenbraun, *J. Electrochem. Soc.* **2009**, *156*, H734.

(168) T. S. Tripathi, M. Karppinen, *Chem. Mater.* **2017**, *29*, 1230.

(169) S.-W. Kang, J.-Y. Yun, Y. H. Chang, *Chem. Mater.* **2010**, *22*, 1607.

(170) Z. Zhong, X. Wang, J. Ding, N. Yuan, *Thin Solid Films* **2015**, *589*, 673.

(171) Z. Guo, H. Li, Q. Chen, L. Sang, L. Yang, Z. Liu, X. Wang, *Chem. Mater.* **2015**, *27*, 5988.

(172) Z. Li, R. G. Gordon, D. B. Farmer, Y. Lin, J. Vlassak, *Electrochem. Solid-State Lett.* **2005**, *8*, G182.

(173) Z. Li, A. Rahtu, R. G. Gordon, *J. Electrochem. Soc.* **2006**, *153*, C787.

(174) S. O. Kucheyev, J. Biener, T. F. Baumann, Y. M. Wang, A. V. Hamza, Z. Li, D. K. Lee, R. G. Gordon, *Langmuir* **2008**, *24*, 943.

(175) O. Seitz, M. Dai, F. S. Aguirre-Tostado, R. M. Wallace, Y. J. Chabal, *J. Am. Chem. Soc.* **2009**, *131*, 18159.

(176) M. Dai, J. Kwon, M. D. Halls, R. G. Gordon, Y. J. Chabal, *Langmuir* **2010**, *26*, 3911.

(177) D. J. Hagen, I. M. Povey, S. Rushworth, J. S. Wrench, L. Keeney, M. Schmidt, N. Petkov, S. T. Barry, J. P. Coyle, M. E. Pemble, *J. Mater. Chem. C* **2014**, *2*, 9205.

(178) J. Mao, E. Eisenbraun, V. Omarjee, A. Korolev, C. Dussarrat, *IEEE Trans. Semicond. Manuf.* **2013**, *26*, 17

(179) D. J. Hagen, J. Connolly, R. Nagle, I. M. Povey, S. Rushworth, P. Carolan, P. Ma, M. E. Pemble, *Surf. Coat. Technol.* **2013**, *230*, 3.

(180) K.-M. Park, J.-K. Kim, B. Han, W.-J. Lee, J. Kim, H.-K. Shin, *Microelectron. Eng.* **2012**, *89*, 27.

(181) J. Mao, E. Eisenbraun, V. Omarjee, C. Lansalot, C. Dussarrat, *Mater. Res. Soc. Symp. Proc.* **2010**, *1195*, B12-05.

(182) D.-Y. Moon, W.-S. Kim, T.-S. Kim, B.-W. Kang, J.-W. Park, S. J. Yeom, J. H. Kim, *J. Korean Phys. Soc.* **2009**, *54*, 1330.

(183) H.-C. Yoon, J.-H. Shin, H.-S. Park, S.-J. Suh, *J. Nanosci. Nanotechnol.* **2015**, *15*, 1601.

(184) K.-H. Park, A. Z. Bradley, J. S. Thompson, W. J. Marshall, *Inorg. Chem.* **2006**, *45*, 8480.

(185) D.-Y. Moon, D.-S. Han, S.-Y. Shin, J.-W. Park, B. M. Kim, J. H. Kim, *Thin Solid Films* **2011**, *519*, 3636.

(186) D.-Y. Moon, W.-S. Kim, J.-W. Park, *J. Nanosci. Nanotechnol.* **2012**, *12*, 3661.

(187) A. Turgambaeva, N. Prud'homme, V. Krisyuk, C. Vahlas, *J. Nanosci. Nanotechnol.* **2011**, *11*, 8198.

(188) J.-M. Park, K. Jin, B. Han, M. J. Kim, J. Jung, J. J. Kim, W.-J. Lee, *Thin Solid Films* **2014**, *556*, 434.

(189) J. S. Thompson, L. Zhang, J. P. Wyre, D. J. Brill, K. G. Lloyd, *Thin Solid Films* **2009**, *517*, 2845.

(190) Z. Li, R. G. Gordon, *Chem. Vap. Deposition* **2006**, *12*, 435.

(191) D. Alburquenque, V. Bracamonte, M. Del Canto, A. Pereira, J. Escrig, *MRS Commun.* **2017**, *7*, 848.

(192) A. M. Alexander, J. S. J. Hargreaves, C. Mitchell, *Top. Catal.* **2013**, *56*, 1963.

(193) M. Daub, M. Knez, U. Goesele, K. Nielsch, *J. Appl. Phys.* **2007**, *101*, 09J111.

(194) K. B. Klepper, O. Nilsen, H. Fjellvåg, *Thin Solid Films* **2007**, *515*, 7772.

(195) M. Diskus, O. Nilsen, H. Fjellvåg, *Chem. Vap. Deposition* **2011**, *17*, 135.

(196) B. Han, K. H. Choi, K. Park, W. S. Han, W.-J. Lee, *Electrochem. Solid-State Lett.* **2012**, *15*, D14.

(197) D. K. Nandi, J. Manna, A. Dhara, P. Sharma, S. K. Sarkar, *J. Vac. Sci. Technol. A* **2016**, *34*, 01A115.

(198) T. Q. Ngo, A. Posadas, H. Seo, S. Hoang, M. D. McDaniel, D. Utess, D. H. Triyoso, C. B. Mullins, A. A. Demkov, J. G. Ekerdt, *J. Appl. Phys.* **2013**, *114*, 084901.

(199) Z. Zhang, H. C. Nallan, B. M. Coffey, T. Q. Ngo, T. Pramanik, S. K. Banerjee, J. G. Ekerdt, *J. Vac. Sci. Technol. A* **2019**, *37*, 010903.

(200) Z. Zhang, T. Dwyer, S. M. Sirard, J. G. Ekerdt, *J. Vac. Sci. Technol. A* **2019**, *37*, 020905.

(201) T. Iivonen, M. Kaipio, T. Hatanpää, K. Mizohata, K. Meinander, J. Räisänen, J. Kim, M. Ritala, M. Leskelä, *J. Vac. Sci. Technol. A* **2019**, *37*, 010908.

(202) E. Lindahl, M. Ottosson, J.-O. Carlsson, *Surf. Coat. Technol.* **2010**, *205*, 710.

(203) D. Rüffer, R. Huber, P. Berberich, S. Albert, E. Russo-Averchi, M. Heiss, J. Arbiol, A. Fontcuberta i Morral, D. Grundler, *Nanoscale* **2012**, *4*, 4989.

(204) G. Wang, Z. Gao, S. Tang, C. Chen, F. Duan, S. Zhao, S. Lin, Y. Feng, L. Zhou, Y. Qin, *ACS Nano* **2012**, *6*, 11009.

(205) G. Wang, Z. Gao, G. Wan, S. Lin, P. Yang, Y. Qin, *Nano Res.* **2014**, *7*, 704.

(206) L. Assaud, E. Monyoncho, K. Pitzschel, A. Allagui, M. Petit, M. Hanbücken, E. A. Baranova, L. Santinacci, *Beilstein J. Nanotechnol.* **2014**, *5*, 162.

(207) Z. Gao, M. Dong, G. Wang, P. Sheng, Z. Wu, H. Yang, B. Zhang, G. Wang, J. Wang, Y. Qin, *Angew. Chem.* **2015**, *127*, 9134.

(208) A. Pereira, J. L. Palma, J. C. Denardin, J. Escrig, *Nanotechnology* **2016**, *27*, 345709.

(209) J. Zhang, C. Chen, W. Yan, F. Duan, B. Zhang, Z. Gao, Y. Qin, *Catal. Sci. Technol.* **2016**, *6*, 2112.

(210) E. Dashjav, M. Lipińska-Chwałek, D. Grüner, G. Mauer, M. Luysberg, F. Tietz, *Surf. Coat. Technol.* **2016**, *307*, 428.

(211) T. Törndahl, M. Ottosson, J.-O. Carlsson, *J. Electrochem. Soc.* **2006**, *153*, C146.

(212) P. J. Soininen, K.-E. Elers, V. Saanila, S. Kaipio, T. Sajavaara, S. Haukka, *J. Electrochem. Soc.* **2005**, *152*, G122.

(213) T. Waechtler, S. Oswald, N. Roth, A. Jakob, H. Lang, R. Ecke, S. E. Schulz, T. Gessner, A. Moskvinova, S. Schulze, M. Hietschold, *J. Electrochem. Soc.* **2009**, *156*, H453.

(214) R. Becker, A. Devi, J. Weiß, U. Weckenmann, M. Winter, C. Kiener, H.-W. Becker, R. A. Fischer, *Chem. Vap. Deposition* **2003**, *9*, 149.

(215) J. Jokinen, J. Keinonen, P. Tikkanen, A. Kuronen, T. Ahlgren, K. Nordlund, *Nucl. Instrum. Methods Phys. Res. B* **1996**, *119*, 533.

(216) A. Baiker, M. Maciejewski, *J. Chem. Soc. Faraday Trans. 1* **1984**, *80*, 2331.

(217) A. Leineweber, H. Jacobs, S. Hull, *Inorg. Chem.* **2001**, *40*, 5818.

(218) Z. Li, R. G. Gordon, V. Pallem, H. Li, D. V. Shenai, *Chem. Mater.* **2010**, *22*, 3060.

(219) N. Popović, Ž. Bogdanov, B. Goncić, S. Štrbac, Z. Rakočević, *Appl. Surf. Sci.* **2008**, *255*, 4027.

(220) G. Sauthoff. *Intermetallics*; P. Gregory, D. Hollis, U. Anton, Eds.; VCH Verlagsgesellschaft mbH: Weinheim, Federal Republic of Germany, 1995.

(221) K. A. Benavides, I. W. H. Oswald, J. Y. Chan, *Acc. Chem. Res.* **2018**, *51*, 12.

(222) R. B. van Dover, E. M. Gyorgy, R. J. Cava, J. J. Krajewski, R. J. Felder, W. F. Peck, *Phys. Rev. B* **1993**, *47*, 6134.

(223) B. L. Drake, F. Grandjean, M. J. Kangas, E. K. Okudzeto, A. B. Karki, M. T. Sougrati, D. P. Young, G. J. Long, J. Y. Chan, *Inorg. Chem.* **2010**, *49*, 445.

(224) T. He, Q. Huang, A. P. Ramirez, Y. Wang, K. A. Regan, N. Rogado, M. A. Hayward, M. K. Haas, J. S. Slusky, K. Inumara, H. W. Zandbergen, N. P. Ong, R. J. Cava, *Nature* **2001**, *411*, 54.

(225) H. Hegger, C. Petrovic, E. G. Moshopoulou, M. F. Hundley, J. L. Sarrao, Z. Fisk, J. D. Thompson, *Phys. Rev. Lett.* **2000**, *84*, 4986.

(226) C. Petrovic, P. G. Pagliuso, M. F. Hundley, R. Movshovich, J. L. Sarrao, J. D. Thompson, Z. Fisk, P. Monthoux, *J. Phys. Condens. Matter* **2001**, *13*, L337.

(227) T. Takeshita, W. E. Wallace, R. S. Craig, *J. Catal.* **1976**, *44*, 236.

(228) E. Casado-Rivera, Z. Gál, A. C. D. Angelo, C. Lind, F. J. DiSalvo, H. D. Abruña, *ChemPhysChem* **2003**, *4*, 193.

(229) Y.-L. Kim, H.-Y. Lee, S.-W. Jang, S.-J. Lee, H.-K. Baik, Y.-S. Yoon, Y.-S. Park, S.-M. Lee, *Solid State Ionics* **2003**, *160*, 235.

(230) N. Mahmood, C. Zhang, F. Liu, J. Zhu, Y. Hou, *ACS Nano* **2013**, *7*, 10307.

(231) L. O. Vogt, C. Villevieille, *J. Electrochem. Soc.* **2016**, *163*, A1306.

(232) J. Hassoun, S. Panero, P. Simon, P. L. Taberna, B. Scrosati, *Adv. Mater.* **2007**, *19*, 1632.

(233) N. M. Pereira, C. T. Sousa, C. M. Pereira, J. P. Araújo, A. F. Silva, *Cryst. Growth Des.* **2017**, *17*, 5208.

(234) C. Xian, J. Wang, *RSC Adv.* **2018**, *8*, 213.

(235) A. Onda, T. Komatsu, T. Yashima, *Chem. Commun.* **1998**, *2*, 1507.

(236) S. Furukawa, K. Ozawa, T. Komatsu, *RSC Adv.* **2013**, *3*, 23269.

(237) Z. Yi, X. Tian, Q. Han, J. Lian, Y. Wu, L. Wang, *RSC Adv.* **2016**, *6*, 39818.

(238) P. S. Goley, M. K. Hudait, *Materials* **2014**, *7*, 2301.

(239) P. D. Ye. Germanium Can Take Transistors Where Silicon Can't. In *IEEE Spectrum*, 2016; https://spectrum.ieee.org/semiconductors/materials/germanium-can-take-transistors-where-silicon-cant (accessed March, 2019).

(240) S. Gaudet, C. Detavernier, A. J. Kellock, P. Desjardins, C. Lavoie, *J. Vac. Sci. Technol. A* **2006**, *24*, 474.

(241) H. J. Ahn, J. Moon, Y. Seo, T. I. Lee, C.-K. Kim, W. S. Hwang, H.-Y. Yu, B. J. Cho, *IEEE Trans. Electron Devices* **2017**, *64*, 2599.

(242) J. Y. Spann, R. A. Anderson, T. J. Thornton, G. Harris, S. G. Thomas, C. Tracy, *IEEE Electron Device Lett.* **2005**, *26*, 151.

(243) I. M. Neklyudov, A. N. Morozov, *Physica B* **2004**, *350*, 325.